BENEFICIATION STUDIES OF BANDED IRON ORES

Ph. D. THESIS

by

VEERANJANEYULU RAYAPUDI

DEPARTMENT OF METALLURGICAL AND MATERIALS ENGINEERING
INDIAN INSTITUTE OF TECHNOLOGY ROORKEE
ROORKEE - 247667 (INDIA)
AUGUST, 2019

BENEFICIATION STUDIES OF BANDED IRON ORES

Ph. D. THESIS

Submitted in partial fulfilment of the
requirements for the award of the degree

of

DOCTOR OF PHILOSOPHY

in

Metallurgical and Materials Engineering

by

VEERANJANEYULU RAYAPUDI

DEPARTMENT OF METALLURGICAL AND MATERIALS ENGINEERING
INDIAN INSTITUTE OF TECHNOLOGY ROORKEE
ROORKEE - 247667 (INDIA)
AUGUST, 2019

INDIAN INSTITUTE OF TECHNOLOGY ROORKEE

STUDENT'S DECLARATION

I hereby request you that the work presented in the thesis entitles "**BENEFICIATION STUDIES OF BANDED IRON ORES**" is my own work carried out during a period from December, 2015 to August, 2019 under the supervision of Dr. Nikhil Dhawan, Assistant Professor, Department of Metallurgical and Materials Engineering, Indian Institute of Technology Roorkee, Roorkee.

The mater presented in the thesis has not been submitted for the award of any other degree of this or any other Institute.

R. Veeranjaneyulu

Dated: August 13; 2019 (VEERANJANEYULU RAYAPUDI)

SUPERVISOR'S DECLARATION

This is to certify that the above mentioned work is carried under my supervision

Nikhil Dhawan 13/08/2019

Dated: August 13; 2019 (NIKHIL DHAWAN)

CONTENTS

ABSTRACT

The present work investigates the utilization/beneficiation of low-grade iron ores to meet the steel vision 2030 of 300MT steel production. Due to limited rate of crude steel production and depletion of high-grade iron ores, processing of alternative iron resources such as low-grade iron ores is inevitable. The low-grade iron ores do not respond to conventional beneficiation techniques because of their complex chemical association. In this study detailed study of low-grade iron ores i.e., banded iron ores were carried out such as mineral identification, characterization studies, magnetic property studies, and wet chemical analysis to develop suitable beneficiation process. The processing of banded iron ores include first part deals with comminution studies (breakage rate characteristics through ball mill /Compression mode breakage) and second part deals with up-gradation (iron grade, yield, and iron recovery) of banded iron ores.

In comminution studies, BHJ ore was found harder than BHQ and BMQ. Thermal treatment of banded iron ores causes massive random micro-cracks which enhances breakage kinetics. Compression testing of banded iron ores yielded finer size reduction than ball mill due to induced microcracks. But the introduction of compression comminution could not lead to any improvement in the concentrate through the downstream magnetic separation process.

The up-gradation of banded iron ores included physical separation, microwave exposure, and carbothermal reduction (conventional/microwave). It was found that BHJ/BMQ can be upgraded and the concentrate can be used as feed for pellet making for blast furnace through microwave processing. The microwave exposed BMQ, produced a concentrate under optimal condition with 60.1% Fe grade, 99% Fe recovery at 71% yield in a single step. Whereas microwave exposed BHJ under optimal conditions, yielded an iron- concentrate with 61% Fe, 85% Fe recovery at 50% yield and BHQ yielded concentrate with Fe_G of 56.30%, Fe_R of 50.68% and a yield of ~27%. Effective conversion of the hematite phase to magnetite phase was observed in conventional carbothermal reduction process which helped ineffective separation of iron values from gangue. Carbothermal reduction was evaluated using Box Behnken statistical design and was found effective for iron enrichment. Under optimal condition, carbothermal reduction of BHQ produced a concentrate of Fe_G of 57.6%, Fe_R of 68% and a yield of 35.7%. Where as in BHJ concentrate enriched to Fe_G of 61.2%, Fe_R of 82% and a yield of 52% and coarser particle size produced the fused fraction consisting of ~ 85%Fe with retained austenite and martensitic iron phases.

In microwave carbothermal reduction the formation of spheroidal ferrite ball was observed within 10 min with the addition of a minimal amount of charcoal dosage at a microwave power of 900 W. Microwave carbothermal reduction of BHJ under optimal condition yielded a magnetic

concentrate having ~61.6% Fe, ~73.4% recovery at a yield of 44% and can be used for blast furnace feedstock. Similarly, other experimental condition yielded a magnetic concentrate with ~49.1% Fe, ~89.3% recovery at a yield of 59.7% with significant amount of ferrite balls. The microwave carbothermal reduction of BHQ yielded Fe_G of 57.6%, Fe_R of 47% and a yield of 24% at optimum condition and other optimal condition yielded a less grade with a significant amount of ferrite balls. It was found that a small fraction of microwave irradiated ore-charcoal mixture was rapidly melted to produce pure ferrite balls with Fe ~93 %. The iron grade deteriorated at prolonged exposure due to the formation of fayalite phase. The optical micrograph of the ferrite ball reveals the presence of retained austenite and martensitic iron phase with a saturation magnetization of ~200 emu/g.

Keywords: Low-grade iron ore, magnetic separation, microwave, carbothermal reduction, ferrite, grade, recovery.

ACKNOWLEDGMENTS

The work presented in this thesis would not have been possible without lots of blessing of Almighty GOD.

First and foremost, I would like to extend my sincere gratitude to my research supervisor, **Dr. Nikhil Dhawan** for his continuous help, suggestions, advice, inspiration, continuous motivation, encouragement, and continuous mental and moral support, throughout my Ph.D. work. His enthusiasm, integral view on research and his mission for providing high-quality work, has made a deep impression on me. During our course of interaction during the last three and half years, I have learned extensively from him, including how to raise new possibilities, how to approach a problem by systematic thinking, data-driven decision making and exploiting serendipity. I owe him lots of gratitude for having me shown this way of research. I am really glad to be associated with the legend like **Dr. Nikhil Dhawan** in my life.

I would like to thank and acknowledge the funding agencies Science Engineering Research Board (SERB) for providing early-career research funds via grants ECR/00874/2016, SER-878-MMED and SER-999-MMED.

I express my deep sense of gratitude to **Prof. Amit K Sen**, SRC Chairman and members of SRC **Prof. R. Krishnamurthy**, **Dr. Devendra Puri,** for their kind co-operation in my Research work. And also extend my gratitude to **Prof. Ujjwal Prakash**, DRC Chairman. I also thank all the faculty members of the department.

I am indebted to **Prof. G. P. Chaudhari**, Head of the department of metallurgical and materials engineering, for his support and ever helping attitude throughout the entire period of my Ph.D. work. I also extend my gratitude to **Prof. Anjan Sil** for his continuous encouragement and support.

I extend my humble thanks to **Prof. Ajit K. Chaturvedi**, Director, IIT Roorkee for his kind cooperation and extending all necessary help during my Research work.

I also thank senior lab technicians Mr. Dinesh Kumar, and Mr. Dhan Prakash and all other lab technicians for their support during my experimental works irrespective of time.

I thank my lab colleagues and other co-research scholars Amit Barnwal, Ashwini Kumar, Neha Shukla, Shrey Agrawal, Singh Rahul Kumar Sunil, Sanjay, Akeshwar Singh Yadav, Nilesh Kumar, Narsimha Vinod Pullagara, Hari Raj, Ravi Raj, Abhishek Maurya, Anurag Singh, Shivani Gupta, Manish Gupta, Kamlesh Kumar Meena, Kshetrimayum Premi Devi, Suprio Pal for their countless support for clearing my critical doubts during my experimental work.

I especially thank my hard-working father and mother **Rayapudi Koteswararao** and **Koteswaramma,** sacrificed their life and provided unconditional love and care, also always

provided a lot of freedom to continue higher studies irrespective of family problems. I also extend my thanks to my brother and sister-in-law **Rayapudi Hanumantha Rao** and **Sunita**, for their continuous love and moral support. I am grateful to have such a wonderful uncles and aunties **Rayapudi Venkateswara Rao & Kamala** and **Rayapudi Kotaiah & Sowjanya,** who dragged me towards studies and continuously encouraged and showed love by providing financial support for my whole study career. I extend my thanks to my beloved sisters and brothers namely **Dr. Sravani, Anurag, Nikhila and Saranya** for their continuous support.

Last but not least a very special thanks to my wife **Saranya**, who came into my life only 3 years back but well understood my inner feelings regarding studies in a very short duration of time. I have no words to express my feelings for her contribution and support. She sacrificed a lot and took whole responsibility for the smooth running of our family life and provided continuous encouragement and moral support when a whenever a tough situation arises. I also extend thanks to my cute daughter **Ritwika (smiley)**, who gave special encouragement to do work so faster.

I would also like to extend my thanks to family relatives and my friends for their speechless support during my studies.

(Veeranjaneyulu Rayapudi)

LIST OF FIGURES

LIST OF TABLES

CHAPTER 1

INTRODUCTION

1.1 Importance of iron ore deposits in the world and India

The applications of steel have become vital in the industrial revolution because of its less consumption of production energy as compared to aluminum production i.e., approximately 25% less. High-grade iron ores are the major source for production of crude steel/pig iron. The enhanced industrial revolution led to an increased crude steel production approximately increasing 5% every year. Iron is the prime backbone for the world's industrial growth. India is the fourth largest iron ore producer country in the world. Iron is the most used metal in the earth because it possesses high strength compared to other metals and cheaper due to its low production cost. It has a wide variety of applications such as to make alloy steels, to use in construction, to use in the automobile sector, to use in water transportation pipes, to use as a catalyst, to make magnets, and also it has many other applications.

1.2 Global iron ore resources

The most important iron ore resources of the world are located in former USSR (Kerch, Krivoirog and Kursk), Brazil (Minas Gerais and Mato Grosso), USA (Lake Superior, Alabama and Utah), Canada (Quebec, Labrador, Ontario and British Columbia), Australia (Hammersley Iron province, WA) and India (Jharkhand, Orissa, Chhatisgarh, Karnataka andGoa). The world's total crude ore resources are estimated as 173, 500 million tones (MT) crude ore containing 83730, 000 MT iron. Australia ranks first with 24, 000 MT of reserves and 50, 000 MT of reserve base, followed by Brazil with 17, 000 and 32, 000 MT of reserves and reserve base respectively as shown in Table 1.1 (MCS, 2019).

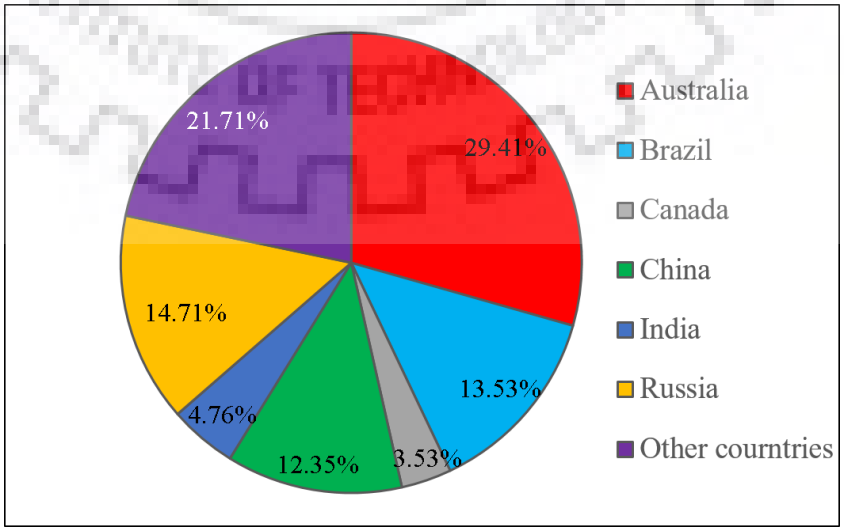

Figure 1.1 Distribution of total iron ore resources in India

Table 1.1 World iron ore reserves in million tones (M.T.) (MCS, 2019)

Country	**Crude ore**	**Iron content**
United states	2,900	760
Australia	50,000	24000
Brazil	32,000	17000
Canada	6,000	2300
China	20,000	6900
India	5,400	3200
Iran	2,700	1500
Kazakhstan	2,500	900
Russia	25,000	14000
South Africa	1,200	770
Sweden	1,300	600
Ukraine	6,500	2300
Other countries	18,000	9500
World total (rounded)	**1,73,500**	**83,730**

Global crude steel production was increased by approximately 4 % in 2018 and by 1.5% in 2019. The increased pressure on steel producers across the world to increase efficiency, reduce energy consumption, and meet environmental benchmarks continued the slow decline in the use of low-grade iron ore and spurred investment in the production of iron metallic and high-grade iron ore products, such as pellets (MCS, 2019).

Table 1.2 World mine production in million tones (M.T.) for the year 2017-2018 (MCS, 2019)

Country	**Usable ore**		**Iron content**	
	2017	2018	2017	2018
United states	47,900	49,000	30300	32000
Australia	8,83,000	9,00,000	547000	560000
Brazil	4,25,000	4,90,000	269000	310000
Canada	49,000	49,000	29000	29000
China	3,60,000	3,40,000	223000	210000
India	2,02,000	2,00,000	125000	130000
Iran	40,100	40,000	26300	26000
Kazakhstan	39,100	40,000	10900	12000
Russia	95,000	95,000	61200	61000
South Africa	81,100	81,000	52600	52000
Sweden	27,200	27,000	16900	17000
Ukraine	60,500	60,000	37800	38000
Other countries	1,19,000	1,20,000	72200	72000
World total (rounded)	24,28,900	24,91,000	1501200	1549000

1.3 Iron ore resources in India

Hematite and magnetite are the major resources of iron ores in India. Most of the hematite resources (approximately 95%) are confined in the states of Orissa, Jharkhand, Chhattisgarh, Karnataka and Goa and the rest of the resources are present in Maharashtra, Madhya Pradesh, Uttar Pradesh, Rajasthan and Assam as shown in Fig. 1.2. Magnetite reserves are mostly present in eco fragile Western Ghats of India which require special mining methods due to environmental issues. Therefore, at present, iron/steel industries are making use of hematite reserves. One third of the hematite reserves is mainly situated in eastern region of India i.e., Orissa (33.9%) and the rest are Jharkhand (26.30%), Chattisgarh (18.80%), Karnataka (12.30%), Goa (5.30%) and in other states are 3.40% (Iron and steel, 2020). There are different iron-bearing minerals in nature which are utilized for the extraction of iron and steel. The list of this mineral along with their properties is shown in Table 1.3. Hematite is the most abundant iron-bearing mineral expensively used iron and steel industries. These iron oxides are mainly associated with impurities such as silica, clay, alumina, calcite an appetite.

Table 1.3 Important iron-bearing minerals and their physical properties

Chemical formula	Iron (Fe) %	Magnetic	Specific gravity	Hardness	Magnetic intensity (Gauss)
Hematite (Fe_2O_3)	69.94	No	5.3	6.5	13000-18000
Magnetite (Fe_3O_4)	72.36	Strong	5.15	5.5 to 6	0-1000
Goethite (FeO(OH))	62.85	No	3.8	5 to 5.5	15000-18000
Siderite ($FeCO_3$)	48.2	No	3.96	3.5	10000-18000
Illmenite ($FeTiO_3$)	36.8	Weakly	4.5 to 5	5 to 6	8000-16000

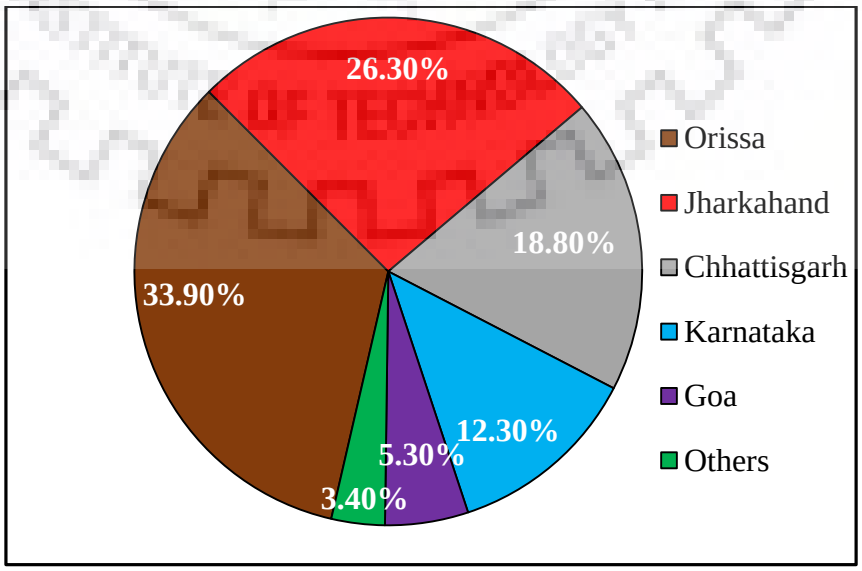

Figure 1.2 State-wise total resources of hematite iron ore as on 1.4.2010 (Iron and steel, 2020)

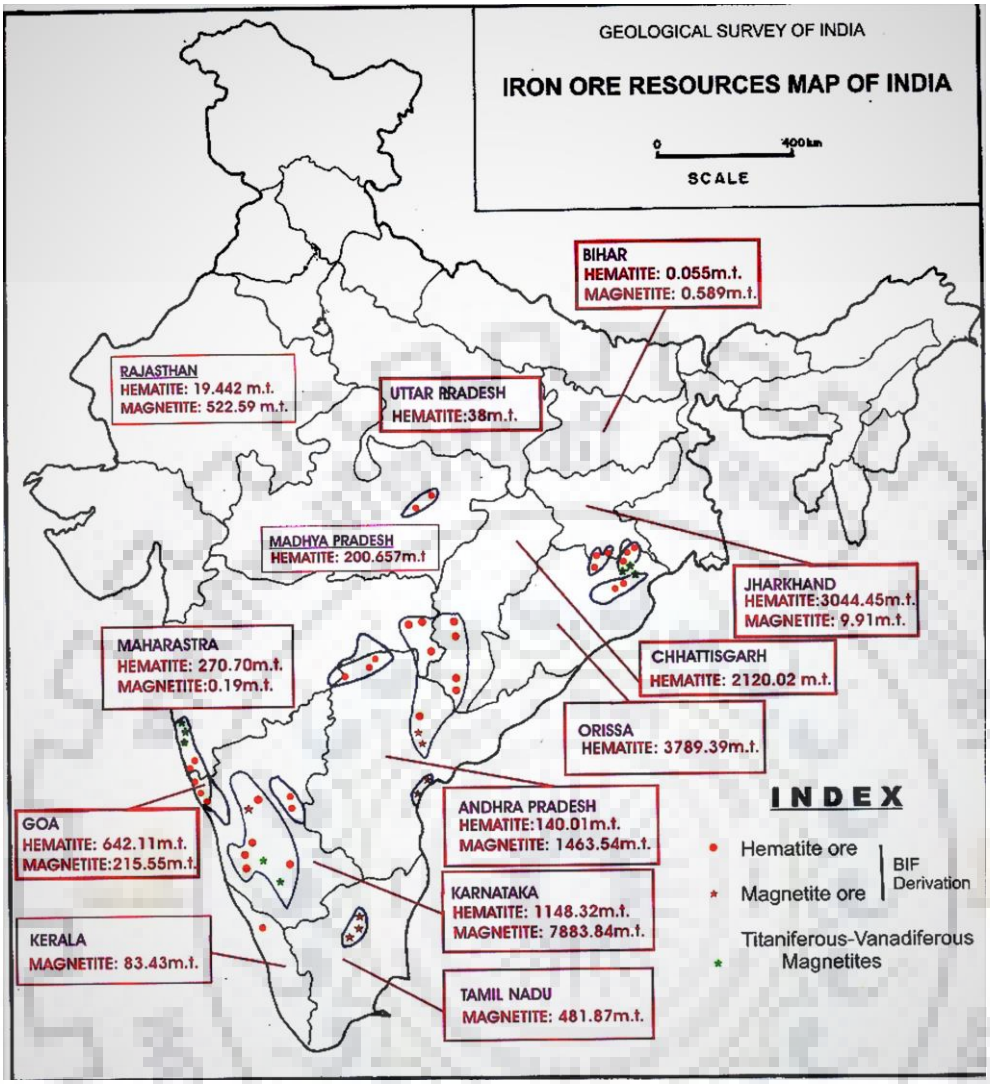

Fig. 1.3 Distribution of iron ore resources in India

1. 4 Banded iron ores and their formation

Banded iron formations (BIFs) are iron oxide and silica-rich chemical sedimentary rocks, most of which were deposited in great abundance during a ~800-million-year span from Late-Archean to mid-Proterozoic (ca 2.7-1.9 Ga) (Poveromo et al., 1999). The banded colors, usually on a cm-scale are due to differing amounts and oxidation states of Fe-containing minerals: hematite, magnetite, grunerite, siderite and sometimes pyrite. Banded iron formations are a distinctive type of rock often found in old sedimentary rocks. The structures consist of repeated thin layers of iron oxides, either magnetite or hematite, alternating with bands of iron-poor shale and chert. Large deposits of this type are observed in Canada, the United States, South Africa, Australia, India, Russia and Ukraine (Huston et al., 2004).

The basic banded iron ores formations are of two types Algoma type and superior type. Algoma-type is oldest (formed primarily in the Archaean) and naturally smaller in size usually less than

100 meters in thickness and some extent (few kilometers) in the lateral direction. Algoma-type BIFs are generally found in volcanic rocks in greenstone belts. The formation process involves the chemical precipitation of iron in anoxic environments. The oxidized (can be due to ultraviolet radiation) iron slowly precipitate and sink to the bottom of the seafloor as a layer by layer. The continuous shifting of oxygen levels caused to form magnetite/hematite beds continuously interlayered with crystalline or amorphous quartz/jasper. The evaporation of seawater promoted local silica over-saturation which resulted in silica precipitating as a gel on the seafloor. Whereas Superior type BIFs were formed by chemical precipitation in shallow waters, importantly due to the low atmospheric and ocean oxygen levels, resulting in high iron levels in the seas and these are large in size, more than 100 kilometers in thickness and more than 100 kilometers in the lateral direction. Under calm shallow conditions, the oxygen released during photosynthesis by blue-green algae would merge with the iron creating magnetite, which would then fall off and deposit on the seafloor.

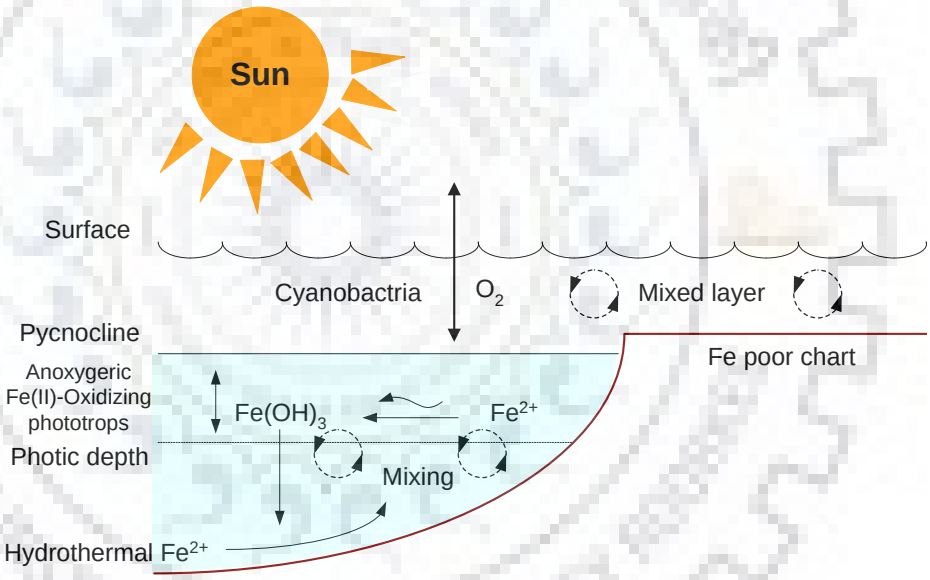

Figure 1.4 Precipitation of Fe_2O_3 in sea/ocean

1. 5 Banded iron ore deposits in India

India has huge resources of low-grade iron ores which are associated with volcano-sedimentary banded iron ores (BHQ, BHJ, BMQ; B-banded, H- Hematite, M-Magnetite, Q-Quartzite, J-Jasper) are of Precambrian age with age in excess of 2.5 billion years and the iron content of 30-35%. India has the fifth largest iron ore reserves in the world whereas Australia, Russia, Brazil, and India are having more resources in the series order.

The low grade and friable nature of the banded iron ores, inhibits the direct use in the iron making process. It is reported that beneficiation steps are mandatory to yield a suitable concentrate 60-62% Fe with 30% recovery only. The most important step from product quality and economic

perspective is confined to comminution or size reduction step. The majority of energy (more than 50%) is consumed in the comminution step with process efficiency as low as 1-2%. This is attributed both to ore response and inefficient action of comminution machine. The ore response is weak if there is liberation issue i.e., intimate association and/or inclusion of impurities within iron mineral (IBM, 2017).

Iron ore is the most important raw material for the production of iron and steel. As per Indian Steel Policy, 300 million tons of steel are required to meet vision 2030 which require approximately 550 million tons of high-grade ores. India does not have enough high-grade hematite ores but has abundant resources of low-grade iron ores (banded hematite quartzite/Jasper (BHQ, BHJ) and banded magnetite quartzite (BMQ). Indian hematite deposits belong to the Precambrian iron ore series and the ore occurs as banded, laminated, friable and also in powder form. During conventional mining of hematite ores, there is a significant generation of low grade banded ores such as BHQ, BHJ, and BMQ which ends up in unused stockpile at the mine sites due to a lack of suitable beneficiation technology (IBM, 2017; Rath et al., 2014). The iron bands in such ores are of hematite, magnetite and the silica bands are either quartz or reddish jasper and the thickness of the bands also varies from 0.5 to 1.5 cm. It is believed that the formation of these banded ores is either through replacement of silica by iron or by leaching of silica under suitable conditions or from the precipitation of iron from the Earth's ancient oceans (IBM, 2017). Also, these ores possess quite different characteristics in terms of beneficiation primarily because of negligible alumina content and excessive silica content compared to conventional hematite ores. The complex association of silica-iron phase i.e., soft-hard lamellae structure, and fine liberation size (<100 microns) prohibits the direct use of these low-grade iron ores in the steel production cycle. The iron content in these ores varies from 30-45% and the rest being siliceous impurities with traces of alumina, and are mainly found in the states of Karnataka, Orissa, Chattisgarh, and Rajasthan, India.

The investigations on the beneficiation of banded iron ores (BHQ, BHJ, and BMQ) are limited and mainly involve processing techniques such as flotation, high-intensity magnetic separation, jigging and reduction roasting. At present some of the iron ore companies in India are evaluating these ores of setting up beneficiation plants to recover the iron value. As per literature, the enrichment of low-grade iron ores requires stringent processing/ beneficiation techniques which include carbothermal reduction roasting, ultrasonic radiation, colloidal magnetic coating and microwave treatment to achieve suitable concentrate for blast furnace feed (Rath et al., 2014; Sahoo et al., 2014; Singh et al., 2015; Rath et al., 2016; Ponomar 2017; Das et al. 2018). The major difficulty in the upgradation of these ores includes the complex mineralogical association

of silica phase with hematite and very fine liberation size ~ 10μm (Das, 2010; Sahoo, 2016; Rath el., 2014). The jasper phase is very fine-grained and entrainment of hematite grains within jasper leads to liberation issues resulting in ineffective beneficiation even after fine grinding (Makhija et al., 2013). The carbothermal reduction involves roasting of the ore in a reducing environment at 500 to 700°C resulting in a partial reduction of hematite to magnetite followed by application of low-intensity magnetic separation (LIMS) to produce iron-rich magnetic product and tailings. The process suffers due to an associated energy penalty with roasting but offers advantages as magnetic separation is simpler and more selective than other separation techniques (e.g., floatation) along with reduced grinding costs due to the increased friability of the roasted ore, and improved settling and filtration characteristics of the ore due to dehydroxylation of clays during roasting (Iwasaki and Prasad, 1989; Faris et al., 2017). In the reduction studies of low-grade iron ores, on an average 10-15% increment in grade with 50-70% Fe recovery is reported (Singh et al., 2015; Das et al., 2018). Recently, a BHJ ore (~47% Fe) is reduced (900°C, 90 min, the coal-to-feed ratio of 0.15, coal size −3.35+1 mm and ore size −1 mm) yielded a concentrate of ~66% Fe with an iron recovery of ~72%. The siliceous tailings generated were further smelted in an arc furnace for the production of ferrosilicon alloy (Ray et al., 2018).

The absence of alumina in the BHJ sample is highly advantageous and makes it more desirable for blast furnace ironmaking considering the ill effect of alumina on slag behavior. BHJ ore resembles taconite ore processed in North America in terms of structure (bands) of iron phase and silica phase. However, the absence of the magnetite phase in BHJ makes it difficult to upgrade compared to conventional beneficiation of taconite ore. The application of microwaves on magnetite and taconite ore leads to selective thermal expansion resulting in less comminution energy and a cleaner mineral liberation thereby significantly improving the concentrate grade and metal recovery (Walkiewicz et al., 1991; Tavares and King, 1999). The unique applications of microwaves in extractive metallurgy processes include faster and controlled temperature ramp-up enhanced kinetics, rock disintegration, better liberation, and floatation, enhanced magnetic properties, improved drying and rheological properties along with better separation (Standish and Huang, 1991; Kingman and Roason, 2000; Ishizaka and Nagata, 2008; Pickles, 2009; Barani et al., 2011; Omran et al; 2014, Hartlieb et al, 2016). It is known that sulfides and oxides respond very well to microwave radiations, whereas, gangue minerals such as silicates are week receptors to microwaves (Kingman and Roason, 2000). Since BHJ ore consists of iron oxide (hematite) and silica (quartz) an attempt is made to make use of selective heating of iron oxide with microwave irradiation.

CHAPTER 2
LITERATURE REVIEW

2.1 Comminution studies of banded iron ores

India has abundant resources of banded iron ores such as (BHQ, BHJ, B-banded, H- Hematite, Q-Quartzite, J-Jasper) with an iron content of 30-40%. The low grade, complex association of silica-iron phase i.e., soft-hard lamellae structure, and fine liberation size (<75 microns) inhibits the direct use in the iron making process. Recently, NMDC, Hyderabad reported that beneficiation steps are mandatory to yield a suitable concentrate 60-65% Fe with 30% recovery only. It is well understood that comminution plays a key role in the process as it kicks starts the mineral beneficiation process. Comminution consumes up to 3% of all-electric power generated in the world and it accounts for about 50 to 80% of the total energy consumption in the mining operations (Abouzied et al. 2009; Wills and Finch, 2016; Fuerstenau, 2002; Liu et al. 2017), while only 1 to 2% is utilized for the production of the new surface area. During size reduction processes, the utmost concentration is on the interrelated phenomena of absorbed energy, utilized energy, reduction ratio, grinding limit, and particle size distributions of the comminuted product (Gutsche et al. 1993; Fuerstenau, 1995). This is attributed both to ore response and the inefficient action of comminution machine. The energy efficiency in grinding is governed by two factors, namely the form by which energy transforms into particles and the particle/particle interactions. Therefore, there have always been increasing efforts to enhance the comminution efficiency considering the fact that ores are getting harder and meanwhile, finer grinding is becoming a necessity. Tumbling mills have been the long-standing workhorse of the mining industry. Ball mills use a charge of steel balls to grind the ore particles in slurry water. Ball mills take millimeter size particles produced in previous grinding stages and finish these particles to a fine top size often below 45 microns. The ore response is weak if there is liberation issue i.e., intimate association and/or inclusion of impurities within iron mineral (IBM, 2017)

The purpose of comminution in mineral processing is almost always to achieve levels of liberation for minerals which allow the required separation efficiencies. The size reduction includes particle breakage which is a complex phenomenon as it involves different modes of breakage such as impact, abrasion, and compression (Schonert, 1986). The most efficient methods involve single particle breakage slowly under pure compression and by the compressive loading of a bed of particles in a piston-die arrangement. In this mode, comminution occurs primarily by very high localized inter-particle stresses generated within the particle bed (Fuerstenau and Favela, 1997; King 2001; Munn et al. 1996; Tavares, 2004).

Another way of enhanced comminution is pre-treatment of ore such as thermal treatment (heating, microwave) and using grinding additives. The thermal treatment of ore brings about thermal fracturing by exploiting differences in the magnitude of the thermal expansion coefficient of various phases in the lattice, and thereby a reduction in ore strength. Whereas, the addition of chemical additive as grinding aid modifies the flow of pulp in the grinding mill and influences on re-agglomeration of the freshly produced fines (Bhattacharyya et al., 2016); Rao et al., 1991; Veasey and Wills, 1991; King 2001). Literature reveals that microwave preheating of an iron ore improved grinding efficiency by 5-10% but this improvement was not enough to compensate for the energy consumption of the microwave preheating (Tavares, 2004). Intuitively, it seems that microwave treatment is more effective for abrasion breakage mechanism as abrasion is a surface phenomenon and microwave treatment is more effective at surface heating. The microwave treatment effect is pronounced in coarse sizes due to more defects (cracks) whereas, for medium-fine sizes flaws are depleted and the observed strength approaches the high intrinsic strength of the solid, thereby microwave effect becomes minimal as shown in Fig. 2.1.

Up to now, Indian iron industry is using soft ores with high grade and most of the plant comminution circuits were designed on conventional soft ore parameters. With the scarcity of high-grade ores and strict mines regulation, the immediate use of abundant low grade banded iron ores widely available looks quite promising. These ores require substantial comminution in order to achieve effective liberation i.e., around 50 to 75 micron. Besides, the ore resembles a composite structure i.e., layers of hematite/magnetite with silica, which acts as a soft-hard lamellae structure (IBM, 2011). The key aspect of thermal treatment is the ability to heat minerals selectively, rather than heating bulk rock

2.2 Microwave exposure of banded iron ores

The application of microwaves on magnetite and taconite ore leads to selective thermal expansion which results in less comminution energy and a cleaner mineral liberation thereby significantly improving the concentrate grade and metal recovery (Walliewicz et al. 1991).

The power absorption and heat transfer with in microwave are strongly dependent on particle size. Microwave heating is non-contact selective heating, and energy transfer instead of heat transfer, rapid heating, material – selective heating, heating initiation from the interior of a material and high level of safety and automation (Hague et al., 1999). Though the volumetric heating feature enhances the heat transfer process in a material but selection of particle size is crucial (Peng et al., 2010). Microwave treatment offers enhanced magnetic susceptibility which

facilitates the separation from complex ores. It is reported that some of the sulfides and oxides such as chalcopyrite, hematite, and magnetite are strong absorbers of microwaves, whereas, silicates do not respond well to microwaves (Pickles, 2009; Walliewicz et al., 1991). Quartz (SiO_2) is a diamagnetic mineral and therefore cannot be concentrated magnetically. The microwave treatment on iron ores such as magnetite and taconite leads to selective thermal expansion and provides cleaner mineral liberation, reduced grinding energy and hence leads to better concentrate grade and recovery (Amini et al., 2018). The microwave absorption by the magnetite phase mainly depends on the particle size, where fine particles (< 20 μm) acts as transparent material (Cheng et al., 2002). The heating rate of magnetite ore increased with increasing microwave power, sample mass and the particle size of ore and the peak shifting (XRD peak) was observed after microwave irradiation (Rajavaram et al. 2016).

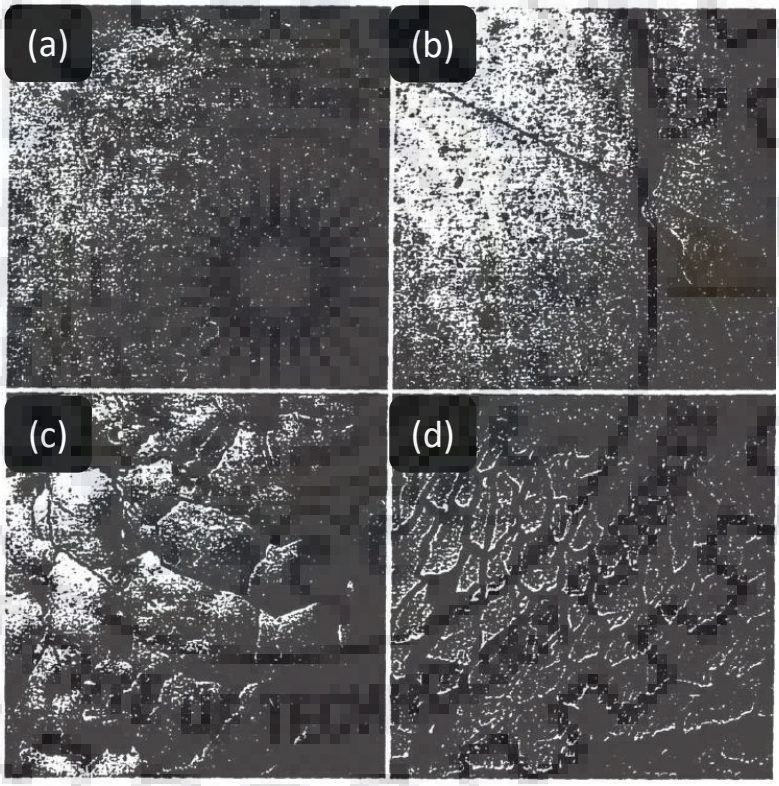

Figure 2.1 Micrographs of untreated a) and conventionally heated and water quenched quartz particles, b) heated to 200ºC, c) heated to 600ºC and d) heated to 1000ºC. (Tavares et.al.1995)

The unique applications of microwaves in extractive metallurgy processes include enhanced kinetics, rock disintegration, better liberation and floatation, better rheological properties, drying and improved recovery (Pickles 2009; Jena et al. 2016; Barani, et al. 2011; Omran et al. 2014). The literature review suggests that using microwaves as a pre-treatment process in beneficiation

of iron ores increases iron recovery, enhances the magnetic properties, easy removal of phosphorous and improves separation (Das, et al. 2010; Makhija, et al. 2013). Microwave radiation has a positive impact on magnetic susceptibility, which facilitates the separation of mineral phases from complex ores. It is known that sulfides and oxides respond very well to microwave radiations whereas gangue minerals such as silicates are not much receptive to microwaves. Some minerals such as chalcopyrite, hematite, and magnetite readily heat and show increased magnetic properties on microwave exposure of only 650 watts (Pickles, 2009). Compared to other iron oxide compounds, magnetite readily absorbs microwaves and the heating rate depends on both density and particle size (Hayashi, et al. 2010, Standish, et al. 1991, Yoshikawa, et al. 2009). It was also reported that the enrichment of magnetite ore (feed Fe: 50.16%) can be done by using microwave treatment followed by magnetic separation (8000 Gauss) to achieve 96.99% enrichment, 67.81% grade for iron, at 180-watt power for 7 min (Agacayak et. al. 2011). It was found that microwave treatment of pure magnetite leads to the generation of high temperature ~1000 °C and new phase nanoscale FeO was observed (Kato et al. 2011, Yoshikawa et al. 2011; Tripathy et al. 2018).

The investigations on beneficiation of banded iron ores (BHQ, BHJ, and BMQ) are limited and mainly involve processing techniques such as flotation, high-intensity magnetic separation, jigging and reduction roasting. The major difficulty in the upgrading of these ores includes the complex mineralogical association of silica phase with hematite and very fine liberation size ~ 10μm. Also, the jasper phase of quartzite is very fine-grained and entrainment of hematite grains within jasper leads to liberation issues resulting in ineffective beneficiation even after fine grinding. The conventional beneficiation of BHJ/BHQ ores does not yield satisfactory iron grade and recovery; therefore, alternative methods such as colloidal magnetic coating and reduction roasting are reported. In these studies, on an average 10-15% increment in grade with 50-70% Fe recovery is reported (Sahoo et al. 2016; Singh et al. 2015; Das et al. 2018). Recently, BHJ ore (~ 47% Fe) reduced in the carbothermal environment (900 °C, 90 min, the coal-to-feed ratio of 0.15, coal of size −3.35+1 mm and ore of size −1 mm) yielded a concentrate of ~66% Fe with the recovery of ~72%. The siliceous tailings generated were further smelted in an arc furnace for the production of ferrosilicon alloy (Ray et al. 2018). Recently scrubbing followed by multiple-step low magnetic separation process was reported for the recovery of magnetite from BMQ ore with a concentrate ~65.1% Fe at a yield of 24.6% (Tripathy et al. 2018). Recently, it is reported that application of microwave pre-treatment reduces the ore hardness causing the ore fracture with no effect on the original mineralogical characteristics. However, the response of microwave

irradiation strongly depends on the mineralogy or the water content of the rock (Singh et al. 2017, Cheng et al. 2018, Hartlieb et al. 2017).

2.3. Carbothermal reduction

The literature reveals the iron oxides can be reduced to magnetite and metallic iron through conventional carbothermal reduction (Das et al. 2018, Ray et al. 2018, Faris 2017, Yu et al. 2017, and Long et al. 2014, Zhu et al. 2013). In order of increasing reduction kinetics and to reduce the energy consumed during conventional carbothermal reduction few researchers were tried carbothermic reduction through microwave technology (Hayashi et al. 2013, Peng et al. 2017, Castro et al. 2012, Omran et al. 2014).

As per literature, the enrichment of low-grade iron ores require stringent processing/ beneficiation techniques which include carbothermal reduction roasting, ultrasonic radiation, colloidal magnetic coating and microwave treatment to achieve suitable concentrate for blast furnace feed (Rath et al. 2014; Sahoo et al. 2014; Singh et al. 2015; Rath et al. 2016; Ponomar 2017; Das et al. 2018). During conventional mining of hematite ores, there is a significant generation of low grade banded iron ores such as BHQ, BHJ, and BMQ which ends up in unused stockpile at the mine sites due to a lack of suitable beneficiation technology (IBM 2017, Rath et al. 2014). The iron bands in these ores are of hematite, magnetite and the silica bands are either quartz or reddish jasper and the thickness of the bands also varies from 0.5 to 1.5 cm. It is believed that the formation of these banded ores is either through replacement of silica by iron or by leaching of silica under suitable conditions or from the precipitation of iron from the Earth's ancient oceans (IBM 2017). Also, these ores possess quite different characteristics in terms of beneficiation primarily because of negligible content and excessive quartz content which makes them quite hard as compared to conventional hematite ores. The complex association of silica-iron phase i.e., soft-hard lamellae structure, and fine liberation size (<100 microns) prohibits the direct use of these low-grade iron ores in the steel production cycle. The iron content in these ores varies from 30-45% and the rest being siliceous impurities and is mainly found in the states of Karnataka, Orissa, Chattisgarh, and Rajasthan, India. The investigations on the beneficiation of banded iron ores (BHQ, BHJ, and BMQ) are limited and mainly involve processing techniques such as flotation, high-intensity magnetic separation, jigging and reduction roasting. At present some of the iron ore companies in India are evaluating these ores for setting up beneficiation plants to recover the iron value. The major difficulty in the upgradation of these ores includes the complex mineralogical association of quartz phase with hematite and very fine dispersion along with liberation size ~ 10μm (Rath et al. 2014, Das et al. 2010). The major difficulty in the

upgradation of these ores includes the complex mineralogical association of silica phase with hematite and very fine liberation size ~ 10μm (Das 2010; Sahoo 2016; Rath el. 2014). The jasper phase is very fine-grained and entrainment of hematite grains within jasper leads to liberation issues resulting in ineffective beneficiation even after fine grinding (Makhija et al. 2013). The carbothermal reduction involves roasting of the ore in a reducing environment at 500-700°C resulting in a partial reduction of hematite to magnetite followed by application of low-intensity magnetic separation (LIMS) to produce iron-rich magnetic product and tailings. The process suffers due to an associated energy penalty with roasting but offers advantages as magnetic separation is simpler and more selective than other separation techniques (e.g., floatation) along with reduced grinding costs due to the increased friability of the roasted ore, and improved settling and filtration characteristics of the ore due to dehydroxylation of clays during roasting (Iwasaki and Prasad 1989; Faris et al. 2017; Uwadiale 1992). In the reduction studies of low-grade iron ores, on an average 10-15% increment in grade with 50-70% Fe recovery is reported (Singh et al. 2015; Das et al. 2018). Recently, a BHJ ore (~47%Fe) is reduced (900 °C, 90 min, the coal-to-feed ratio of 0.15, coal size −3.35+1 mm and ore size −1 mm) yielded a concentrate of ~66% Fe with an iron recovery of ~72%. The siliceous tailings generated were further smelted in an arc furnace for the production of ferrosilicon alloy (Ray et al. 2018).

The absence of alumina in the BHJ/BHQ sample is highly advantageous and makes it more desirable for blast furnace ironmaking considering the ill effect of alumina on slag behavior. BHJ/BHQ ore resembles taconite ore processed in North America in terms of structure (bands) of iron phase and silica phase. However, the absence of the significant amount of magnetite phase in BHJ/BHQ makes it difficult to upgrade compared to conventional beneficiation of taconite ore. The application of microwaves on magnetite and taconite ore leads to selective thermal expansion resulting in less comminution energy and a cleaner mineral liberation thereby significantly improving the concentrate grade and metal recovery (Walkiewicz et al. 1991; Tavares and King1999). The unique applications of microwaves in extractive metallurgy processes include faster and controlled temperature ramp-up enhanced kinetics, rock disintegration, better liberation, and floatation, enhanced magnetic properties, improved drying and rheological properties along with better separation (Standish and Huang 1991; Kingman and Roason 2000; Ishizaka and Nagata 2008; Pickles 2009; Barani et al. 2011; Omran et al 2014; Hartlieb et al, 2016). It is known that sulfides and oxides respond very well to microwave radiations whereas gangue minerals such as silicates are week receptors to microwaves (Kingman and Roason 2000). Since BHJ/BHQ ore consists of iron oxide (hematite) and silica (quartz) an attempt is made to make use of selective heating of iron oxide with microwave irradiation. The

prime objective of microwave reduction is to selectively transform the hematite phase in the ore to magnetite followed by a low-intensity magnetic separator to obtain a suitable iron concentrate. The conversion of hematite to magnetite is not likely to be the limiting factor as reduction of ferric iron to ferrous iron is a fast process and the magnetizing roasting of oxidized iron ores has been carried out at temperatures as low as 350–400 °C using CO, H_2, and syngas (Fruehan 1977; Faris et al. 2017). The complete conversion of hematite to magnetite or metallic iron, the high coercitivity of the magnetic concentrate hampers its magnetic separation due to its due to the formation of very strongly magnetic phases (Youssef et al. 1998). It is also reported initial stage of reduction (Fe_2O_3-Fe_3O_4-Fe_xO) depends on carbon gasification, further stage (Fe_xO-Fe) of reduction depends on the wustite reduction which is considered as the rate-limiting step for the later stage of kinetics (Srinivasan et al. 1977).

However, it is worthwhile to mention that BHJ/BHQ ore consists of dual-phase i.e., alternate bands of hematite and jasper phase in bonded form. Therefore, it is expected that the reduction conditions will be quite different from the ideal thermodynamic conditions as reported by many researchers for hematite based samples (Iwasaki and Prasad 1989; Standish and Huang 1991; Ishizaki and Nagata 2008; Barani et al. 2011; Hayashi et al. 2013; Omran et al. 2014; Rath et al. 2016; Ponomar et al. 2017; Yu et al. 2017). Microwave reduction is highly non-isothermal process and bearing this in mind, the effect of reductant dosage, temperature, and microwave power on reduction was pursued. The previous studies do not emphasize the carbon requirement, underlying reduction mechanism and hence lack the systematic approach for the evolution of iron oxides during reduction. There are research works for up-gradation of low-grade iron ores but to the best of our knowledge, no systematic investigation employing microwave carbothermal reduction has been carried out on low-grade ore such as BHJ/BHQ ore.

Compared to the reduction of iron oxides in conventional heating, the solid-state reaction occurred at low temperatures and in a different sequence for the microwave irradiation reduction (Standish et al. 1991; Ishizaki et al. 2008; Hayashi et al. 2013). The microwave electromagnetic field selectively induces the magnetite dissociation which is a strong microwave absorbing material, to produce oxygen gas that can react with solid carbon, to produce CO and CO_2 gases. It is reported that as the fraction of carbonaceous material increases, the maximum temperature attained also increases, resulting in the higher reduction reaction rate (Standish et al. 1991; Hayashi et al. 2013; Mishra et al. 2016). Also, the main heat source of microwave heating is carbonaceous material rather than iron oxides. Also, it takes a longer time to initiate the hematite reduction than magnetite because of hematite is hardly heated from room temperature by microwave (Hayashi et al. 2013).

Microwave reduction is a highly non-isothermal process and considering this the effect of reductant dosage, temperature and microwave power on the reduction process was pursued. The previous studies do not emphasize the carbon requirement, underlying reduction mechanism and hence lack the systematic approach for the evolution of iron oxides during reduction. There are research works for up-gradation of low-grade iron ores but to the best of author's knowledge, no systematic investigation employing microwave carbothermal reduction has been carried out on BHJ/BHQ ore. The purpose of this research is, therefore, to find out optimal microwave conditions for the up-gradation of the typical Indian BHJ ore. It is expected that this study is likely to have an impact on the allied industries which are gearing up to utilize similar ore to meet the ever-increasing steel demand.

CHAPTER 3
MATERIALS AND METHODS

3.1 Characterization studies of BMQ, BHJ, and BHQ.

The banded iron ore samples are shown in Fig. 3.1 were procured from different mines from the states of Karnataka (BHQ and BHJ) and from (BMQ) Rajasthan, India. The as-received samples were visually inspected and identified several bands in lieu of thickness. The visible bands were maybe silica-rich or iron-rich phases. The photograph of the as-received samples as shown in Fig 3.2a reflects the banded structure of ores with varying band thickness. In each iron ore, the band thickness varies from 0.5 mm to 6 mm and sometimes can be viewed as thin and thick bands. The Mohr hardness of the sample is measured at approximately 7-7.5, 6-7 and 5-5.5 for BHJ, BHQ, and BMQ respectively. The optical micrograph of the feed samples shown in Fig. 3.1b indicates the dispersed and interlocked structure of hematite within the quartzite matrix and reflects the complex chemical association of iron oxide along with impurities. The chemical composition of these ores is shown in Table 3.1 indicates the iron values along with quartz as a significant impurity. Alumina is present in a very low percentage compared to silica which facilitates the processing of banded iron ores. The total iron content present in the feed based on wet chemical analysis is ~41% Fe, 37% Fe and 31% Fe in BMQ, BHJ, and BHQ respectively. The minimal alumina content in these ores makes it favorable for blast furnace ironmaking considering the ill effect of alumina on slag behavior. The Loss of Ignition (LOI) for each ore is calculated and is found approximately less than 2 wt. %. The X-ray diffraction spectra (XRD) analysis as shown in Fig. 3.2a indicates hematite and quartzite as major phases along with traces of magnetite phase in BHJ ore. The thermogravimetric analysis (TGA) shown in Fig. 3.2b reveals a weight loss (approximately 2-3%) between 350°C-800°C due to ore dehydroxylation. The major minerals identified through a light microscope and XRD analysis are Hematite and quartz along with micro/macro bands as shown in Fig. 3.1b.

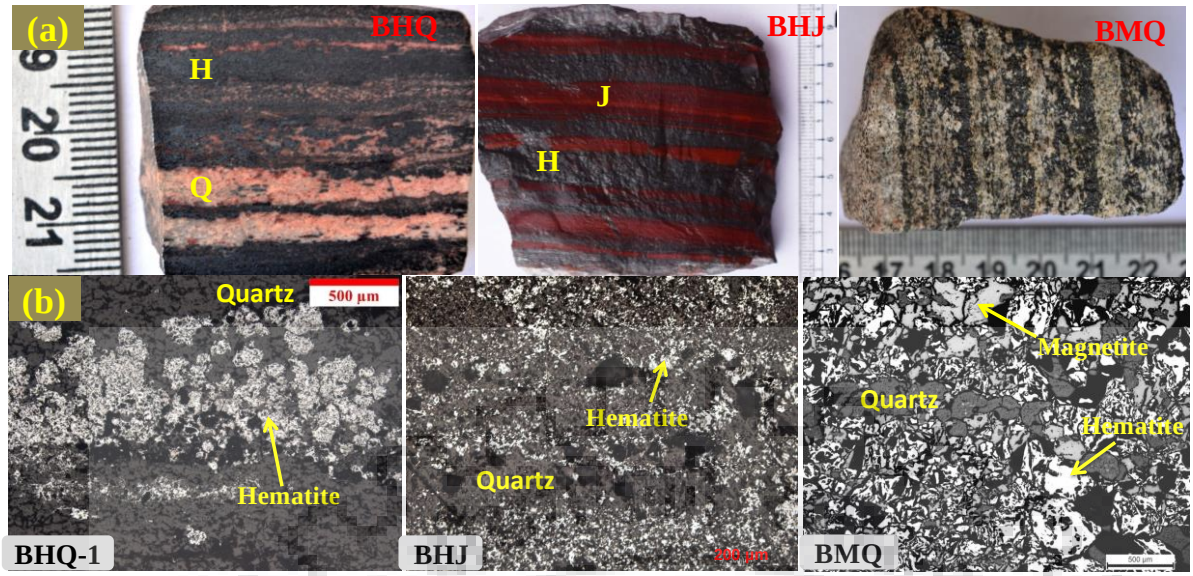

Figure 3.1 (a) Hand specimen photographs (b) Optical microscopy of feed sample (where H – Hematite, Q – Quartz, J – Jasper M-Magnetite)

Table 3.1 Wet-chemical analysis of different ores

	Weight (%)		
Constituent	BHQ	BHJ	BMQ
SiO_2	51.85	45.2	29.3
TiO_2	0.03	0.01	0.14
Al_2O_3	0.24	0.26	2.39
Fe_2O_3	44.37	51.8	43.1
FeO	1.71	1.9	14.3
MnO	0.06	0.06	4.5
MgO	0.06	0.01	1.5
CaO	0.04	0.02	2.1
Na_2O	0.09	0.05	0.26
K_2O	0.02	0.01	0.59
P_2O_5	0.08	0.06	0.35
LOI	0.45	0.62	1.52

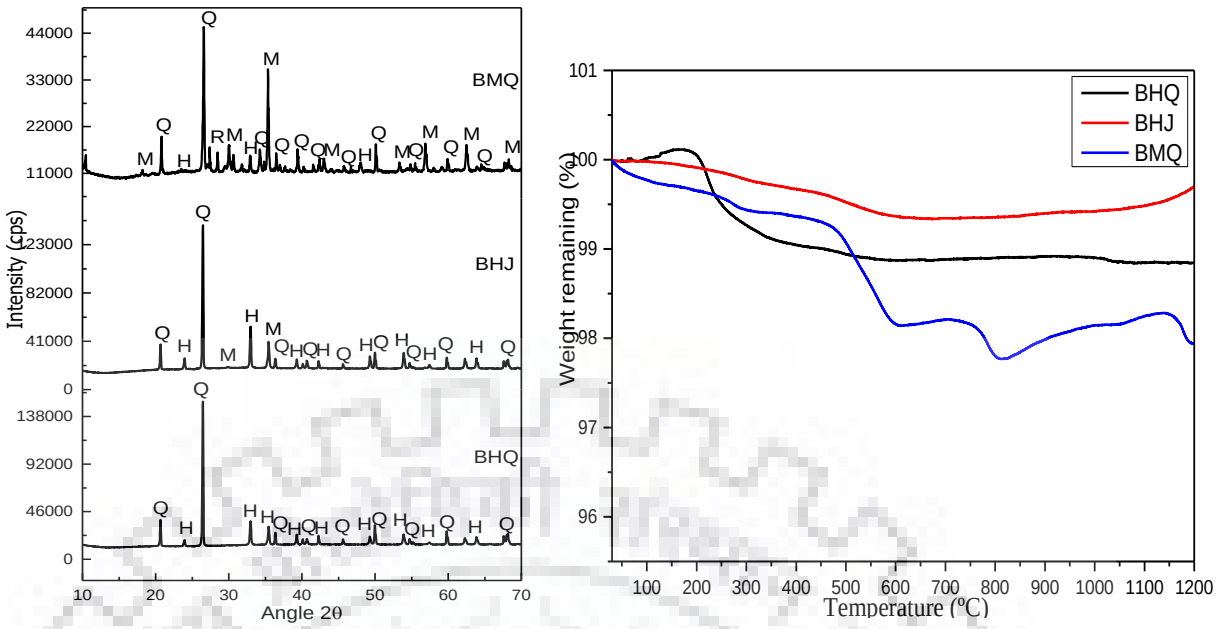

(a) (b)

Figure 3. 2 Characteristics of sample (a) XRD spectra (b) TGA curve

3. 2 Ore preparation (crushing, grinding and sieving)

The as-received ore was stage-wise crushed using primary jaw crusher, secondary jaw crusher and followed by roll crusher. The product was further sieved using sieve shaker to nominal feed size which is less than - 6.3×4.75 mm. The photographs of the primary and secondary and tertiary crushers and vibratory sieving test assembly are as shown in Fig. 3.3. The representative sample was prepared by using a standard lab-scale riffler.

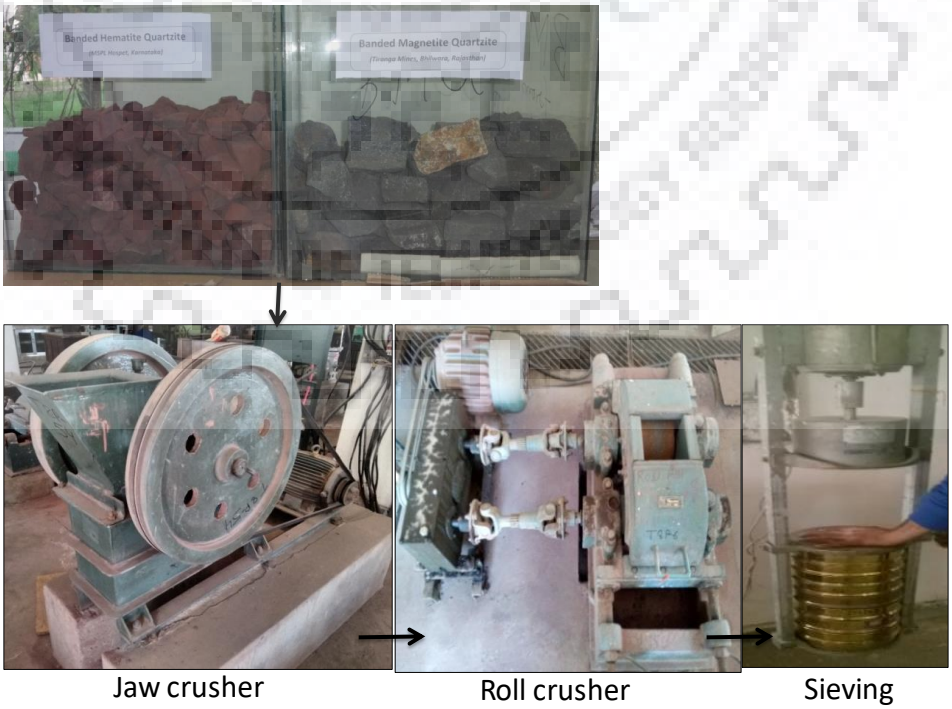

Figure 3.3 Photograph received sample and the size reduction mechanism

3.3 Comminution studies of banded iron:

3.3.1 Mono size preparation (Sieving):

The crushed sample was sieved to different mono sizes i.e., 6.30×4.75 mm, 4.75×3.30 mm, 3.30×2.38 mm and 2.38×1.41 mm for performing laboratory grinding experiments.

3.3.2 Grinding and compressing testing machine

It was envisaged that it is very important to conduct comminution studies with different breakage modes to evaluate the response of complex banded ores. In this context, the ores are subjected to impact-abrasion and compression mode testing using ball mills, and compression testing machine. These different breakage mode tests can provide energy requirement/signature of these ores in different scenarios and their behavior compared to conventional ores can be evaluated. Besides, ore specific breakage distribution function and selection function are delineated which are useful for scale-up to industrial-scale grinding if required. They are determined from the size distributions obtained by short-time grinding tests which are generally applied to one-size-fraction feeds.

3.3.2.1 The Breakage Rate (Selection) Function

Assuming first-order kinetics, the breakage rate is obtained by evaluating the slope of semi-log plots of the fraction retained versus time which generally shows a straight line.

$$\ln\big(R(t)\big) = -K_t t$$

where R_i is the cumulative fraction retained on the lower screen of the size interval *i*. Assuming that the breakage parameters for the coarsest fraction (B_{i1}, K_1) in the mill feed are determined, and assuming B_{ij} as normalizable, the K_2, K_3, …, K_{n-1} can be calculated by the use of a rearranged form of G-H solution given by Eq. (1-3).

$$K_t = \frac{-G_t - H_t - K_{i-1}B_{i,t-1}\frac{R_{i-1}(t)}{R_i(t)} + \sum_{j=1}^{i-2}(K_{j+1}B_{i,j+1} - K_j B_{i,j})\frac{R_j(t)}{R_i(t)}}{1 - \frac{R_{i-1}(t)}{R_i(t)}} \quad (1)$$

$$G_i = -K_i + \sum_{j=1}^{i-1}\frac{R_j(0)}{R_i(0)}(k_{j+1}B_{i,j+1} - k_j B_{i,j}) \quad (2)$$

$$H_i = -\sum_{j=1}^{i-1}\frac{R_j(0)}{R_i(0)}(k_{j+1}B_{i,j+1} - k_j B_{i,j})(G_j - G_i) \quad (3)$$

The selection function can be calculated as per Eq. (4)

$$S = \frac{a x_i^{\alpha}}{1 + (\frac{x_i}{\mu})^{\wedge}} \quad (4)$$

Where x_i is the upper limit of the particle size interval under consideration; the model parameters a and μ are mainly functions of the grinding conditions while α and Λ are material properties.

The first-order breakage law for a given material is shown in Fig. 3.4. The initial straight-line portion of the curve which shows the normal breakage behavior is the area where S has not passed through the maximum. The second portion, an area where S has passed the maximum, shows the abnormal breakage behavior. According to Griffith theory of breakage, this trend can be attributed to the fact that very fine particles are hard to break. This suggests that the breakage rate increases with increase in particle size. However, for too large particles that cannot be correctly nipped and fractured by the balls, therefore the rate of breakage steadily drops and tends to zero. The factors affecting the selection function are the mill diameter, mill speed, media load and size, and particle hold up. The specific rate of breakage increases steadily with a particle size which reflects the decreasing strength of the particles as size increases. This is attributed to the greater density of micro flaws in the interior of the larger particles and to the greater likelihood that a particular larger particle will contain a flaw that will initiate fracture under the prevailing stress conditions in a mill. As the particle size becomes significant by comparison to the size of the smallest media particles, the prevailing stress levels in the mill are insufficient to cause the fracture and the specific rate of breakage passes through a maximum and decreases with further increase in particle size. The parameter α is determined by taking the first linear region as a power function and calculating its slope.

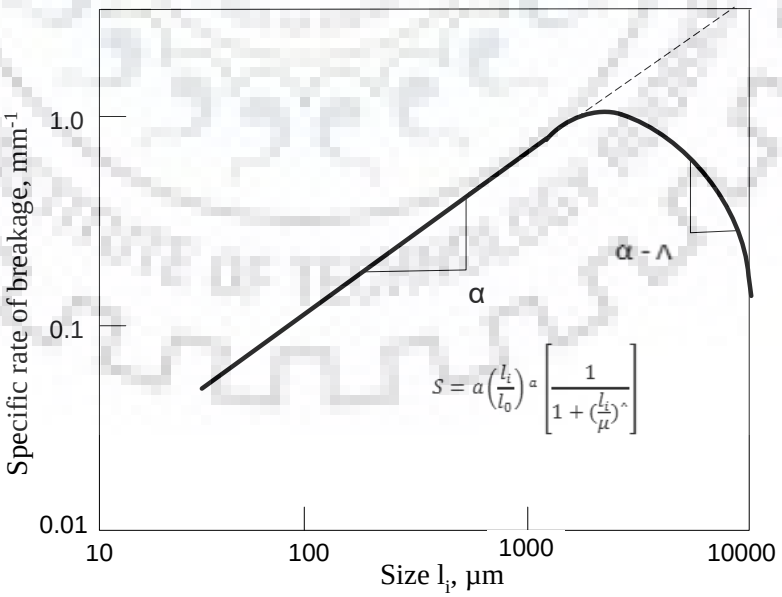

Figure 3.4 Standard First-order breakage law for a given material

3.3.2.2 *The Breakage Distribution Function*

There are many methods of estimating the breakage distribution function described in the literature which is based on non-linear optimization techniques and direct experimental schemes for measuring the feed size distribution parameters from short-time grinding of one-size-fraction feed (Kapur, 1982). Based on the nature of the terms in the right-hand-side of the Kapur's size-discretized batch grinding equation for a given ore and type of mill being used (Subasinghe et al., 2004). The B_{ij} estimation as shown in Eq. (5-8);

$$\frac{dR_i(t)}{dt} = -K_i R_i(t) + \sum_{j=1}^{i-1}[K_{j+1}B_{i,j+1} - k_j B_{i,j}]R_j(t) \quad \text{for i=1, 2, 3……..n} \quad 5$$

When the right-hand side of the equation is small it leads to a first-order relationship known as a linearized form of the batch grinding equation. This form of the batch grinding equation utilizes cumulative size basis rate of breakage without using breakage distribution function assuming compensation condition is valid. The advantage of this scheme is that the reasonable approximations can be achieved by utilizing a single parameter which implicitly represents the change in breakage rate and distribution functions.

$$R(x_i, t) = R(x_i, 0)\exp(z_t t^{P_i}) \quad 6$$

where, $R(x_i, t)$ and $R(x_i,t)$ are the mass retained of mineral m coarser than size i at time t and 0, respectively. Z_i is the rate of breakage of mineral coarser than size i. p_i is a function which corrects the equation for non-first order kinetics.

(Herbst and Fuerstenau 1968) assumed the right-hand-side of the equation to be constant for smaller sizes in the initial stages of grinding a coarse ore. This is called zero-order production of fines and used to estimate grinding characteristics such as breakage rate and distribution functions.

$$\frac{dY_i(t)}{dt} = F_i$$

Where $Y_i\ (t) = 1 - R_i(t)$ and F_i is the production rate of fines. A sufficient condition for this phenomenon to occur is $B_{ij}\ K_j = Fi$ for $j=1, \ldots, i-1$.

(Austin and Luckie, 1972) proposed three methods of estimating B_{ij}. BII is the one based on the solution of batch grinding equation given by the compensation condition and is claimed to correct for the secondary breakage.

$$B_{i,1} = \frac{Log[(1 - P_i(0))/(1 - P_i(t)]}{Log[(1 - P_2(0))/(1 - P_2(t)]}, \qquad i > 1 \quad 7$$

where $P_i$is the mass fraction of material in a certain size.

(Kapur, 1982) developed a method (G-H) for estimating breakage distribution functions;

$$\ln \frac{R_i(t)}{R_i(0)} = G_i.t.+.\frac{H_i}{2!}.t^2 + \frac{I_t t^3}{3!} + \cdots \quad (8)$$

where G_i, Hi, Ii, … are coefficients of the series expansion which were defined in the above equations. When a single sized feed is used then for all size fractions $R_i(0)$ = 1.0. In addition, if short grind times are used then the higher-order terms of the above equation may be neglected. The coefficients are related to the breakage rate of the top size and the cumulative breakage distribution function, i.e. for i = 2, 3, 4, …

A mathematical expression for obtaining B_{ij} which describes it as a sum of two components arising from impact and shatter breakage, respectively as shown in Eq. (9) (Klimpel and Austin, 1984);

$$B_{ij} = \emptyset \left(\frac{x_i}{x_j}\right)^{\gamma} + (1-\emptyset)\left(\frac{x_i}{x_j}\right)^{\beta} \quad (9)$$

Assuming B_{ij} to be normalizable and independent of grinding environment, the model parameters Φ, γ, β can be directly determined via single particle breakage tests such as drop weight and slow compression. However, this method cannot simulate the complex grinding environment within a tumbling mill. Instead, afore mentioned methods, Zero Order Production of Fines (Herbst and Fuerstenau, 1968), BII (Austin and Luckie, 1972) and G-H (Kapur, 1982), were compared and the most reliable one for the entire range of operating conditions was preferred for determination of B_{ij}.

In general, B_{ij} is considered to be normalizable with respect to size and independent of grinding environment in the population balance models. Therefore, all the variations on particle size distribution are attributed to the breakage rate function.

The present work focuses on lab-scale comminution studies using ball mill system photograph shown in Fig. 3.5 to determine energy signature of BHQ, BHJ, and BMQ. Breakage/distribution function was determined mono-size particles breakage in ball mill. To measure the patterns of energy utilization in particle bed mode of mono and natural sizes, these ores are broken in compression testing machine at different conditions and comparison studies are made with conventional ball mills. Finally, a relationship between the comminution energy and the resulting product size distribution can be examined for the ores tested.

The ore is subjected to impact-abrasion and compression mode using ball mill and compression testing setup as shown in Fig. 3.6. The grinding mill used (L×D, 11.5×10 inches) in this study is an instrumented lab scale ball mill with four equally spaced square lifters and is equipped with a variable frequency drive and torque-meter to record actual comminution power. A stainless steel

ball load of different sizes 1/2 inch to 1-1/2 inch weighing 20.7 kg corresponding to 30% filling and at 70% critical speed was used. The grinding experiments were performed in batch mode in both dry and wet condition for different mono-size samples. Similarly, for compression tests a predetermined amount of sample approx. 500 g was subjected to a dynamic load (1-10 kN/s) in a designed compression die set up and maximum load leading to actual work done was recorded with time. The photograph of the compression test set up is as shown in Fig. 3.7. The product is dry screened for 30 min and product size distribution is measured. Similarly, the sample was pre-treated in the microwave (~ 1 - 6 min) and conventional heating at 500 to 700°C for 30-60 min.

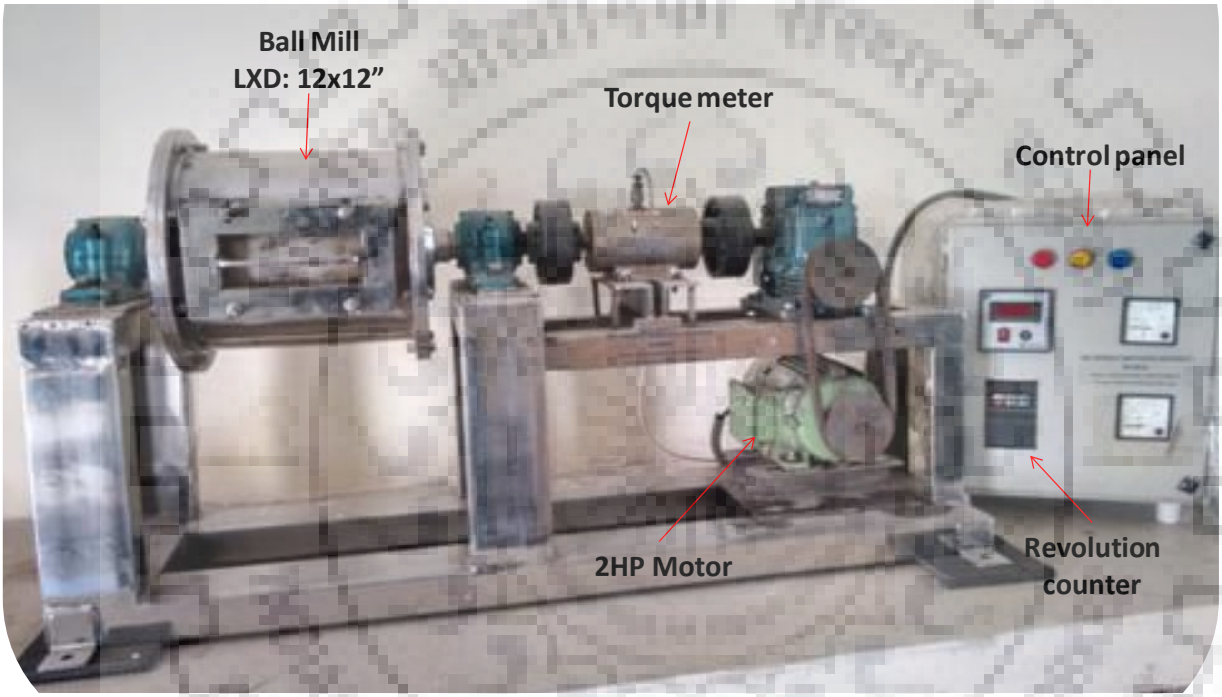

Figure 3.5 Photograph of a laboratory scale ball mill system

The mechanism inside the ball milling system as shown in Fig. 3.6, consisting of equally distributed different particle sizes and different ball sizes. The grinding efficiency or the output product was characterized by input feed parameters (flow rate, percentage of solids, and size distribution), dimension of the ball mill (length, diameter, and speed), liner profile design and corresponding material, grinding ball mill diameter, and the properties of ore (grindability, specific gravity, and composition) and product is mainly defined by its size distribution. The systematic experimental procedure followed in the present study is as shown in Fig. 3.8.

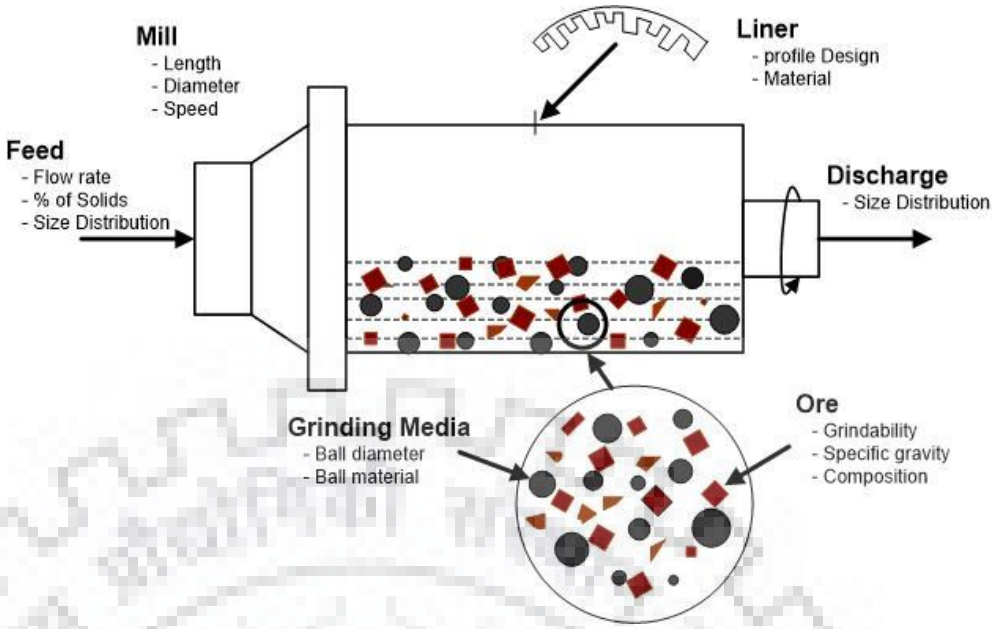

Figure 3.6 Breakage inside the ball mill by impact and compressive forces

Figure 3.7 Compression test setup

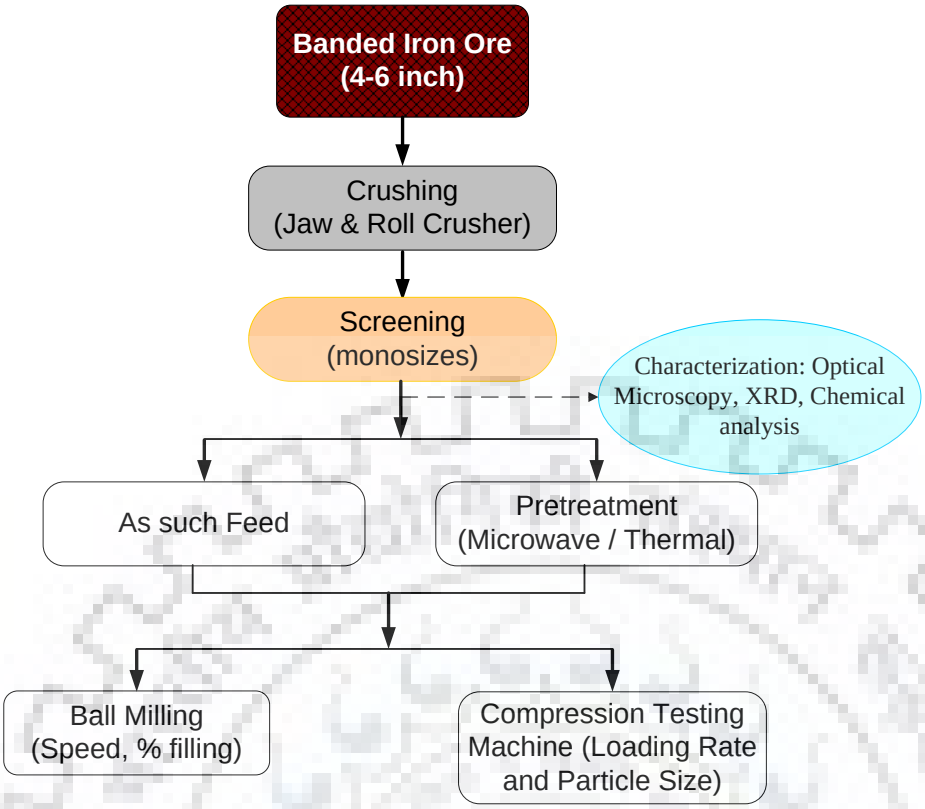

Figure 3.8 Experimental plan for comminution studies of iron ore

3.4 Beneficiation of banded iron ores

In part of the upgradation of banded iron ores, initially, the ores were a test though physical separation route to convert i.e., spiral separation (gravity separation) and magnetic separation.

3.4.1 Spiral concentrator (gravity separation)

Spiral concentrator separates the heavier mineral and lighter minerals based on their density difference. The concentrate purity depends mainly on the liberation size of the ore/sample. The concentrate purity controlled by the pulp density, the density of valuable minerals and the impurities and liberation size of the minerals. Feed size of minus 75 µm was maintained for the spiral concentrator. The spiral concentration is carried out in a laboratory spiral concentrator (INSMART make) consisting of seven turns with an outer diameter of 250 mm. The representative sample in slurry form is subjected to a laboratory-scale spiral concentrator (Insmart make) having seven turns with an outer diameter of 250 mm and is circulated in a closed-loop for 30 min. The heavier minerals (concentrate) were collected from the center and the lighter minerals (tailings) were collected from the outer area of the spiral concentrator. The concentrate and tailings were collected for equal time intervals and the concentrate obtained was recirculated several times to improve the purity.

3.4.1.1 Magnetic separation

The ore was subjected to magnetic separation (WHIMS, INSMART make) from 1000 to 16000 gauss. Initially the slurry, the powder ore sample: water ratio is maintained as 1:20 and thoroughly mixed before subjected to magnetic separation. The flow velocity of the slurry is maintained 0.6 L/min uniform throughout the experiment. The uniformly mixed slurry was poured through steel wool matrix placed in between magnetic rods. The magnetic rods are magnetized by 4 magnetic coils placed (two coils on each side). The feed ore size sample was maintained below minus 150 µm. The photographs of the wet high-intensity magnetic separator (WHIMS) and spiral concentrator are shown in Fig 3·9.

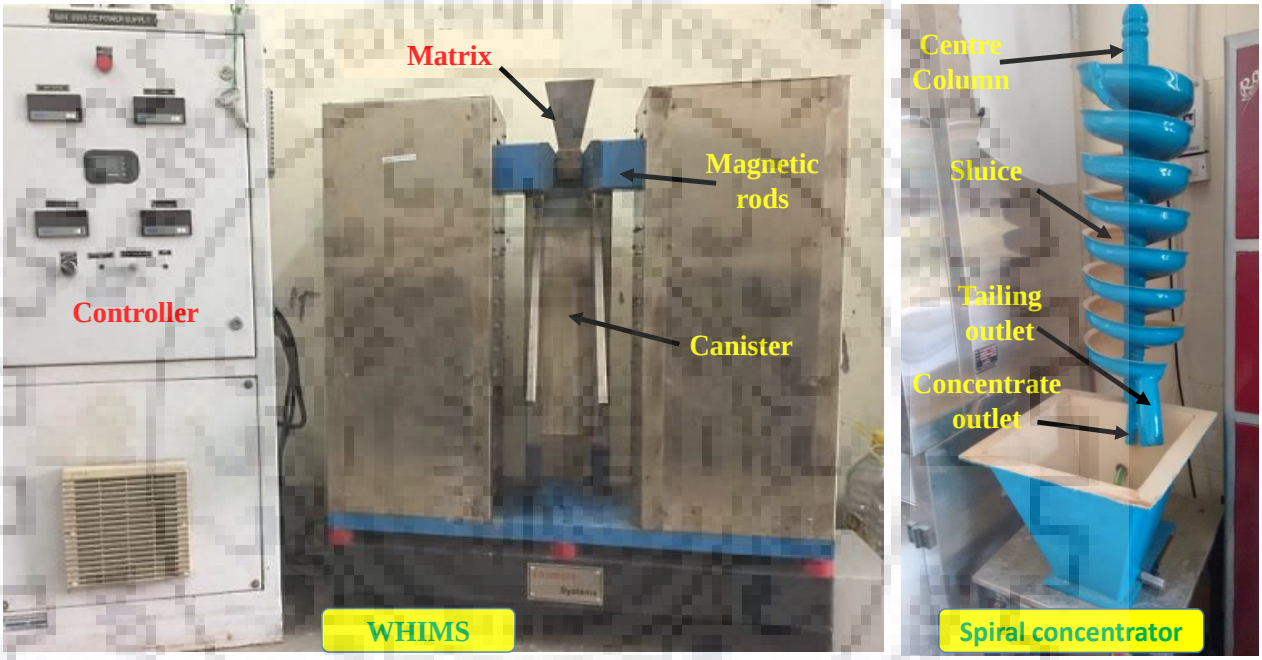

Figure 3.9 Photograph of the WHIMS and Spiral concentrator

3.4.2 Microwave exposure of banded iron ores:

3.4.2.1 Fundamentals of microwave

The complete microwave experimental setup is shown in Fig. 3. 10. A microwave is a form of non-ionizing electromagnetic radiation with a frequency higher than ordinary radio waves but lower than infrared light. It consists of electric and magnetic fields oriented perpendicular to each other. The electric field causes to heat the object by prompting rotation of polar molecules. The microwaves are generated from magnetron and pass to the object through the wave guide. Absorbing capacity of microwaves by the object, depends on the dielectric constant and dielectric loss of the object to heat. The higher the moisture content, the higher the microwave frequency and larger the particle size leading to an increase in depth of penetration of microwaves in the

object and temperature rise. The glass wool prevents the transfer of heat from the refractory crucible to glass plate.

3.4.2.2 Microwave exposure of banded magnetite quartzite ore

The experimental route adopted in this work is shown in Fig. 3. 11a. the sample was exposed to microwave irradiation at pre-determined parameters of time and power. The optimization of different factors was pursued using a Box-Behnken statistical design. All the experiments were carried out in a 28L microwave (LG make, maximum power 900 W) having cavity dimensions as (510 w x 305 h x 495 d mm) with a batch sample size of 25 g. The refractory grade crucible was kept in the center position for all the experiments to negate the effect of the microwave field pattern variation. The temperature attained during the experiment was immediately recorded at the end using an Infrared thermocouple (Extech make). It is important to mention that temperature measurement is of significant concern in the microwave process as a contact type internal thermocouple (metal-based) can also interact with microwaves. The microwave treated sample was immediately quenched in water, pulverized and subsequently subjected to magnetic separation at 1000 Gauss for all the experiments. The quantitative analysis of iron values present in the magnetic concentrate was determined using standard titration procedure, whereas, the phase analysis was studied using XRD. The microwave exposure of BMQ leads to produce promising results, so the similar process was applied on BHJ also.

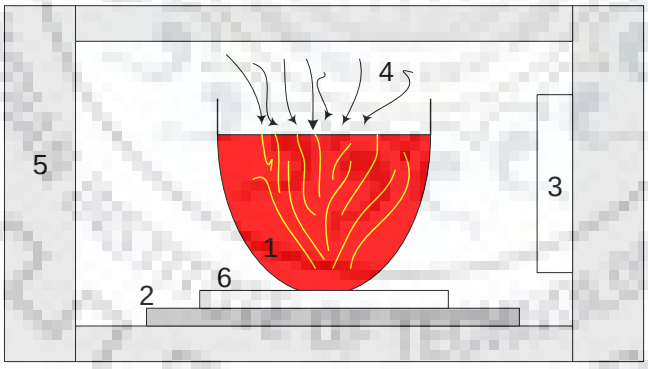

1. Refractory crucible, 2. Base, 3. Magnetron, 4. Microwaves, and 5. Domestic microwave, 6. Glass wool

Figure 3.10 Schematic microwave experimental setup

3.4.2.3 Microwave exposure of banded hematite jasper ore

The experimental procedure followed in the study is shown in Fig. 3. 11b. The route A incorporates conventional physical beneficiation techniques i.e., Wet High-Intensity Magnetic Separation and spiral concentrator. Route B involves microwave exposure of the feed sample followed by Low-Intensity Magnetic separation (LIMS). Route B involves microwave exposure

from 2 to 14 min and the effect of particle size was also investigated using two sizes i.e., coarse; 4.75x3.35 mm and fines; denoting minus 75 microns. It is also important to mention that the microwave treated coarser particles are subjected to grinding and pulverization to reduce the particle size below defined value i.e., 75 microns. The route C involves WHIMS and further, the obtained magnetic fraction is subjected to microwave exposure followed by LIMS respectively. The temperature attained during the microwave exposure is recorded instantly at the end of an experiment using a K-type thermocouple (Extech make). It is important to mention that the temperature measured is on the lower side of the actual experimental temperature because it is measured at the end of the experiment. Next, the microwave exposed sample was water quenched and pulverized in a mortar-pestle below 75 microns and subsequently magnetically separated at 1800 gauss. To enhance further Fe grade (%), Fe recovery (%) and yield (%) in BHJ and BHQ, carbothermal reduction using carbon reductant is attempted.

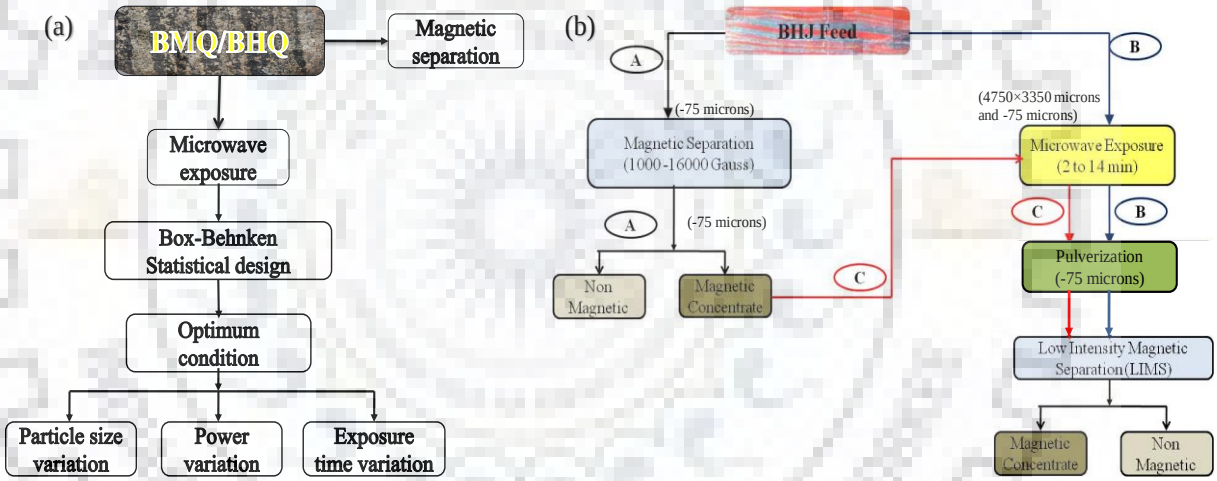

Figure 3.11a Experimental procedure followed in the study (a) BMQ, (b) BHJ

3.4.3 Thermodynamic considerations

As shown in Fig. 3.12, the thermodynamics calculations (FactSage software) employing Gibbs free energy of reduction of oxides and temperature revealed that iron oxide can be reduced to Fe at 700°C, whereas, the other oxides such as Al_2O_3 and SiO_2 cannot be reduced below 1450 °C (Han et al. 2015; Hu et al. 2018). In summary, the reduction is dominated by the direct reduction (with solid carbon) at the initial stage of reduction and is finally determined by the indirect reduction (gaseous CO/CO_2) together with the carbon solution loss reaction. It is generally accepted that the main reduction occurs through the gaseous intermediates CO and CO_2. The initial formation of carbon monoxide is an important step in the overall reaction and can be produced by reaction of solid carbon with oxygen of the entrapped air, reaction of solid carbon

with oxygen gas released by the dissociation of the iron oxide and by direct reduction occurring at the points of contact between the carbon and the iron oxide particles. The reduction is terminated if one or both of the gaseous intermediates (CO/CO_2) become unavailable to the solid reactants. The interfacial chemical reaction involving oxide and carbon is presumed to occur relatively rapidly compared to the diffusion process. The extent of direct reduction is considerable beyond 900°C and that diffusion of iron ions within the oxide crystal, rather than the diffusion of carbon atoms into the iron oxide is the rate-determining stop in the reaction of ferric oxides (Fruehan, 1977; Standish and Huang, 1991; Mishra and Roy, 2016; Iwasaki and Prasad, 1989).

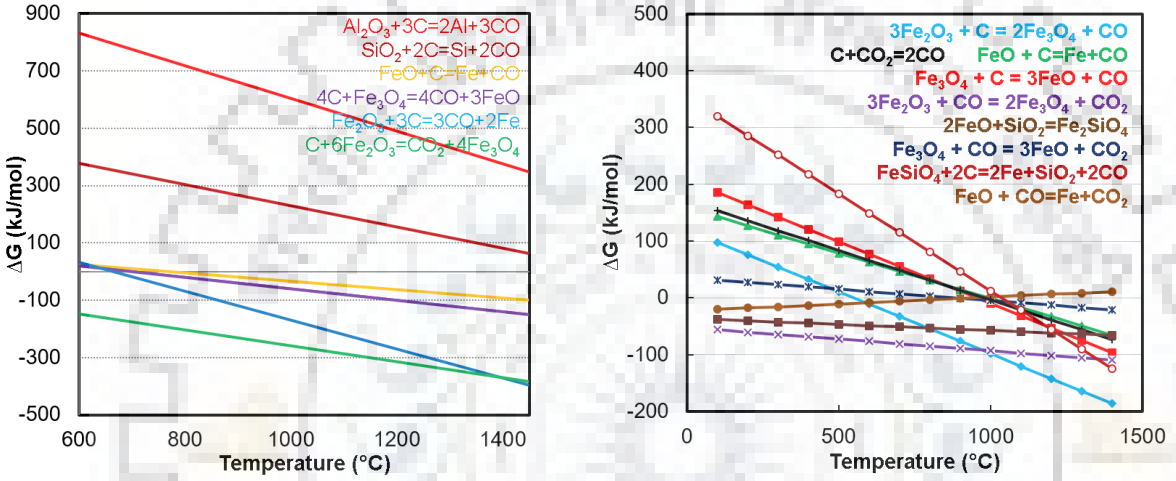

(a) (b)

Figure 3.12 Changes of Gibbs free energy with the temperature at 1 atm for (a) different oxides in the ore (b) iron oxides

Compared to the reduction of iron oxides in conventional heating, the solid-state reaction took place at low temperatures for the microwave irradiation reduction along with different chemical reactions pattern (Standish and Huang, 1991; Ishizaki and Nagata, 2008; Hayashi et al., 2013). The microwave electromagnetic field induces the magnetite dissociation which is a highly microwave absorbing material, to produce oxygen gas that can react with solid carbon, another microwave absorbing the material, to produce CO and CO_2 gases. The microwave absorbing the power of magnetite finishes at about 650°C and its reduction to wustite is accomplished below this temperature. The main heat source of microwave heating is carbonaceous material rather than iron oxides. It takes a longer time to initiate the hematite reduction than magnetite because hematite is hardly heated from room temperature by microwave (Hayashi et al., 2013). The different underlying reduction reactions possible in Fe-O-C-Si system are listed in Table 3.2 (Vandenberg and Dippenaar, 1989; Ishizaki and Nagata, 2008; Han et al., 2015; Lei et al., 2017; Hu et al., 2018).

Table 3.2 Different underlying chemical reactions in Fe-O-C-Si system

Chemical reactions	Change in Gibbs free change (J/mol.)	Eq. No
$3Fe_2O_3 + C = 2Fe_3O_4 + CO$	$\Delta rG_m^\theta = 120000 - 218.46T$	(10)
$Fe_3O_4 + C = 3FeO + CO$	$\Delta rG_m^\theta = 207510 - 217.62T$	(11)
$FeO + C = Fe + CO$	$\Delta rG_m^\theta = 158970 - 160.25T$	(12)
$3Fe_2O_3 + CO = 2Fe_3O_4 + CO_2$	$\Delta rG_m^\theta = -52131 - 41T$	(13)
$Fe_3O_4 + CO = 3FeO + CO_2$	$\Delta rG_m^\theta = 35380 - 40.16T$	(14)
$FeO + CO = Fe + CO_2$	$\Delta rG_m^\theta = -22800 + 24.26T$	(15)
$2FeO + SiO_2 = Fe_2SiO_4$	$\Delta rG_m^\theta = -36200 - 21.09T$	(16)
$FeSiO_4 + 2C = 2Fe + SiO_2 + 2CO$	$\Delta rG_m^\theta = 354140 - 341.59T$	(17)
$C + CO_2 = 2CO$	$\Delta rG_m^\theta = 170700 - 174.5T$	(18)
$2Fe_3O_4 + 3SiO_2 = 3Fe_2SiO_4 + O_2(g)$	$\Delta rG_m^\theta = 471750 - 160.06T$	(19)

3.4.4 Carbothermal reduction of banded iron ores

The carbothermal reduction was conducted for banded iron ores for the conventional route (thermal reduction) and microwave route. Charcoal and other alternative reductants (coconut shell, groundnut shell, cow dung, and goat dung) were used reductants in carbothermal reduction. The chemical analysis and corresponding calorific value of the reductants are shown in Table 3.3.

Table 3.3 Chemical analysis and calorific value of different reductants used

Reductant	**N (%)**	**C (%)**	**H (%)**	**S (%)**	**Calorific value (cal/g)**
Activated Charcoal	0.7	79.66	2.06	0.44	19694.26
Coconut shell	0.01	48.54	5.82	0	8754.93
Groundnut shell	1.25	44.15	5.5	0.32	14406.76
Cow dung	1.65	30.94	4.29	0.34	7777.6
Goat dung	2.46	33.85	4.49	0.61	10176.81

For safety purpose and to delineate the time-temperature plot for different sizes, the preliminary experiments were conducted in a microwave furnace fitted with a K-type thermocouple (Enerzi make, max power 800 W). The time-temperature plot is as shown in Fig. 3.13.

It can be seen that during microwave exposure, the temperature of ~ 400°C is achieved in 12 min and ~ 1100 °C in the presence of a sufficient amount of carbon. The heating rate initially increases

followed by the maximum rate in the middle which subsequently decreases and finally, the temperature saturates. The variation in the heating rate can be attributed to the phase transformation undergoing during microwave irradiation. Carbon is excellent microwave absorber which leads to an initial increase in the heating rate and is confirmed by different heating rates of feed and mixture samples. As the temperature increases, the carbon reduces the hematite phase and converts it into a highly magnetic magnetite phase. The formation of magnetite leads to increased absorption of microwaves which consequently leads to a higher heating rate. As soon as the carbon in the system exhausts and the magnetite transforms into less susceptible iron phases like wustite and fayalite, the heating rate decreases and temperature eventually saturates. The average heating rate during microwave reduction is approximately 85 °C/ min compared to 20 °C/ min in a muffle furnace. On the comparison between the temperature variation in the mixture of ore and carbon at different weight percentage, it can be clearly seen that the heating rate is significantly faster in 11% C due to the transformation of hematite phase in relatively shorter time duration. It can be concluded that the charcoal dosage is the dominant factor for microwave reduction. Based on the time-temperature plot, two zones of varying heating rate were sought around 6 min and 10 min. Also, it is known that the free energies of the different iron phases varies with temperature and is a function of temperature and with the slower cooling rate the probability of phase conversion is high. Therefore, the experiments were conducted for 6 and 10 min at a varying charcoal dosage of 6 to 11% at maximum 900 W power. On the other hand, the temperature of the mixed powder starts to increase abruptly at around 400°C and is considered to be due to thermal runaway of Fe_2O_3.

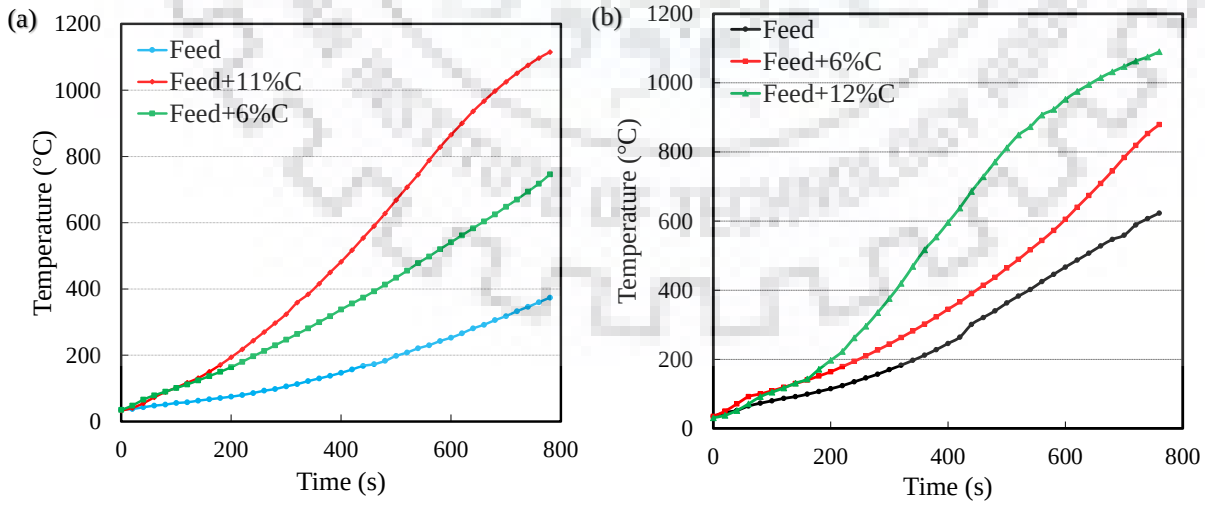

Figure 3.13 Time-temperature plot for the feed and mixture during microwave exposure at 800 W for (a) BHJ and (b) BHQ.

The carbothermal reduction experiments were carried out in a muffle furnace (Carbolite make, CWF 1200) and microwave oven unit (LG make; 900 watts, 2.45 GHz) using activated charcoal as a reductant. The schematic photographs of the muffle furnace, microwave, and microwave furnace used shown in Fig. 3.14. The proximate and ultimate analysis of the charcoal consists of fixed carbon (88%), volatile matter (10.1%), ash (1.1%) and moisture (0.4%) and carbon 79.66%, hydrogen 2%, nitrogen 0.7% and sulphur 0.4 %. The conversion of the hematite phase to the ferrite phase takes place sequentially and the intermediate reduced phases are formed by the chemical reactions stated in Eq. (1) - (4). The stoichiometric carbon required for complete reduction of hematite to metallic iron is calculated as ~5.05 %, 5.55 % and ~6.03 % BHQ and BHJ respectively as per Eq. (5). The grade, yield and iron recovery of the magnetic concentrate is determined using Eq. (20-26) where Fe_{grade} magnetic is iron percentage obtained in magnetic fraction and weight corresponds to respective weight in the fraction.

Figure 3.14 The equipment used for carbothermal reduction

$$3Fe_2O_{3(s)} + 2C_{(s)} + O_{2(g)} \rightarrow 2Fe_3O_{4(s)} + CO_{(g)} + CO_{2(g)} \quad (20)$$

$$Fe_3O_{4(s)} + 2CO_{(g)} + O_{2(g)} \rightarrow 3FeO_{(s)} + 2CO_{2(g)} \quad (21)$$

$$3FeO + 1/2O_{2(g)} \rightarrow 2Fe_3O_{4(s)} \quad (22)$$

$$FeO + 2CO_{(g)} + O_{2(g)} \rightarrow Fe_{(s)} + 2CO_{2(g)} \quad (23)$$

$$Fe_2O_{3(s)} + 3C_{(s)} + \tfrac{1}{2}O_{2(g)} \rightarrow 2Fe_{(s)} + 2CO_{(g)} + CO_{2(g)} \quad (24)$$

$$Fe_{Recovery}\ (\%) = \frac{(Fe_{Grade} \times Weight)_{magnetic}}{(Fe_{Grade} \times Weight)_{feed}} \times 100 \quad (25)$$

$$\text{Yield } (\%) = \frac{\text{Weight}_{\text{magnetic}}}{\text{Weight}_{\text{Total}}} \text{ X } 100 \quad (26)$$

The carbothermal reduction carried out in the microwave is non-isothermal and the temperature attained is measured using a K-type thermocouple immediately after the experiment (Extech

make). The reduced product is water quenched to prevent the re-oxidation of the reduced phases. The reductant dosage was extended up to two times of stoichiometric value as the feed contains approximately ~50% SiO_2 values.

The preliminary experiments were conducted at 900 W, 10 min and 6-12% charcoal to investigate conditions for ferrite formation. For all the ores, within ~10 min, a continuous sharp blue colour flame was observed due to rapid burning of ore and charcoal mixture. The optimization was performed by using statistical designed experiments in ma uffle furnace and microwave reduction. The reduced product and separated ferrite balls/fused iron were polished as per metallurgical standards to identify the structure using optical microscopy (Leica make, 5000M model). The systematic experimental procedure followed for the up-gradation of banded iron ores is shown in Fig. 3.15.

3.5 Tools used for characterization studies

The concentrate obtained through low-intensity magnetic separation process was analyzed by X-ray diffractometer (XRD, Rigaku, Smart Lab) by using Cu-Kα radiation at a step size of 0.02° and scanning rate of 2°/minute to identify the different phases. The different phases present and their association were studied using reflected light microscopy (Leica make). The morphology and elemental analysis were carried out using a Scanning electron microscope (SEM) attached with energy dispersive X-ray spectrometer (EDS). The thermal response of the feed and charcoal mixture was studied by using thermo-gravimetric analysis (TGA) using air as carrier gas at 0.2L/min, 10°/min up to 1200°C to identify weight loss occurs due to dehydroxylation. The morphology and structure of the fussed iron/Ferrite balls formed during carbothermal reduction were studied using optical microscopy (Leica, make, 5000M). The change in the magnetic characteristic of the sample was studied at room temperature using a vibratory sample magnetometer (VSM) in the form of a hysteresis loop.

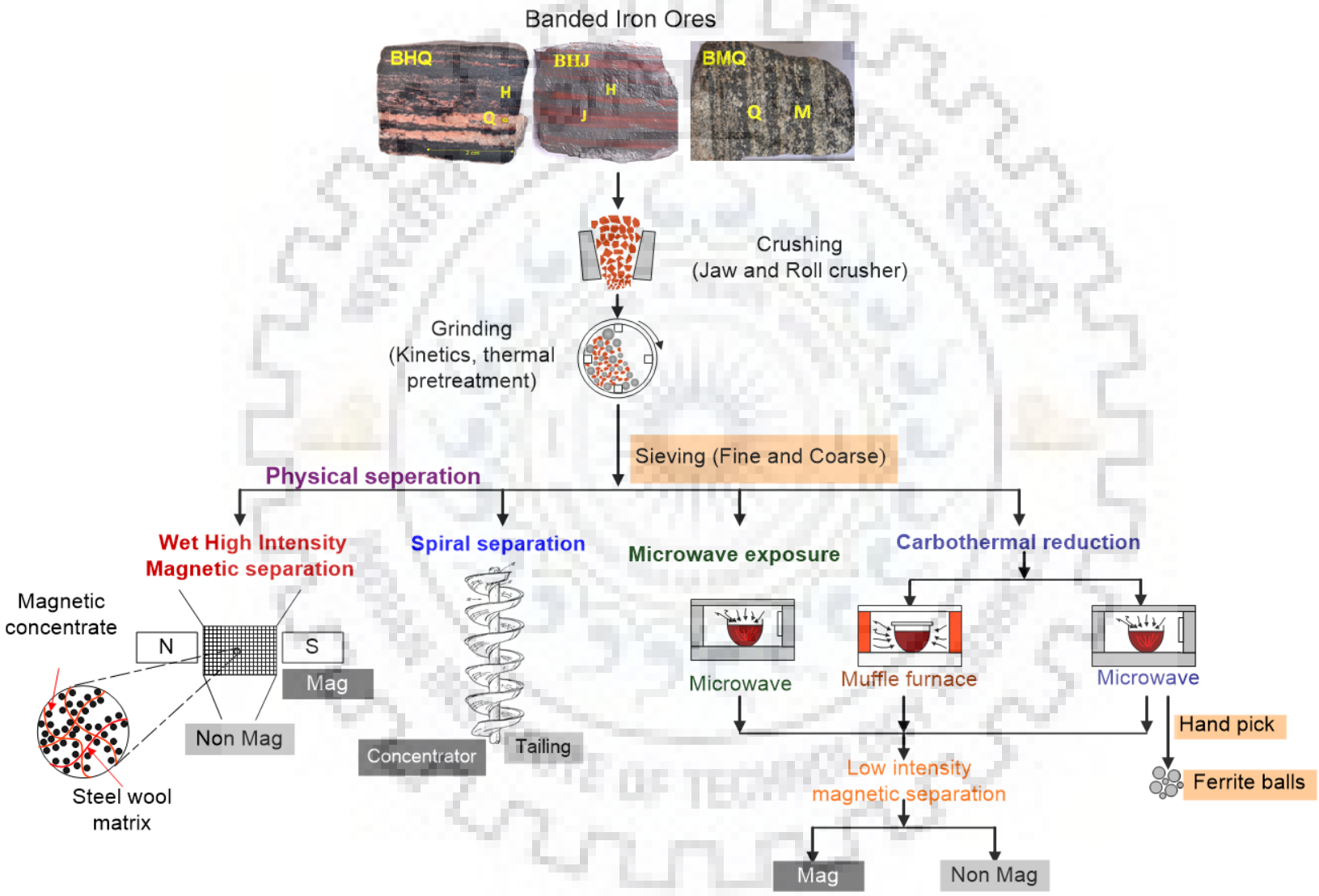

Figure 3.15 The experimental procedure followed

CHAPTER 4
RESULTS AND DISCUSSION

4.1 Comminution studies of banded iron ores

4.1.1 Particle size distribution and selection function studies

The comminution studies of banded iron ores aim in the development of comminution parameters, evaluation of breakage modes and energy signature of complex banded iron ores for determining the ore specific breakage characteristics. Using this information, it is possible to find out the optimum comminution conditions for banded iron ores. To measure the patterns of energy utilization in single-particle breakage, mono-size of banded iron ores were ground in compression testing machine and ball mills. At first, the ball mill grinding experiments were carried in different mills (L×D) to evaluate the rate of grinding (Selection function) and progeny size distribution (breakage function) with corresponding product size distribution. The ball mill grinding process was optimized in terms of ball size, ball filling and grinding time. Next, the grinding was carried out in an instrumented ball mill to record torque values which were further used to calculate comminution power and specific energy (kWh/t). Also, pre-treatment techniques such as thermal treatment and microwave treatment were applied since they can cause a phase change of quartz around 600ºC. As expected, in pre-treated samples (thermal and microwave), random massive micro-cracks were observed. In both pre-treatments, there is no phase change involved in the sample. However, surprisingly in pretreated samples a lot of cracks was observed as compared to the feed sample as shown in Fig. 4.1.1. The heat treatment produces a significant reduction in fracture energy even at moderate temperature because of the superficial cracks induced that offer sites for crack propagation leading to fracture, particularly in brittle solids. If the hot material is rapidly quenched, the internal stresses produce intense micro-cracking and fracture occurs easily during comminution which may reduce the grinding energy. The α-β quartz inversion at 573°C causes a volume growth of 0.86% and causes internal stresses to build up throughout the structure (which causes stress concentrations, and microscopic cracks), and at grain boundaries (Tavares & King 2005). Similarly, microwave pretreated ores show a differential heating due to the different dielectric properties of the various phases present in the ore body. This differential heating leads to fracture along the grain boundary and reduce the bond work index of the material. It is expected that the cracks showed in Fig. 4.1.1 will affect the grinding characteristics of the ore sample.

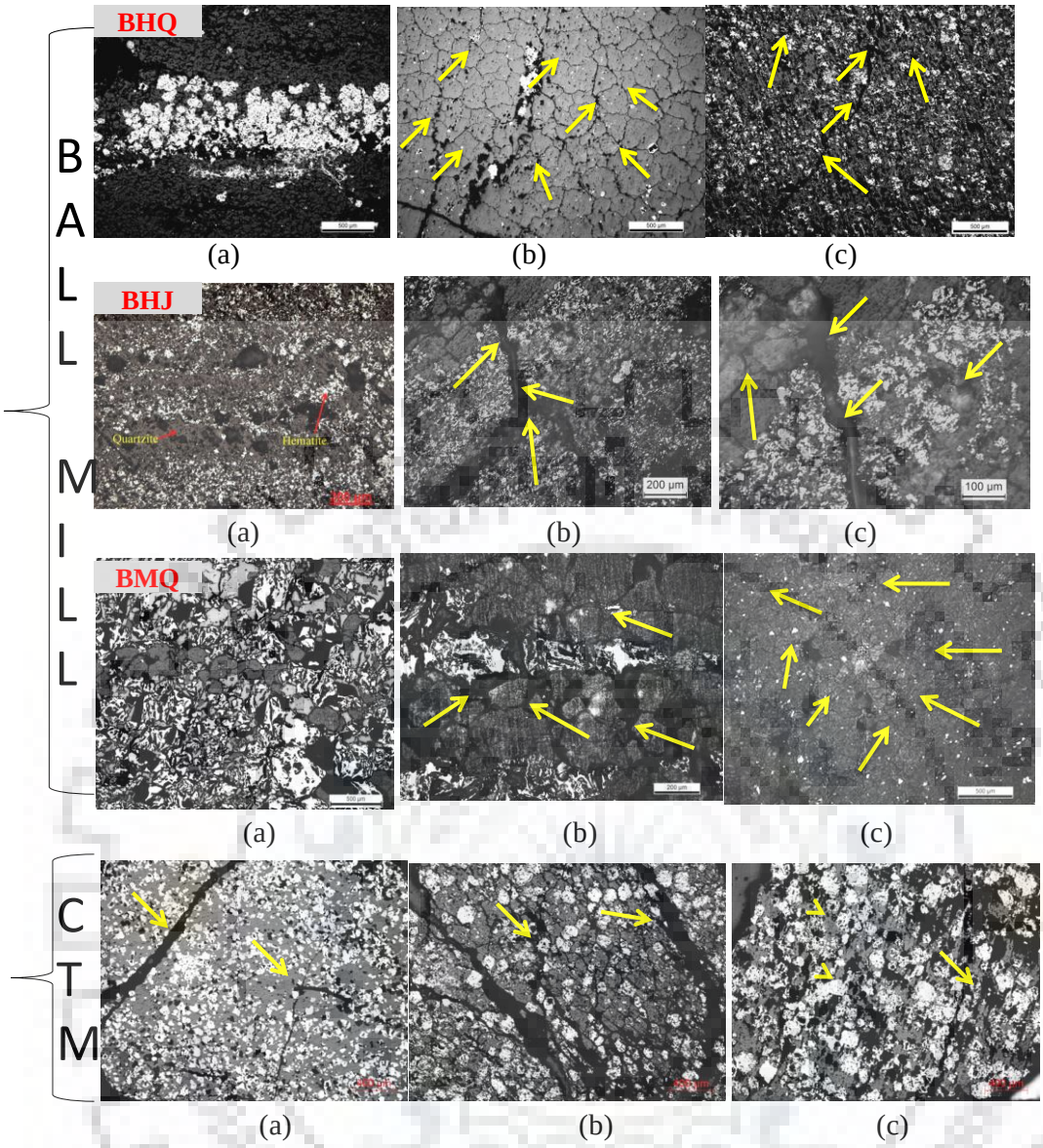

Figure 4.1.1 Optical microscopic images showing cracks (a) Feed (b) muffle furnace exposed (700°C, 60 min) and (c) microwave exposed (900 W, 6 min)

4.1.1 Particle size distribution

Four mono-sizes (6.3×4.75, 4.75×3.35, 3.35×2.38, 2. 38×1.41 mm) of BHQ and BHJ were placed in a microwave for different time intervals to evaluate their microwave response. All the samples corresponding to different sizes were tested batch-wise for 6 min and process temperature was recorded using a K-type infrared temperature sensor. As shown in Fig. 4.1.2, the coarser particle sizes attained higher temperature compared to smaller particle size. This can be attributed to the fact that the microwave treatment effect is pronounced in coarse sizes due to more cracks, whereas, for medium-fine sizes, flaws are depleted leading to minimal microwave effect.

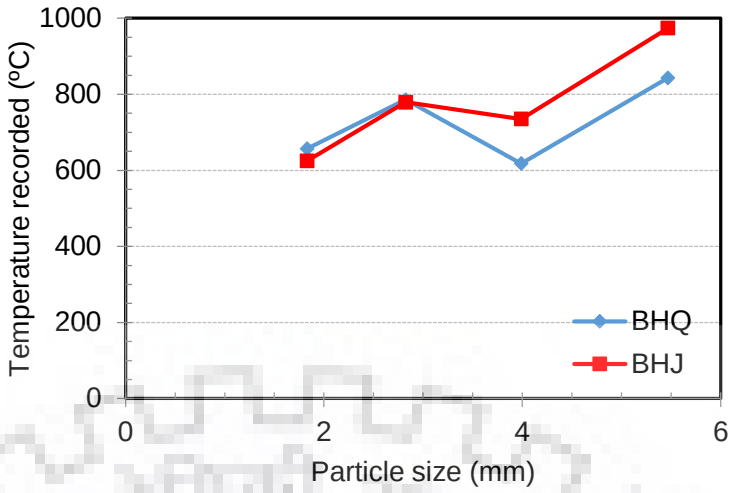

Fig 4.1.2 Temperature attained during microwave pretreatment for different particle

Considering both pretreatments showed promising results in terms of micro-crack generation and significant temperature attained in the microwave, the feed, the pretreated thermal-microwave feed was subjected to ball milling grinding for 1, 2, 4 and 8 min in batch mode. Dry grinding systems have breakage kinetics absolutely linear in nature, thereby indicating that the feed size selection function (S_1) is independent of time and can be evaluated as shown in the Eq. (27).

Selection function,

$$S_1(t) = -\frac{d}{dt}\left[ln\left(\frac{m(t)}{m(0)}\right)\right] \quad (27)$$

Batch grinding operations have been modeled as a first-order kinetic process by employing two parameters; breakage rate parameters (or selection functions) S_i, and the breakage distribution function (*Bij*). The breakage rate functions describe the probability of breakage of particles of different sizes and have units of 1/time. The dimensionless breakage distribution parameters quantify the mass fraction of the breakage product of a given particle size reporting into finer sizes. These parameters play a vital role in predicting the evolution of the entire particle size distribution in a grinding environment, and a knowledge of their true values is essential for simulation, scale-up, control and optimization of grinding processes. They are determined from the size distributions obtained by short-time grinding tests which are generally applied to one-size-fraction feeds (Fuerstenau et al., 2004).

Breakage function is described as the average size distribution resulting from the fracture of a single particle. It is considered as insensitive to most of the parameters including particle size. Assuming first-order kinetics, the breakage rate is obtained by evaluating the slope of semi-log plots of the fraction retained versus time which generally shows a straight line. It is found that

the breakage kinetics is linear, that is the feed size selection function (S-j) is independent of the extent of grind time. Selection function was determined through Herbst and Fuerstenau zero-order method, whereas, breakage functions was evolved through Kapur G-H method.

The results for all the ores at different time intervals using zero-order method are shown in Fig. 4.1.3. Direct experimental schemes for measuring the feed size distribution parameters from short-time grinding of one-size-fraction feed is quite common. Short-time grinding tests were performed for the evaluation of grinding kinetics of BMQ ore sample as shown in Fig. 4.1.4. The ball charge and the feed were put into the mill layer by layer. The grinding times were set as 15, 30, 45, 60, 90, 120, 150 s, cumulatively. After each cycle, wet and dry sieve analyses were performed with representative samples. Then, the samples were added to the ground mill content was again put into the mill layer by layer for further short-time grinding. The procedure was repeated until 75 s of grinding achieved. The obtained size distribution data were evaluated for the determination of breakage parameters using Kapur's G-H method. Different alternatives for effective comminution were tried to reduce the energy requirements for comminution as shown in Fig. 4.1.5. To avoid errors due to particle size distribution, the grinding was carried using mono size fraction (2×1mm, 3.35×2 mm), 4 min grinding time, equilibrium ball size distribution and constant percent mill filling as shown in Fig. 4.1.4. For the sake of brevity, only typical experimental results are shown. For microwave grinding the ore was kept in the microwave for 0.5-6 min and was quenched immediately followed by grinding in ball mill. For thermal pre-treatment, the ore sample was kept in the furnace at 700-950 °C for 30 min. The natural ground sample refers to conventional grinding i.e., with balls in slurry form. The results for both particle sizes 2×1 mm and 3.35×2 mm for alternative comminution are shown in Fig. 4. 1.5. It can be inferred from that thermal treatment is better than natural, and microwave ground products.
Also, it was interesting to see the evolution of selection function both for natural/untreated and thermal grinding at constant ball mill conditions. As expected the rate of breakage or selection function was almost twice i.e., 0.41 min^{-1} compared to 0.24 min^{-1} for natural/untreated grinding. Another way to see the effect was to trace out the product size P_{80} as a function of time. At all-time intervals in can be seen that thermal grinding is better than natural grinding as it yields lower 80% passing values as shown in Fig 4.1.5f.
Once it was determined that thermal treatment is working, the temperature was varied to find the best temperature condition corresponding to grinding performance. As shown in Fig.4.1.4 the reduction ratio is almost constant up to 550 °C and beyond that, it increases sharply. Next, the effect of particle size in thermal treatment was studied. It is evident that the effect of thermal

treatment-quenching is highest in coarse particles and it decreases sharply with a reduction in size. It is important to mention that in case of natural or untreated grinding, coarse particles are easier to break compared to small sizes. This can be explained on the fact that the cracks or defects present in brittle materials such as rock are abundantly present in coarser sizes. Under the application of higher temperature followed by quenching, these cracks are extended due to the difference in thermal coefficient of expansion between different phases and thereby fracture is enhanced.

4.1.2 Thermal treatment for particle size breakage

It can be seen clearly that selection function value (min^{-1}) is higher for pretreated samples compared to the feed sample. As shown in Fig. 4.1.9and 4.1.10, it can be clearly seen that compression testing samples exhibited finer particle size distribution as compared with the ball-milled samples. In another set of experiments, 4.75×3.30 mm particles were comminuted with different combinations such as dry, wet, pre-treated in both ball mill and compression mode and corresponding particle size distributions for all combinations are shown in Fig. 4.10. The specific energy (kWh/t) consumed during comminution for both ball mill and compression unit is calculated using torque value and work done calculated. It is worthwhile to mention that specific energy values are least for compression mode, whereas, it becomes significantly high for ball mill. The specific energy values for heat treatment at 700°C for 60 min time and microwave treatment for 5 min is calculated as extra ~2 and 3 kWh/t units respectively. It can be deduced that compression mode gives finer particle size distribution compared to ball milling. However, pretreatment assisted ball milling gives the finest particle size distribution but at the expense of significantly higher specific energy. The reason for the better performance of compression mode grinding is attributed to the formation of significant cracks. BHQ sample attained a temperature of ~1000°C within 5 min of microwave exposure. Coarse particle sizes respond better to microwave exposure due to more internal flaws. Compression testing mode is more efficient than ball mill grinding with respect to particle size distribution and fineness due to the generation of significant micro-cracks. In pre-treated samples (thermal and microwave), micro-cracks were observed which does not significantly affect downstream operation i.e., magnetic separation as revealed conducted tests. Thermal treatment followed by water quenching was found better for coarser sizes compared to fine sizes.

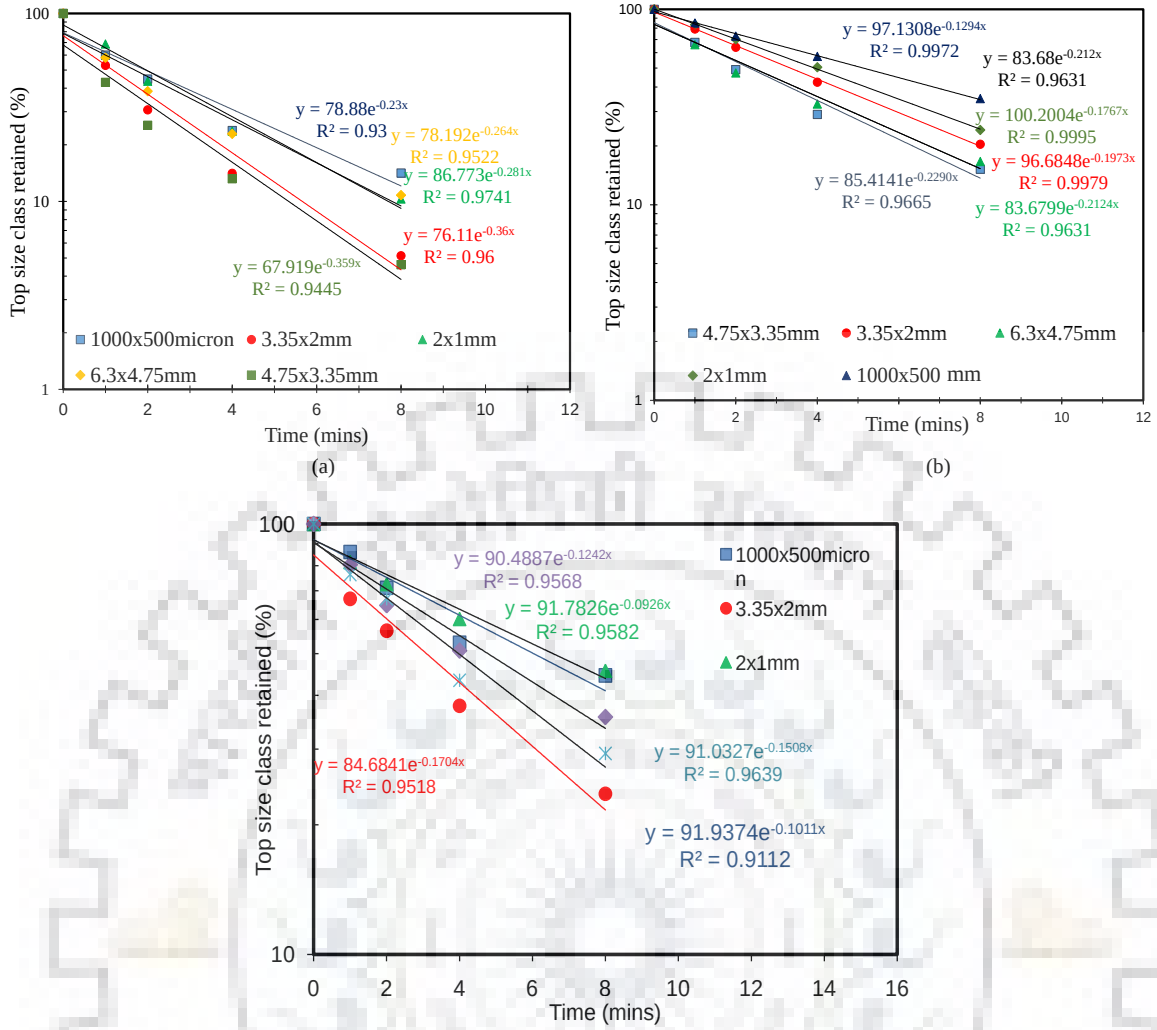

Figure 4. 1.3. Determination of selection function using zero order method for BMQ, BHJ and BHQ sample

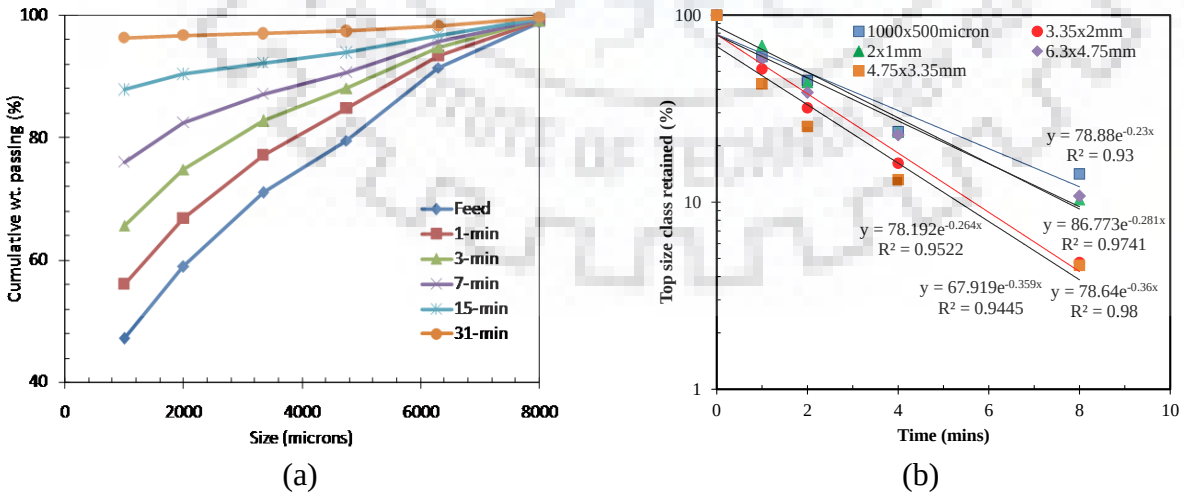

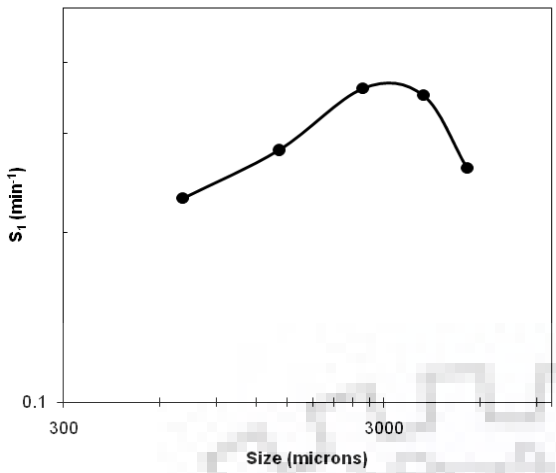

(c)

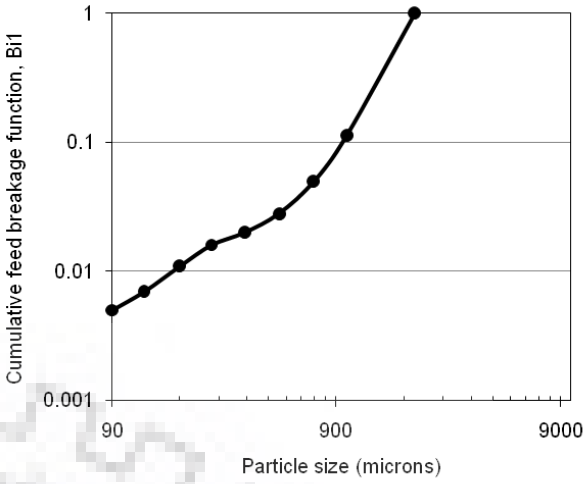

(d)

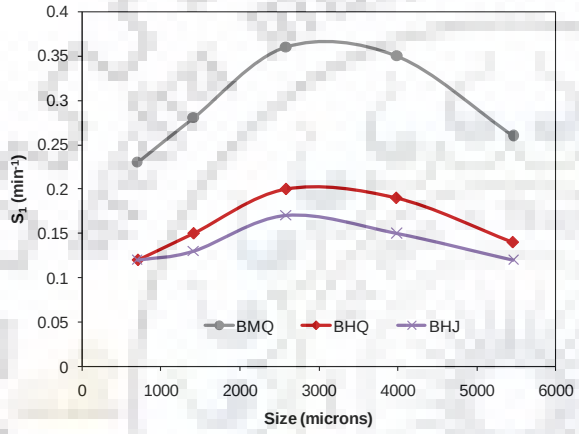

(e)

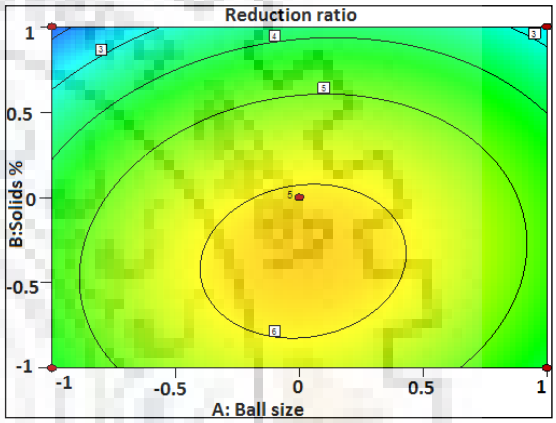

(f)

Figure 4.1.4 (a) Dry batch grinding of different ores in a ball mill (b) Zero-order plot for selection function (c) Variation of selection function with particle size (d) Cumulative breakage distribution functions as per G-H method (e) selection functions of ores (f) contour plot for optimization

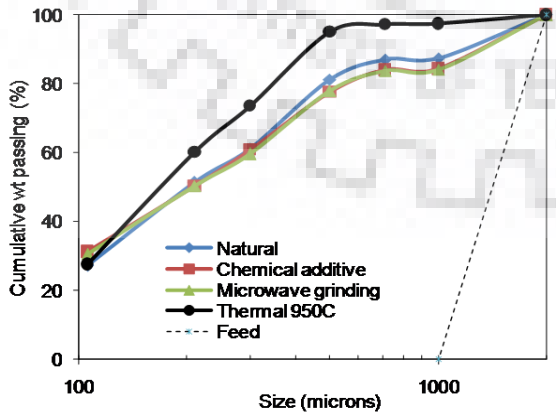

(a)

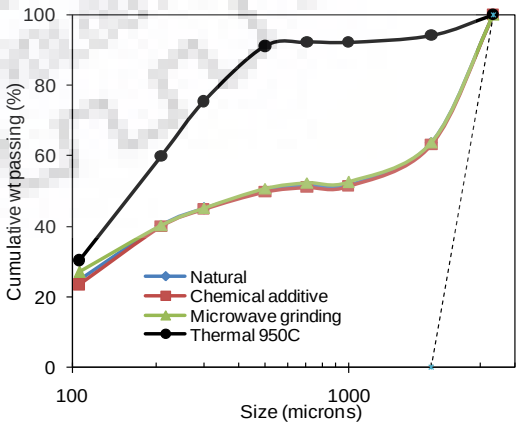

(b)

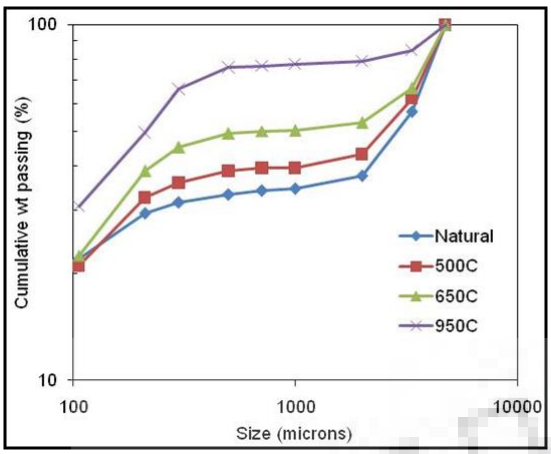

(c)

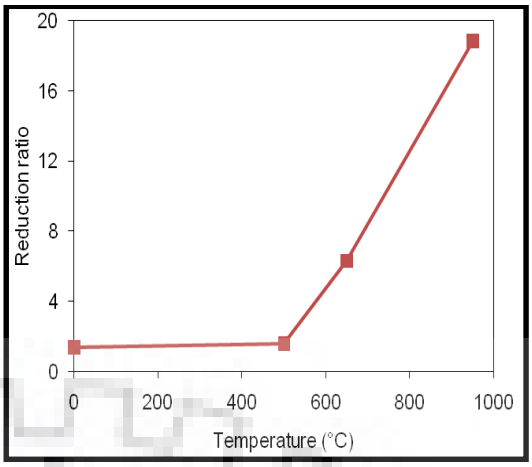

(d)

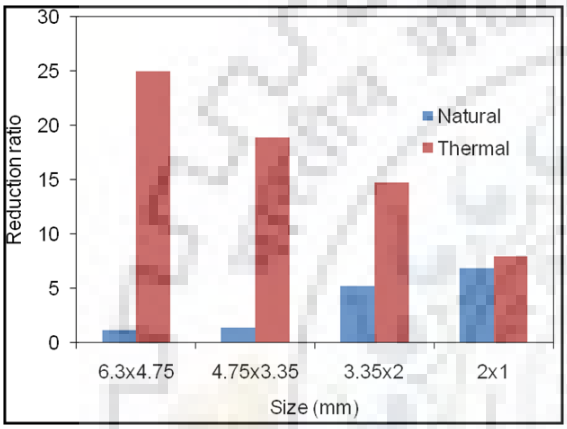

(e)

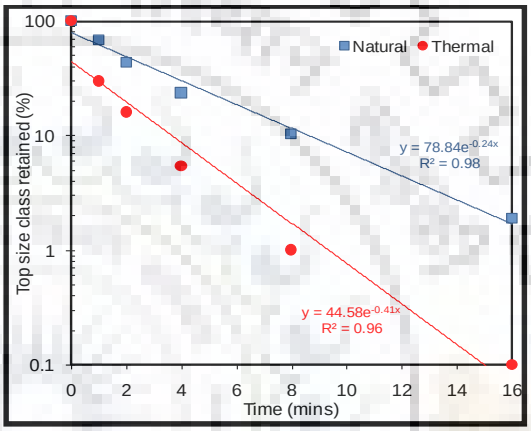

(f)

Figure 4.1.5 Comparison of different comminution alternatives at 4 min for BMQ ore (a) 2×1mm (b) 3.35×2 mm (c) 2×1mm and (d) Variation of reduction ratio as a function of temperature at 4 min for 2×1 mm (e) Comparison of reduction ratio as a function of particle size at 4 min at 950 °C (f) Evaluation of selection function for both natural and thermal treatment 950 °C grinding

The effect of grinding ball on the selection function value is shown in Fig. 4.1.6. It can be concluded that monologizes balls offer high grinding rate compared to mixed balls. Also, it was interesting to see the evolution of selection function both for natural/untreated and thermal grinding at constant ball mill conditions. As expected the rate of breakage or selection function was almost double i.e., 0.41 min^{-1} compared to 0.24 min^{-1} for natural/untreated grinding. At all-time intervals, it can be seen that thermal grinding is better than natural grinding as it yields lower 80% passing values as shown in Fig 4.1.7.

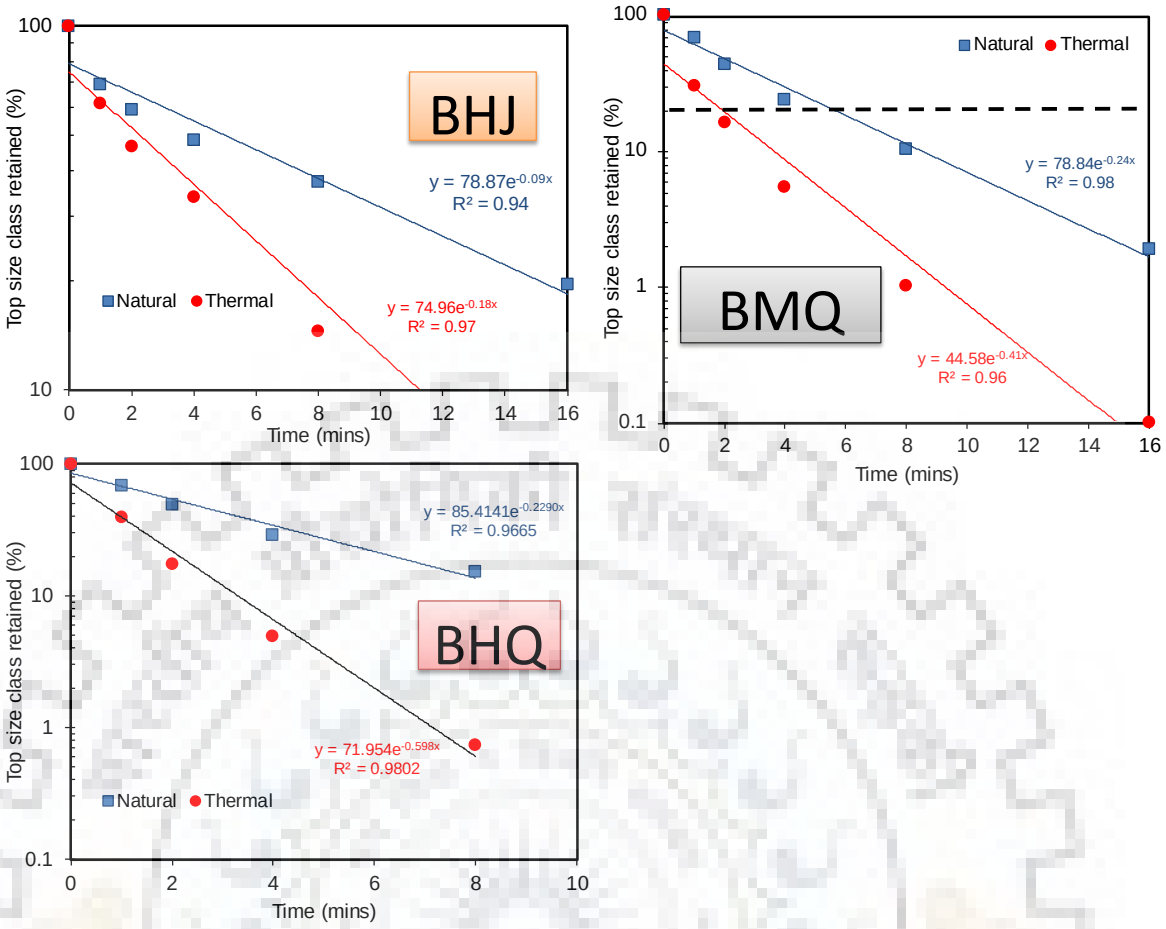

Fig 4.1.6 The plot of coarse selection function (S1) values for different ores for natural and thermal treated samples

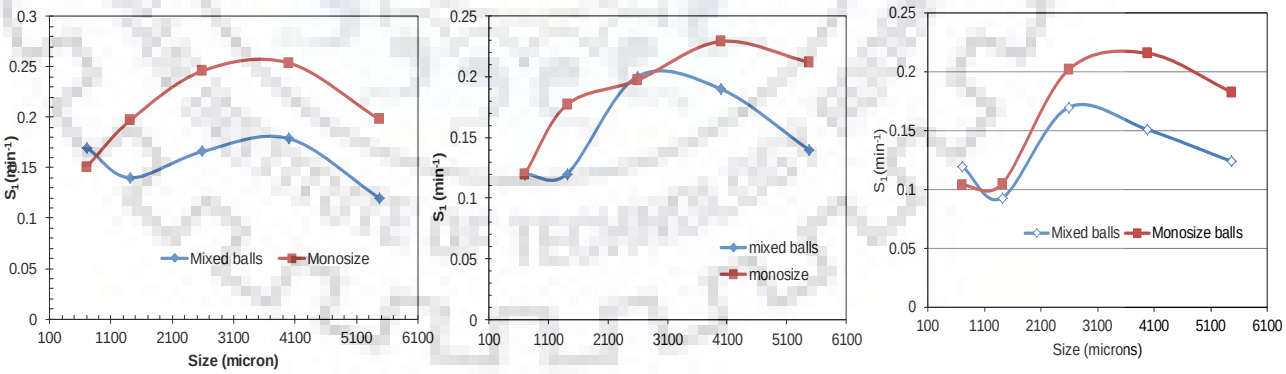

Fig. 4.1.7 Effect of ball size on selection function values

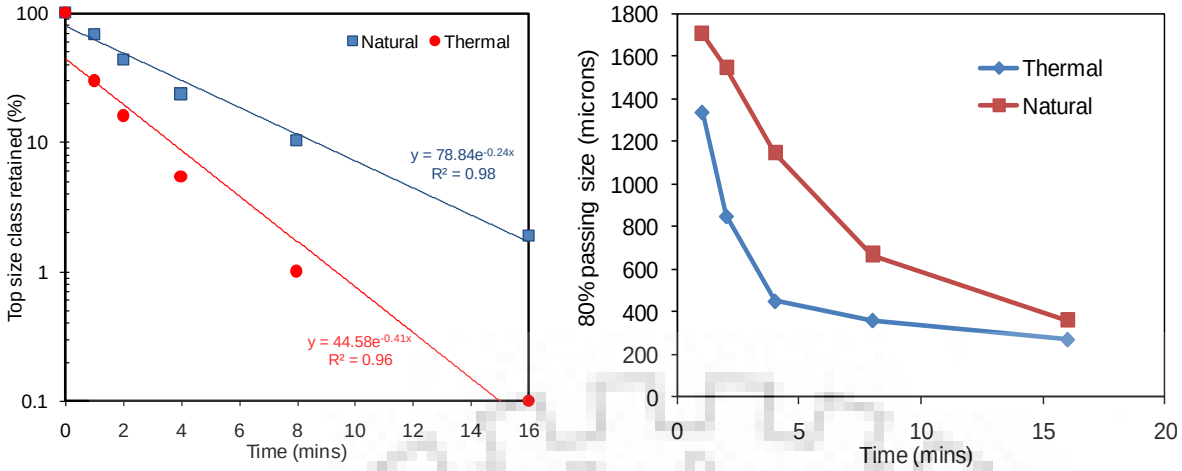

Fig 4.1.8. Evaluation of selection function and particle size d_{80} for both natural and thermal treatment grinding for BMQ ore

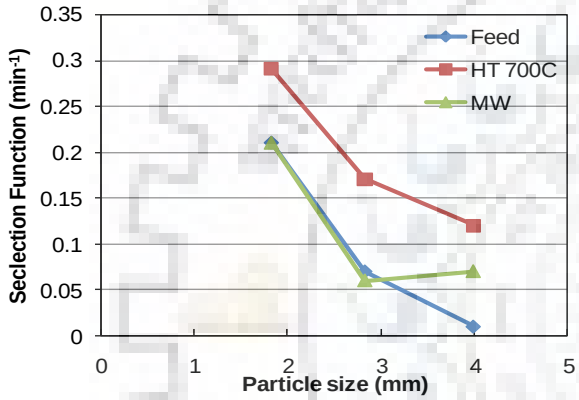

Fig 4.1.9 Variation of top size selection function for different particle sizes

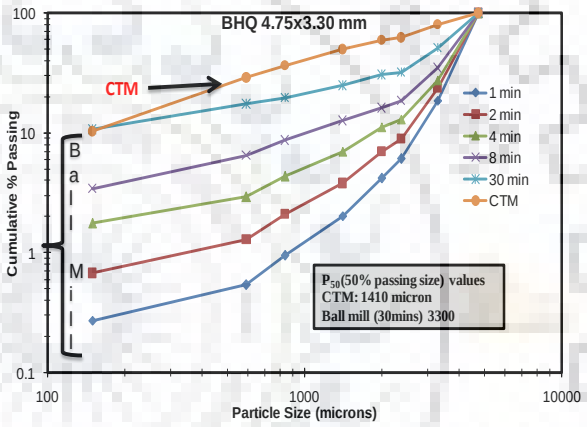

Comparison of the particle size distribution of both modes for 4.75×3.3 mm BHQ sample

Finally, compression mode is found better compared to ball mill with reference to finer particle size distribution at lower specific energy values. The ground samples of ball mill and compression testing were processed with Wet High-Intensity Magnetic Separator (WHIMS) at 10,000 Gauss. Surprisingly, there is not much change in total iron grade and recovery however there is a slight increase in weight percent of the magnetic fraction.

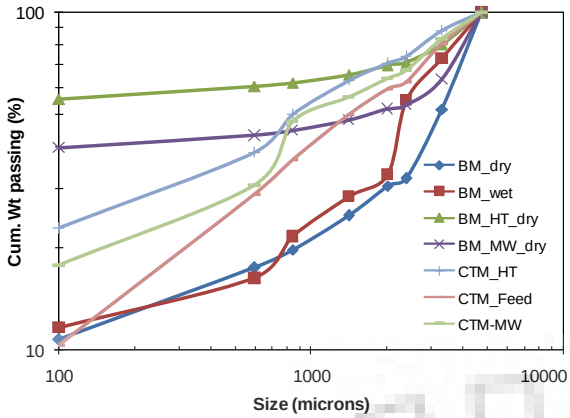

Condition	d/d_{50}	(-100 µm %)	kWh/t
CTM_Feed	2.82	10.34	5.4
CTM_MW	4.01	17.81	6.07
CTM_HT	4.72	22.93	6.59
Ball Mill_Feed dry	1.24	10.69	16.87
Ball Mill_Feed wet	1.74	11.6	11.36
Ball Mill_HT dry	44.3	55.3	18.87
Ball Mill_MW dry	2.32	39.8	19.87

	Constituent	% Fe	Wt.(%)
Feed	Mag.	52.72	30.27
	Non-Mag.	21.22	69.73
HT	Mag.	51.83	36.77
	Non-Mag.	25.91	63.23
MW	Mag.	47.14	34.89
	Non-Mag.	24.35	65.11

WHIMS result for samples at 10,000 gauss

Fig 4.1.10. Particle size distributions for different grinding conditions (4.75×3.30mm) and summary of parameters obtained

4.1.3 Compression testing of banded iron ores

In particle-bed comminution unlike most conventional grinding mills energy is transferred directly to the charge mass and breakage occurs by very high stresses, generated locally, at the contact points between the particles of the tightly compressed bed (Schonert, 2001; Tavares, 2005). For this reason, significantly enhanced energy efficiency is realized when a confined bed of particles is comminuted under sufficiently high compressive loads. The photograph of the compression testing setup along with feed and the compressed product is shown in Fig. 4.1.11.

4.1.3.1 Self-preserving spectrum

It can be seen from Eq. (28) that the particle-size distributions are self-preserving in the sense that a family of distribution curves collapses into a single similarity spectrum when LM(x) is plotted as a function of dimensionless size x/L. From considerations of a phenomenological model of grinding kinetics, the particle-size distributions conform to Eq. (28) are self-preserving in a reduced particle size scale, and the scaling factor, in turn, is the same as the characteristic particle length (Kapur, 1971).

$$M(x) = -\frac{C_o}{L}\left[\frac{x}{L}\right]^{b-1} \exp[-C_1\left[\frac{x}{L}\right]^{a} \quad 28$$

Where M(x) is the mass fraction of particles in the size interval x to x+ ***dx, Co*** is a normalizing factor and a, ***b*** and C, are dimensionless constants. ***L,*** a characteristic particle length or a scaling factor, is the overall index of 'fines' of the particulate assembly.

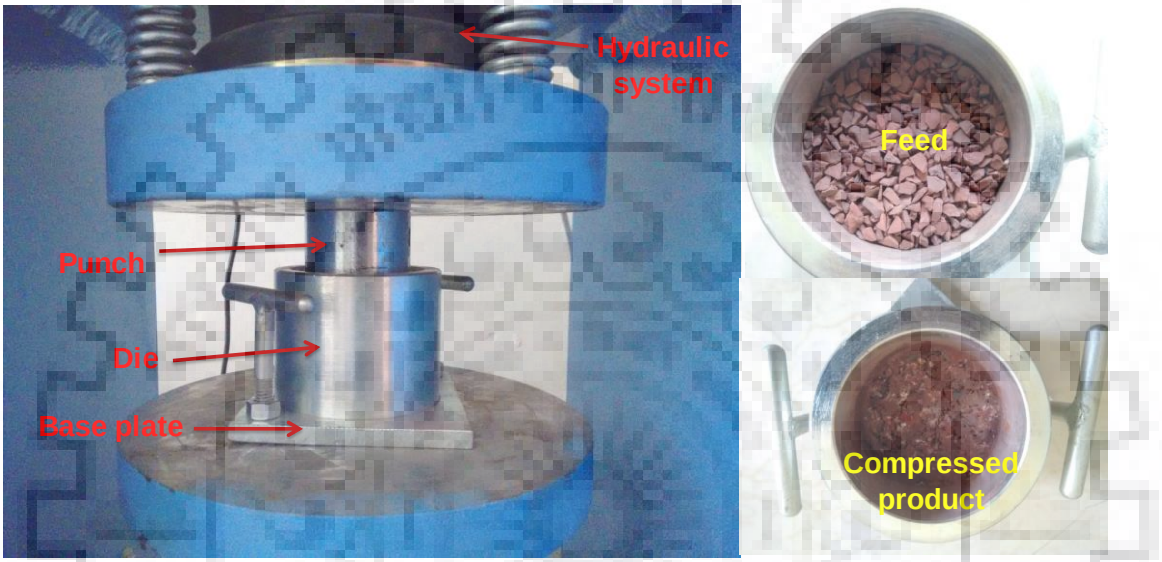

Figure 4. 1. 11 Compression testing setup along with feed and compressed product

4.1.3.2 The size distribution of the broken product

The size distributions of material ground in ball mills follow the Gaudin - Schohmann size distribution with a reasonably long straight line portion in the fine size range and a convex portion near the top of the feed size at higher grinding times (higher energy levels) and a concave portion close to the top of the feed size at shorter grinding times. The slope of the straight-line portion (the distribution modulus) is constant for all grinding times. All of the distributions are reasonably normalizable with respect to the median size, X_{50}, as shown in Fig. 4.1.12. This means that BHQ and BHJ behave the same in the confined compression setup under all of the applied loads for all size fractions. As shown in Fig. 4.1.13a, the pressure developed in bed is increased linearly with increase in compression depth. The developed pressure is more in BHQ compared to other ores. However, the reduction ratio of BHJ is better as compared with other ores. As expected, the specific energy consumed for breaking the various size fractions increased as the applied load increased.

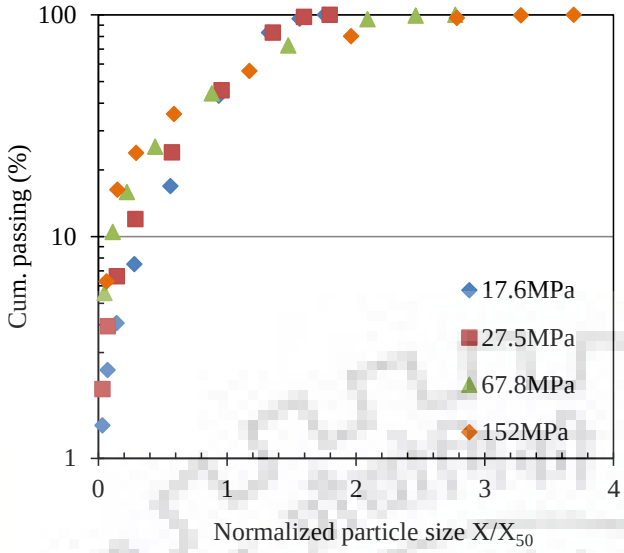

(a) BHQ

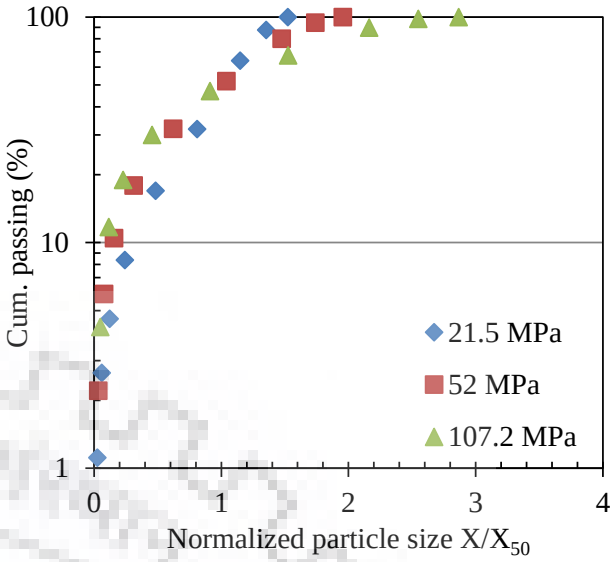

(b)BHJ

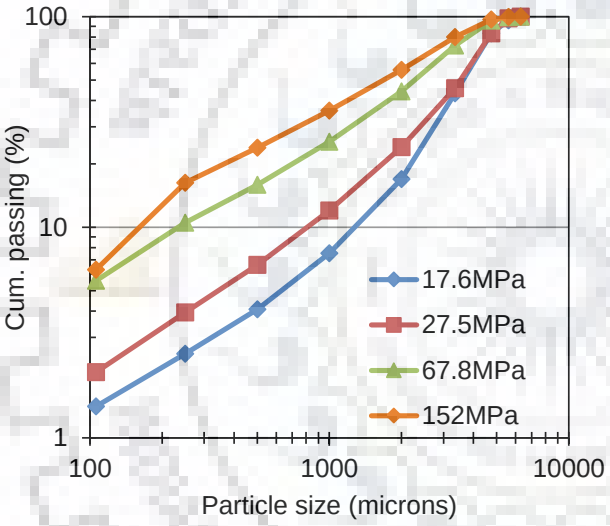

(c) BHQ

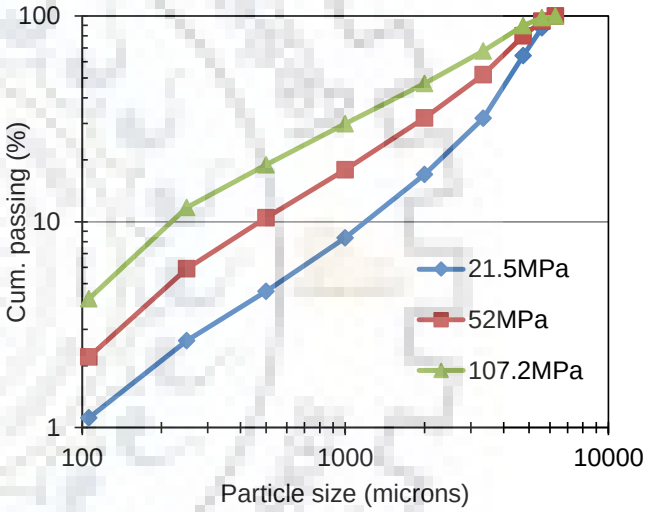

(d) BHJ

Figure 4.1.12 (a&c) Normalized size distributions for all size fractions at pressure and (b&d) product size distribution for the mono size 6.35×4.75mm)

4.1.3.3 Reduction

The reduction ration, X_{50f}/X_{50p}, as a function of the specific energy consumed for the breakage of different size fractions used in this study is shown in Fig. 4.1.14 for different ore samples. As expected, the slope of the relationship increases as the size fraction increases, i.e., the coarser size is more easily crushed in the die compares to the finer sizes. It can be seen that the specific energy consumption in the compression piston die system decreases with increasing size.

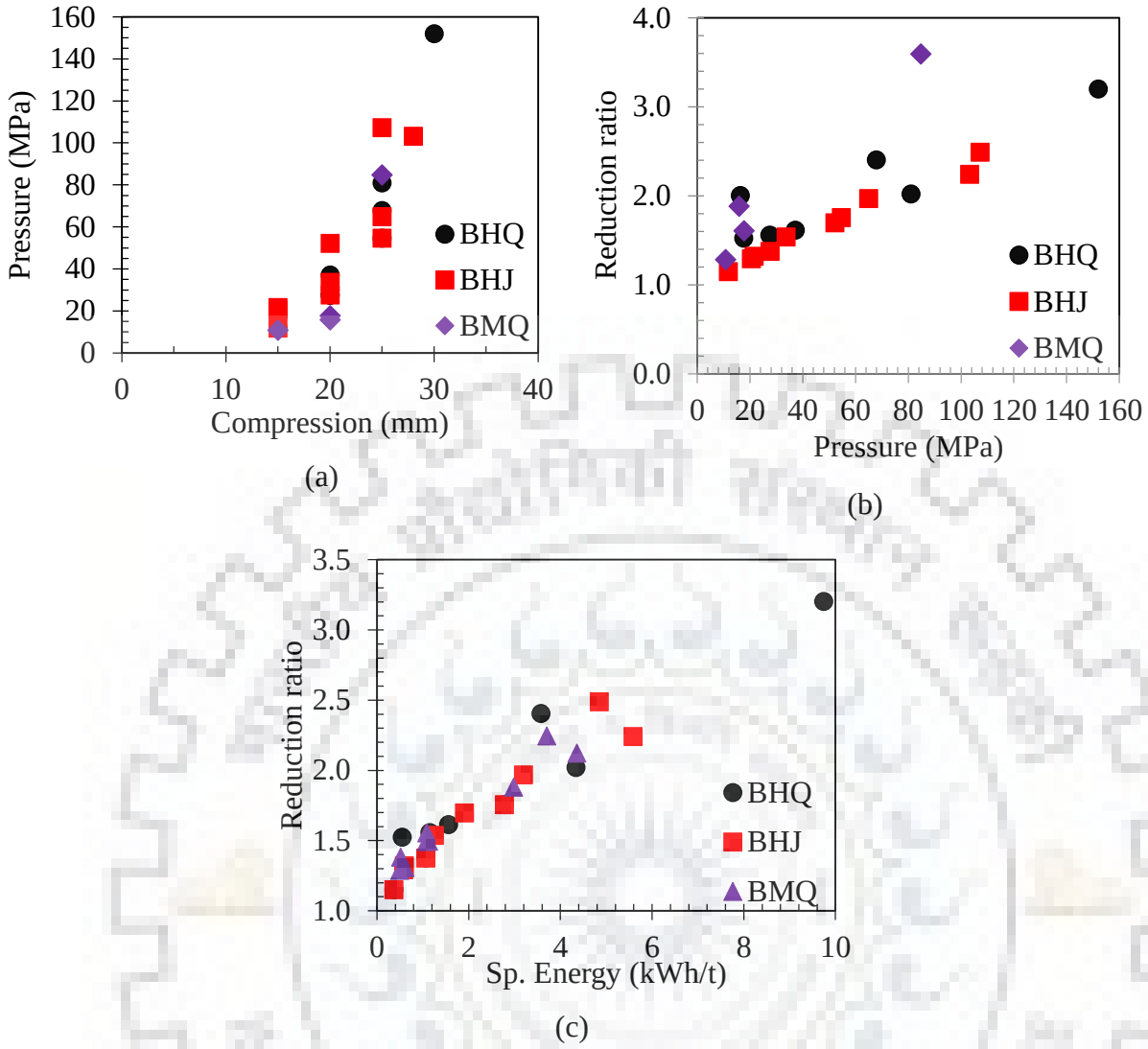

Figure 4.1.13 (a) Effect of compression depth on pressure generation, (b) effect of pressure on reduction ratio and (c) specific energy vs reduction ratio for different ores

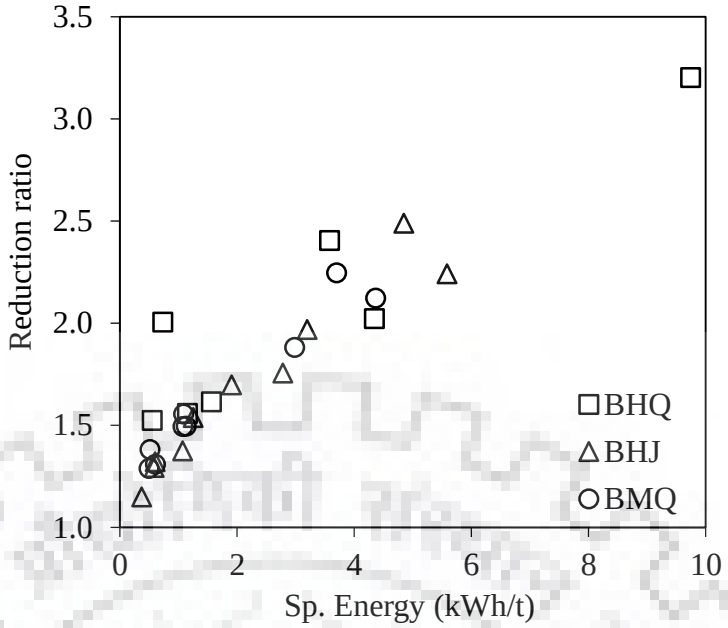

Figure 4.1.14 The reduction ratio for some of the tested fractions as a function of the specific energy consumed for different monosizes

4.2 Up-gradation of banded iron ores

4.2.1 Effect of particle size

The variation of iron grade with particle size is shown in Fig. 4.2.1 (a, b). The particles below 75 microns show comparatively higher iron grade suggesting better separation/liberation of iron phase from quartzite at finer sizes and is chosen as a representative sample with 38.7 % iron BHJ ore whereas for BHQ gives, particle size below 500 microns showed a slightly higher grade compared to coarse sizes. However, no certain trend was observed depicting inadequate liberation because of the dispersion of hematite values in the quartzite matrix for both the ores.

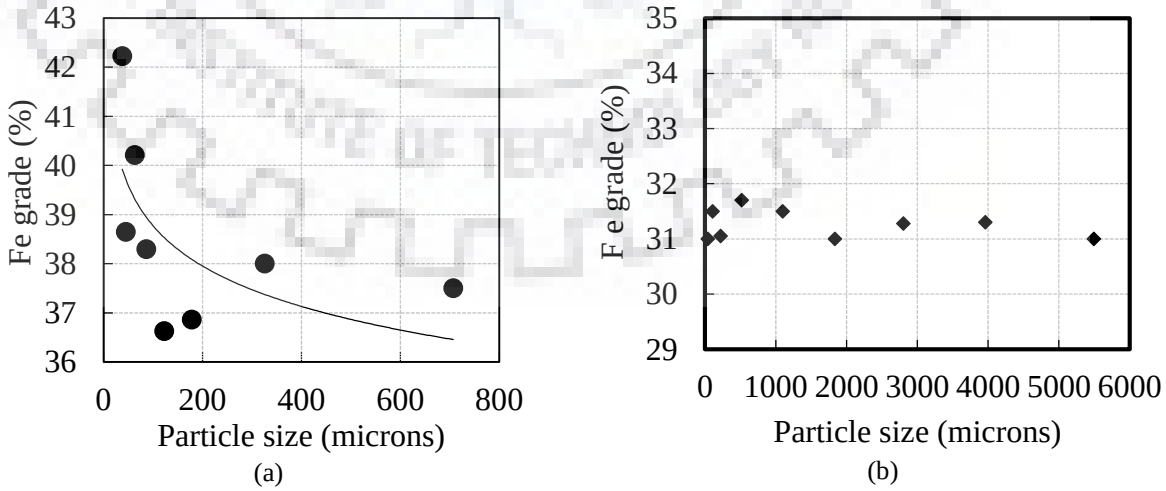

Figure 4.2.1 Variation in iron grade with particle size for (a) BHJ (b) BHQ

4. 2. 2 Physical separation of banded iron ores

4. 2. 2. 1 Sink float test

The spiral concentrator yielded a concentrate with 45.79% iron grade at 64% iron recovery and a yield of ~56.14%. At the optimum condition of 5000-16,000 gauss, a concentrate with 53 % iron grade at 94% iron recovery is obtained with a yield of ~58.6% (for BHJ). The conventional sink float analysis using Bromoform was carried out to assess the liberation size; however, it was found futile due to inadequate liberation. The spiral concentrator yielded a lean concentrate with approximately 35-40% iron grade (Fe_G) at 85-91% iron recovery (Fe_R) for BHQ ore.

4. 2. 2. 2 Magnetic separation of banded iron ores

The representative sample was subjected to magnetic separation for iron enrichment. The variation in the concentrate grade and recovery with magnetic intensity is shown in Fig. 4.2.2 (a,b,c). It is observed that iron grade falls with magnetic intensity, however, recovery increases as weakly bound impurities along with iron values are trapped in the magnetic fraction. The optimum condition of 10,000 Gauss, yielded a concentrate with 49 % Fe grade (Fe_G) and 97% Fe recovery (Fe_R) in case of BMQ, a concentrate with 53 % Fe and 94 % iron recovery producing a yield of ~58.6% is obtained in case BHJ, whereas, in BHQ a concentrate with 49 % Fe grade and 97% Fe recovery is obtained.

As expected, the iron grade decreases whereas iron recovery increases on increasing the magnetic intensity. The observed trend due to the fact that with an increase in magnetic intensity, relatively weaker iron-bearing phase is trapped along with bonded impurities in the magnetic fraction, thereby, increasing the iron recovery in the magnetic concentrate, but the overall iron fraction in the magnetic concentrate decreases. In the case of spiral concentration, as expected insignificant iron enrichment was observed; concentrate with 45.8% iron grade and 64% iron recovery. It can be inferred that low iron recovery in the conventional physical separation process is due to the strong bonding of hematite and jasper quartzite phase. Hence, an alternative treatment is required to weaken the underlying bond to achieve the desired separation. The magnetic separation provides some iron enrichment in the concentrate, but the concentrate is not suitable for the blast furnace feedstock.

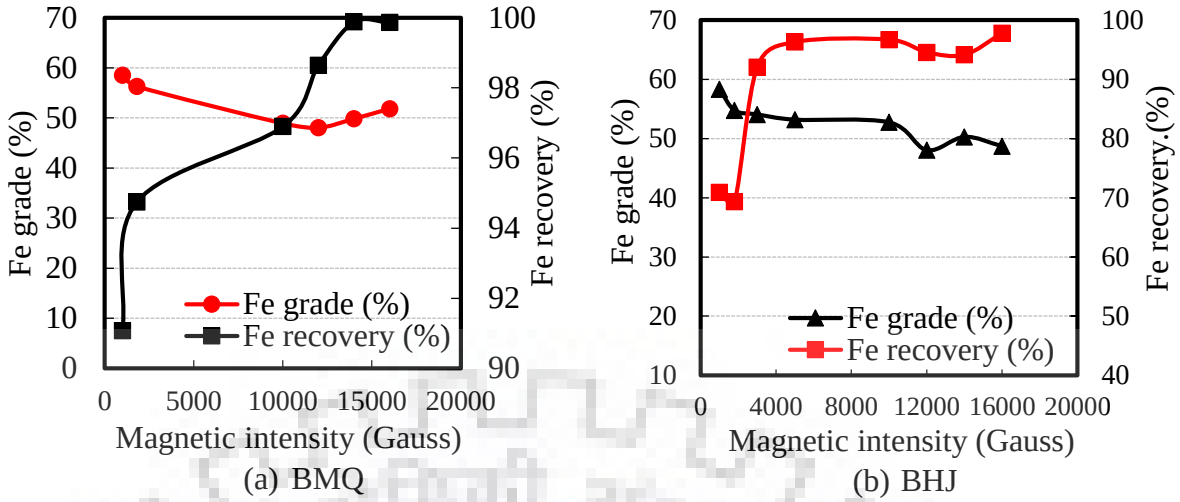

(a) BMQ (b) BHJ

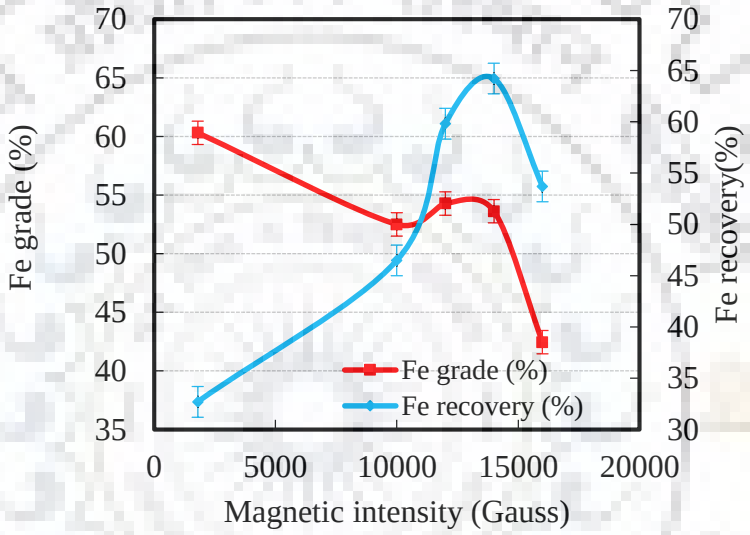

(c) BHQ

Figure 4.2.2. Effect of applied magnetic intensity on iron grade-recovery (a) BMQ, (b) BHJ, and (c) BHQ

4.2.3 Microwave Exposure of banded iron ores

4.2.3.1 Banded magnetite quartzite

It was observed that the conventional magnetic separation was ineffective in the enrichment of iron values. The strong bonding between the iron phase and the impurities prohibits the separation. Hence, the ore was exposed to microwaves to distort the underlying structure by loosening the bond between quartzite and magnetite through preferential heating of magnetite. Preliminary experiments were carried out at a maximum power of 900 W at a residence time of 6-8 min respectively. It was observed that Fe_G ~ 55% and temperature attained was ~ 600 °C. Owing to the positive response of ore towards microwave exposure in preliminary experiments, Box Behnken statistical design with three factors was pursued. In general, the response-surface design includes experimental runs at the boundary conditions of the selected factors, however, it

compensates as it offers better prediction at the center values of the factor (Montgomery, 2016). The microwave exposed sample was immediately quenched and pulverized and subsequently subjected to magnetic separation at 1000 Gauss to assess the iron grade and recovery. The factors involved in the design are microwave power, residence time and particle size. The temperature attained, iron grade, recovery, and yield were recorded as responses. It can be seen from Table 4.2.1 that optimum condition (Expt-4) microwave exposed concentrate yielded 60.09% Fe grade, 99.96% Fe recovery with a yield of 71.2%. It is evident from the results that the range of responses Fe_G: 53-60.7%, Fe_R: 78-99% and Yield 65-85% was significant. Based on the design results, a plot with iron grade-recovery of the concentrate with temperature attained is shown in Fig. 4.2.3 it can be inferred that a good concentrate (with higher grade and higher recovery) is obtained between 475-580 °C. Surprisingly both iron grade-recovery falls at both ends i.e., lower and higher temperature. The range of response parameters were determined with corresponding to 95% confidence interval. Means 95% confidence that the mean population value can exist in between upper and lower limit value. The Optimum Fe grade value obtained from the statistical design is almost equal to upper limit obtained through statistical design. Most of the response values were in between the 95% Confidence Interval. But it is observed the response recovery, is having slight variation with optimal value obtained through statistical designed.

The trend of response variables with significant factors is shown in the form of contour plots in Fig. 4.2.4 (a-d). It can be observed that high microwave power leads to higher attained temperature and higher yield. The grade and recovery of concentrate are confined to a stable range in the given operational parameters. The predicted values for temperature; yield, iron grade, and recovery are in good agreement with model experimental values as shown in Fig. 4.2.5(a-d). It can be observed that the predicted vs. actual plot fits best for yield response and worst for the grade.

Table 4.2.1 Experimental design conditions and responses

Expt. No.	Power (W)	Time (min)	Particle size (µm)	Temp (°C)	Fe_G (%)	Yield (%)	Fe_R(%)
1	720	6	300	549	56.74	74.19	93.89
2	900	14	150	502	53.62	74.15	87.46
3	540	10	300	518	53.62	67.21	78.15
4	720	6	40	539	60.09	71.13	99.96
5	900	10	300	713	56.74	69.04	86.53
6	720	14	300	615	57.19	68.91	85.59
7	900	6	150	756	44.68	85.09	84.09
8	540	14	150	499	60.32	73.65	98.22
9	540	6	150	576	60.54	70.24	91.31
10	720	14	40	553	60.76	66.42	90.05
11	720	10	150	634	53.62	72.37	80.71
12	540	10	40	469	59.20	65.64	87.39
13	720	10	150	613	55.36	71.84	84.86
14	900	10	40	402	56.74	64.37	81.10
15	720	10	150	627	56.19	70.78	82.86
Average (mean)					56.36	71.00	87.48
Standard deviation (s)					4.1	4.96	6.27
(t value*Standard deviation)/Sqrt(sample size)					2.27	2.75	3.47
95% Confidence Interval					56.36 ± 2.27	71 ± 2.75	87.48 ± 3.47

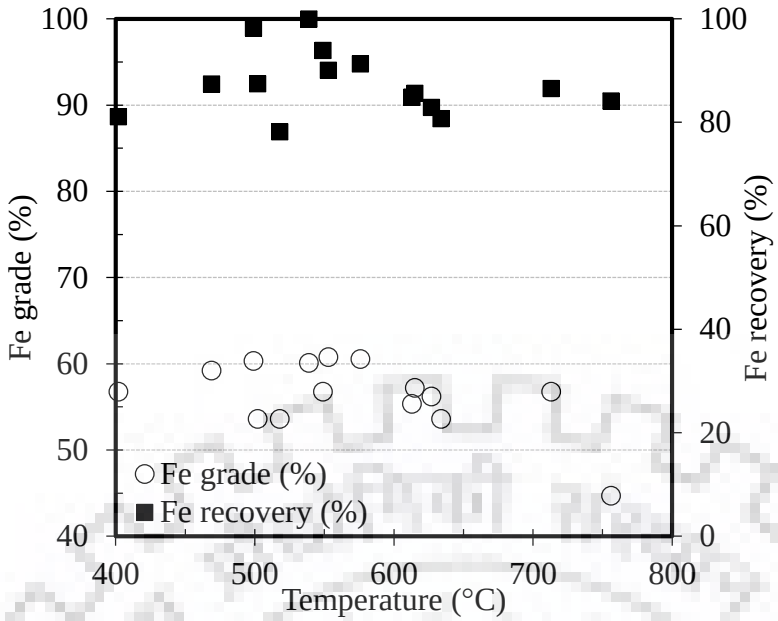

Figure 4.2.3 Effect of temperature attained on iron grade-recovery

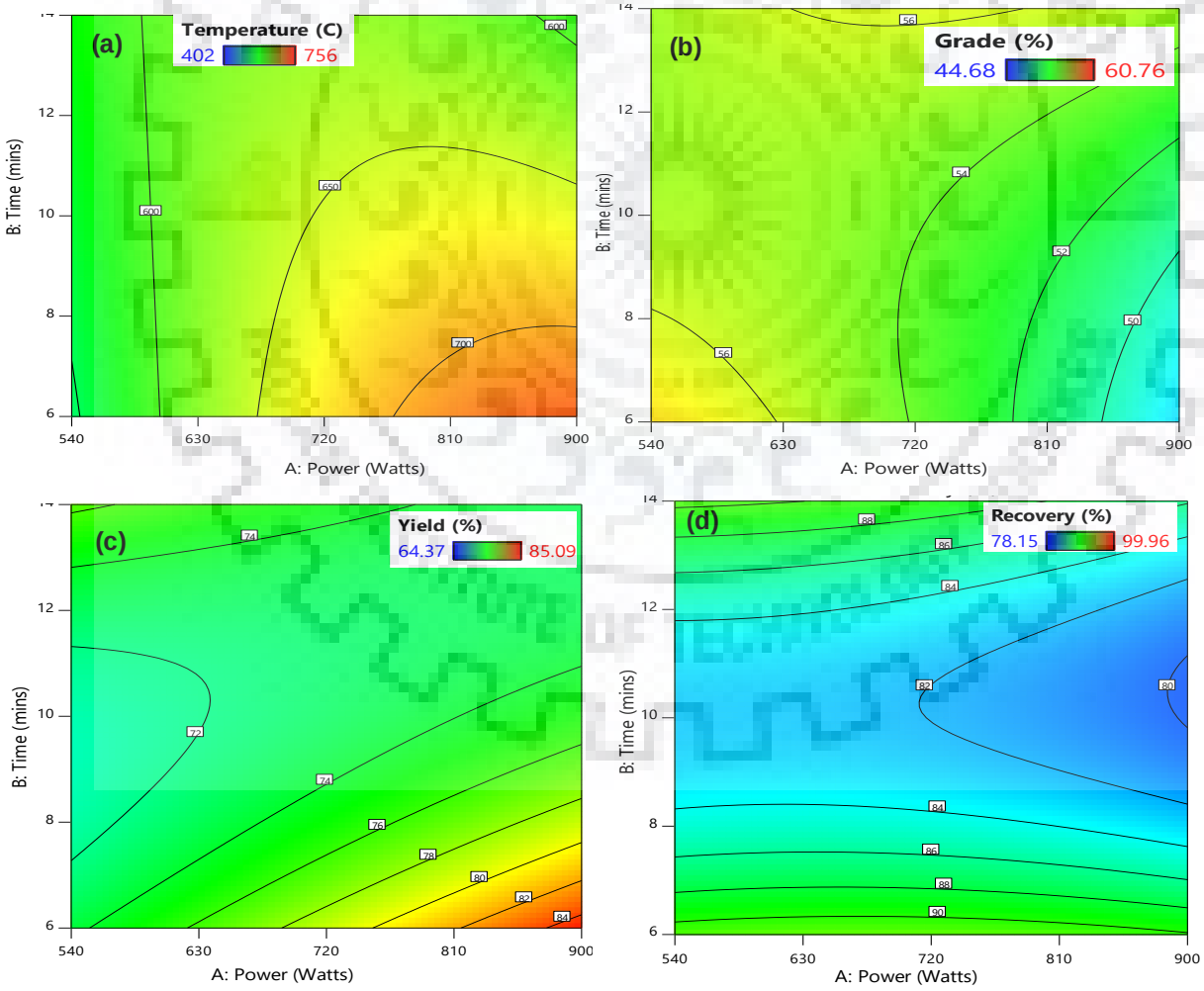

Figure 4.2.4 Contour plots of the influential factors of microwave exposed (a) Temperature, (b) Iron grade, (c) Yield, and (d) Iron recovery

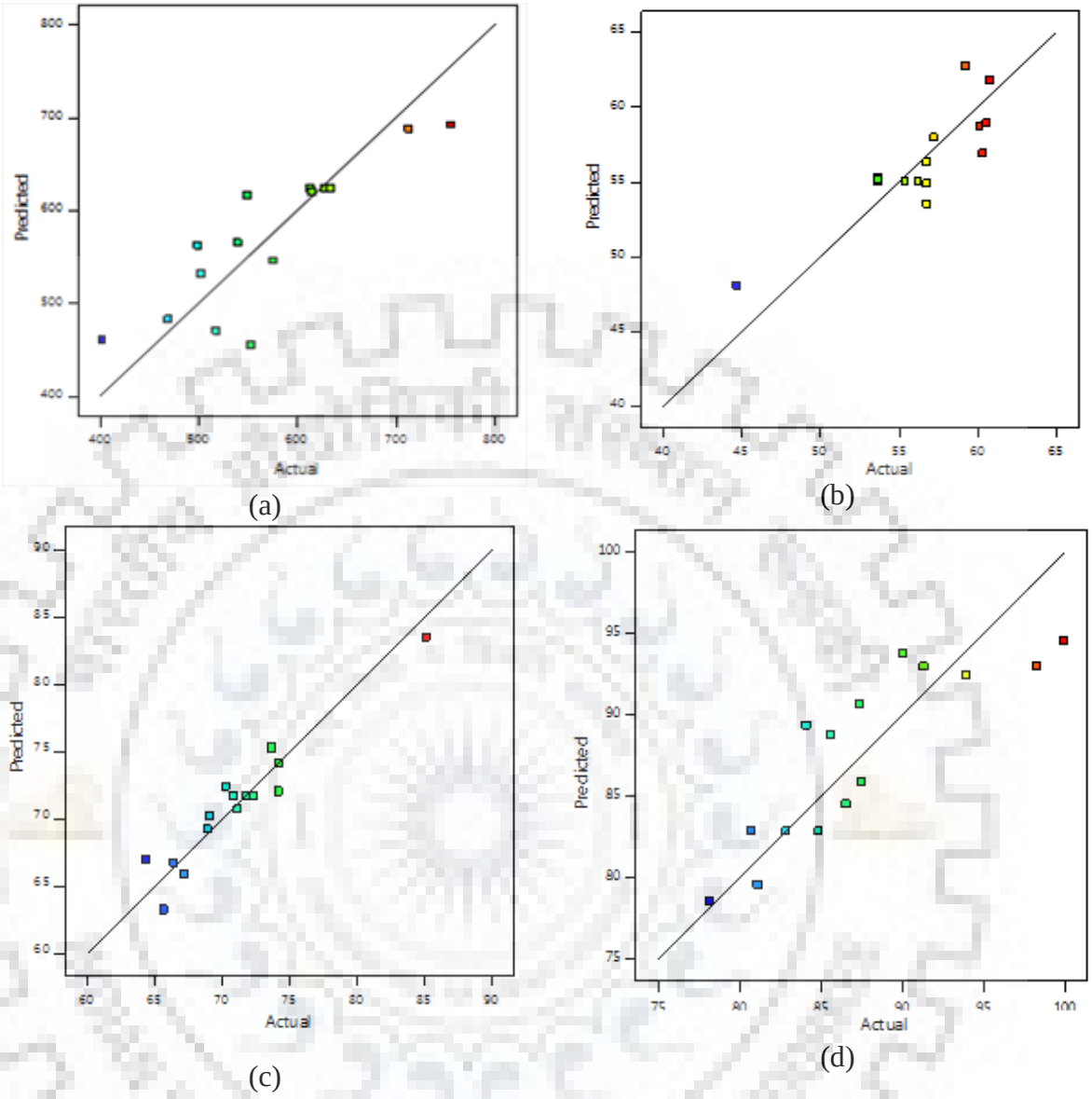

Figure 4.2.5 Predicted vs. actual values of the MW exposed experiments (a) Temperature, (b) Iron grade, (c) Yield, and (d) Iron recovery.

The analysis of statistical design depicts that the temperature and yield experimental values fit well to a modified quadratic model. The statistical parameters such as F-values and p-values of the model are shown in Table 3. The F and p values are more significant for response yield and high F-value of model 5.51 implies that the model is significant for the yield response. Ideally, p-values less than 0.0500 depicts significant model terms and the derived experimental equations for iron grade and recovery are, shown in Eq. (29-32). Based on the ANOVA table, it is observed that the overall interaction of factors is weak, however, for responses yield and recovery, the interaction of Power-Time and Power-Size are significant respectively. Also, the significant factors for all the responses are shown in Table 3. A small value of standard deviation value for

the responses depicts the robustness of the microwave exposure process adopted. The higher value of the regression coefficient (R^2) depicts the good fitting of the underlying quadratic model and it fits best to the yield response compared to recovery, temperature, and grade respectively.

$$\text{Temperature} = -380.6 + 2.1\ \text{Power} + 27.5\ \text{Time} + 0.3\ \text{Size} - 0.06\ \text{Power} * \text{Time} + 0.003\ \text{Power} * \text{Size} + 0.06\ \text{Time} * \text{Size} + -0.001\ \text{Power}^2 - 0.09\text{Time}^2 - 172.4\ \text{Size}^2 \quad (29)$$

$$\text{Grade} = +96.4 - 0.01\ \text{Power} - 3.01\ \text{Time} - 0.2\ \text{Size} + 0.003\ \text{Power} * \text{Time} + 0.0001\ \text{Power} * \text{Size} - 0.0009\ \text{Time} * \text{Size} - 0.00003\ \text{Power}^2 + 0.057\ \text{Time}^2 + 0.0003\ \text{Size}^2 \quad (30)$$

$$\text{Yield} = +42.1 + 0.05\ \text{Power} - 1.7\ \text{Time} + 20.1\ \text{Size} - 0.005\ \text{Power} * \text{Time} + 0.004\ \text{Power} * \text{Size} - 0.03\ \text{Time} * \text{Size} + 8.0504\text{E}^{-06}\text{Power}^2 + 0.2\ \text{Time}^2 - 5.3\ \text{Size}^2 \quad (31)$$

$$\text{Recovery} = +153.98 + 0.002\ \text{Power} - 9.4\ \text{Time} - 0.2\ \text{Size} - -0.001\ \text{Power} * \text{Time} + 0.0002\ \text{Power} * \text{Size} - 0.001\ \text{Time} * \text{Size} - -0.00002\ \text{Power}^2 + 0.5\ \text{Time}^2 + 0.00017\ \text{Size}^2 \quad (32)$$

Table 4.2.2 ANOVA quadratic factors of process responses temperature, grade, yield and recovery

	Temperature		Grade		Yield		Recovery	
Source	**F-value**	**p-value**	**F-value**	**p-value**	**F-value**	**p-value**	**F-value**	**p-value**
Model	1.55	0.33	1.48	0.35	5.51	0.03	1.61	0.31
A-Power	2.89	0.15	3.30	0.12	4.87	0.08	0.44	0.53
B-Time	0.86	0.39	0.81	0.41	5.97	0.058	0.33	0.58
C-Size	3.72	0.11	1.52	0.27	2.75	0.16	0.91	0.38
AB	1.25	0.31	1.63	0.25	8.14	0.03	0.11	0.75
AC	2.41	0.18	1.64	0.25	0.01	0.9	2.72	0.16
BC	0.55	0.49	0.04	0.85	0.03	0.85	0.08	0.78
A^2	0.94	0.37	0.41	0.55	0.04	0.85	0.085	0.78
B^2	0.001	0.97	0.246	0.64	8.69	0.03	8.93	0.03
C^2	3.34	0.13	2.85	0.15	19.00	0.007	0.44	0.53
Std. Dev.	79.18		3.59		2.52		5.32	
Mean	571		56.36		71.00		87.5	
R^2	0.73		0.72		0.9		0.74	
Significant factor sequence	Size>Power>Time		Power>Size>Time		Time>Power>Size		Size>Power>Time	

4.2.3.1.1 Characterization of microwave treated samples

The XRD plot of the feed and selected magnetic concentrates from the design is shown in Fig 4.2.6a. It is important to mention that there is no phase change throughout the experiment, however, there is a slight increase in the intensity of the magnetite phase. The VSM analysis was also carried to evaluate saturation magnetization for selected magnetic concentrates from the design experiments as shown in Fig. 4.2.6b. The saturation magnetization for the feed and optimum condition (experiment no. 4) was observed as 44.04 emu/g and 63.15 emu/g. It clearly reflects the iron enrichment in the concentrate by microwave irradiation and is in confirmation with iron grade results. Next, at optimum condition (720W, 6 min, and minus 75 microns), a coarse size fraction (4.75×3.35mm) is microwave exposed and the optical microscope image of the product is shown in Fig. 4.2.7. The rapid heating of iron oxide phase (magnetite) in a non-heating gangue (quartzite) generated thermal stresses which produced flaws at discrete locations within the matrix and effectively causing fracture at grain boundaries and is in agreement with previous studies (Barani et al., 2011; Kingman and Roason, 2000; Tavares, 1999). The micrographs reveal that significant random cracks in the product compared to the feed and thereby assists in the liberation of iron values. The crushing energy required for microwave-treated particles was significantly lower than the feed as revealed by higher fines generation under the same milling conditions. It can be attributed to the loosening of the strong bond, as quartz undergoes a phase transition at 573°C (α→β) and crack formation is expected due to different coefficient of thermal expansion of magnetite and quartzite phase (Tavares, 1999). The microwave exposure causes selective heating of iron phases revealed by temperature attained. Due to thermal expansion in grains and subsequent water quenching leads to initiation of localized stress and thereby damage. It is expected that microwave exposure offers a pathway for cracks, between mineral and the gangue constituents due to differences in microwave absorption characteristics and thermal expansion coefficient (Rayapudi et al. 2018; Kingman and Roason, 2000; Singh et al. 2017; Cheng et al. 2018; Hartlieb et al. 2018).

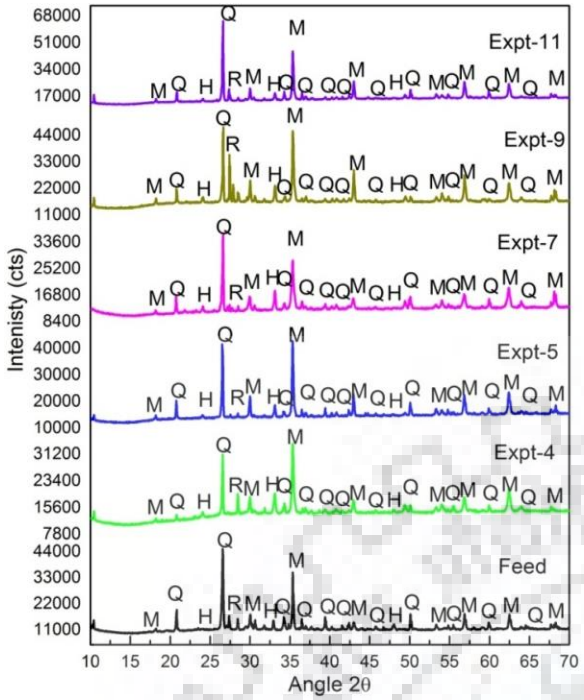

Figure 4.2.6a XRD plot of magnetic concentrates of various experiments

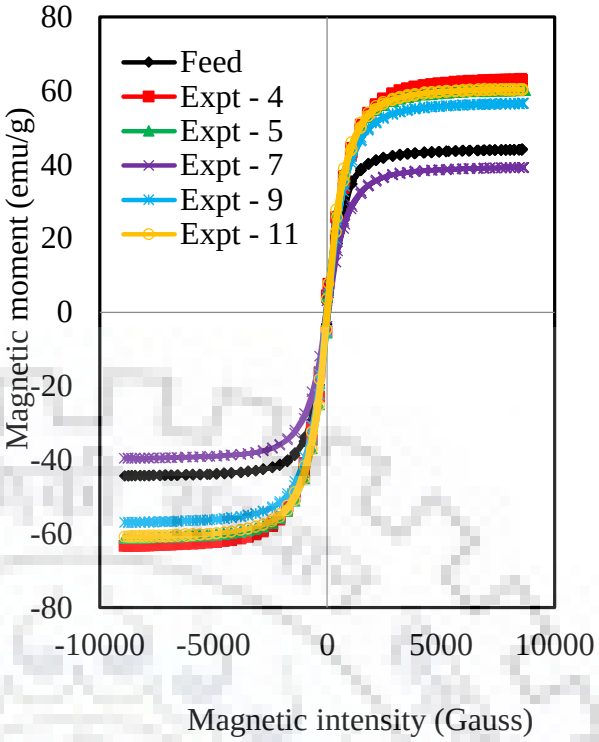

Figure 4.2.6bVSM plot of a magnetic concentrate of various experiments

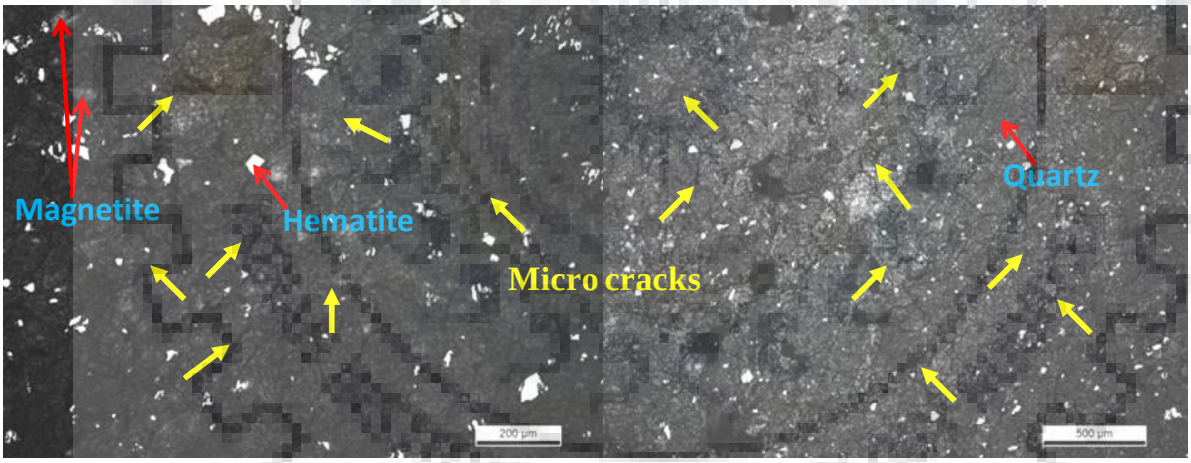

Figure 4.2.7 Optical microscope image of the exposed product at optimal condition (720 W, 6 min)

Considering the positive response of microwaves due to the crack formation, the effect of particle size, microwave power and exposure time were studied for the optimal condition (720 W, 6 min, minus 75 µm) as shown in Fig.4.2.8. It is observed in that with an increase in particle size, temperature attained reaches a maximum at 1000-micron size and decreases with increasing size. Similarly, iron grade and recovery were confined to small variation up to 3000-micron size. As expected the grade will fall due to better microwave exposure of fine particles with high effective surface area compared to coarse sizes. Similarly, with an increase in microwave power, the attained

temperature increases due to higher heating rate available at higher power levels. As expected there is a small variation of both iron grade and recovery which confirms that the optimum condition is a favorable condition for both iron grade and recovery. Next, the effect of exposure time as shown in Fig. 4.2.8b was also evaluated for a shorter time duration at optimum condition (720 W, minus 75 microns). As shown in Fig.4.2.8c, short exposure time (30 s) offers high grade but at the cost of low recovery. All the responses were found constant between 1- 4 min whereas exposure for 6 min remains the optimum condition. Also, it can be observed that iron grade values and saturation magnetization are in good agreement. The VSM analysis was also conducted for verification of optimal condition at different exposure times as shown in Fig. 4.2.8c. At higher exposure time of microwave irradiation, there is a decrease in saturation magnetism value and is in agreement with previous findings (Barani et al., 2011). It is observed that even though the peak height subsequently changes with microwave exposure, however, the position of new peaks cannot be accurately located, due to the threshold limit of the XRD sensitivity.

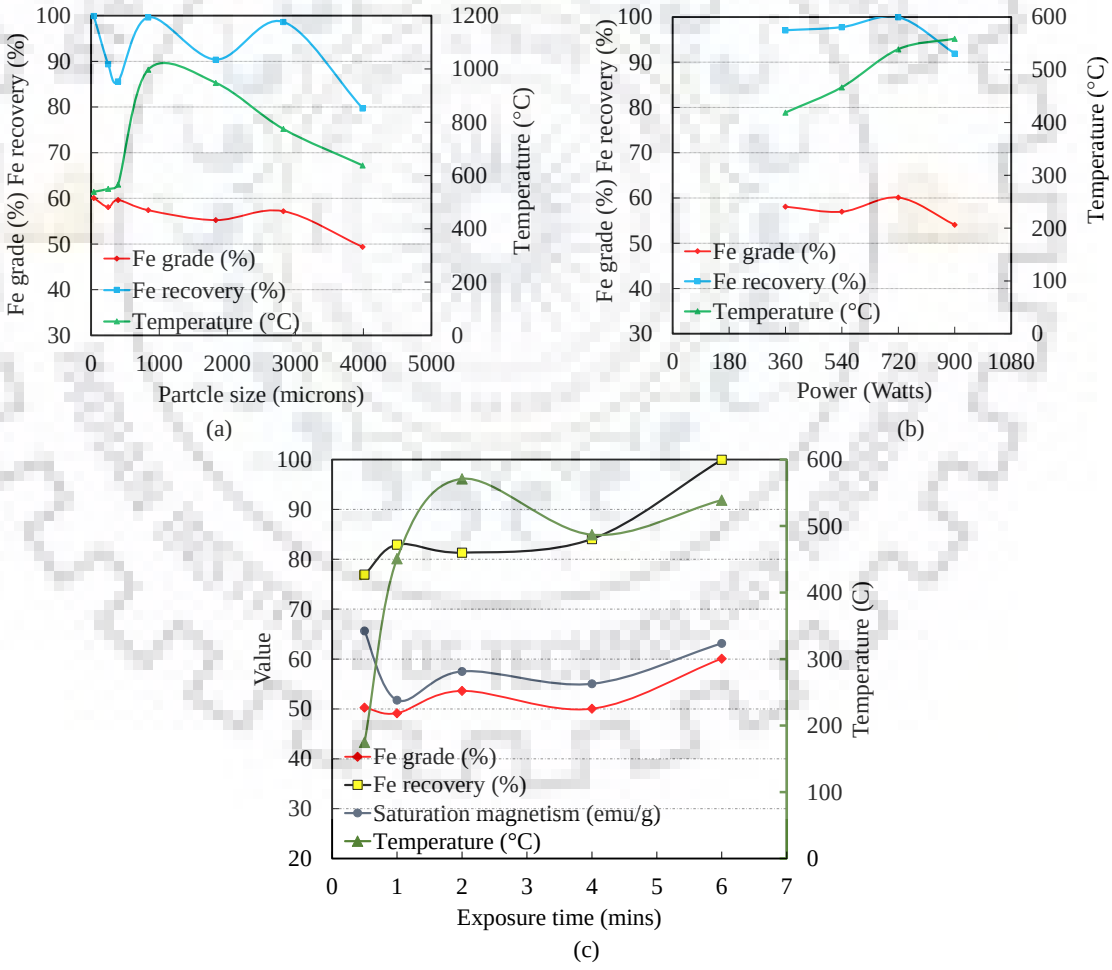

Figure 4.2.8 Variation of iron grade, recovery, and temperature of the optimum magnetic concentrate at 720 W with (a) Particle size (power 900 W) (b) Microwave power (particle size minus 75 microns) and (c) Exposure time.

4.2.3.1.2 Characterization of non-magnetic obtained through microwave treatment:

The by-product obtained through microwave exposed followed by magnetic separation consists of ~ 6% iron grade and the rest are silicon, oxygen and with traces of calcium and manganese and was confirmed through chemical analysis. The SEM-EDS analysis is as shown in Fig. 4.2.9. The X-ray spectra analysis shows the main existing phases are quartz, wollastonite, and traces of magnetite in the non-magnetic fraction.

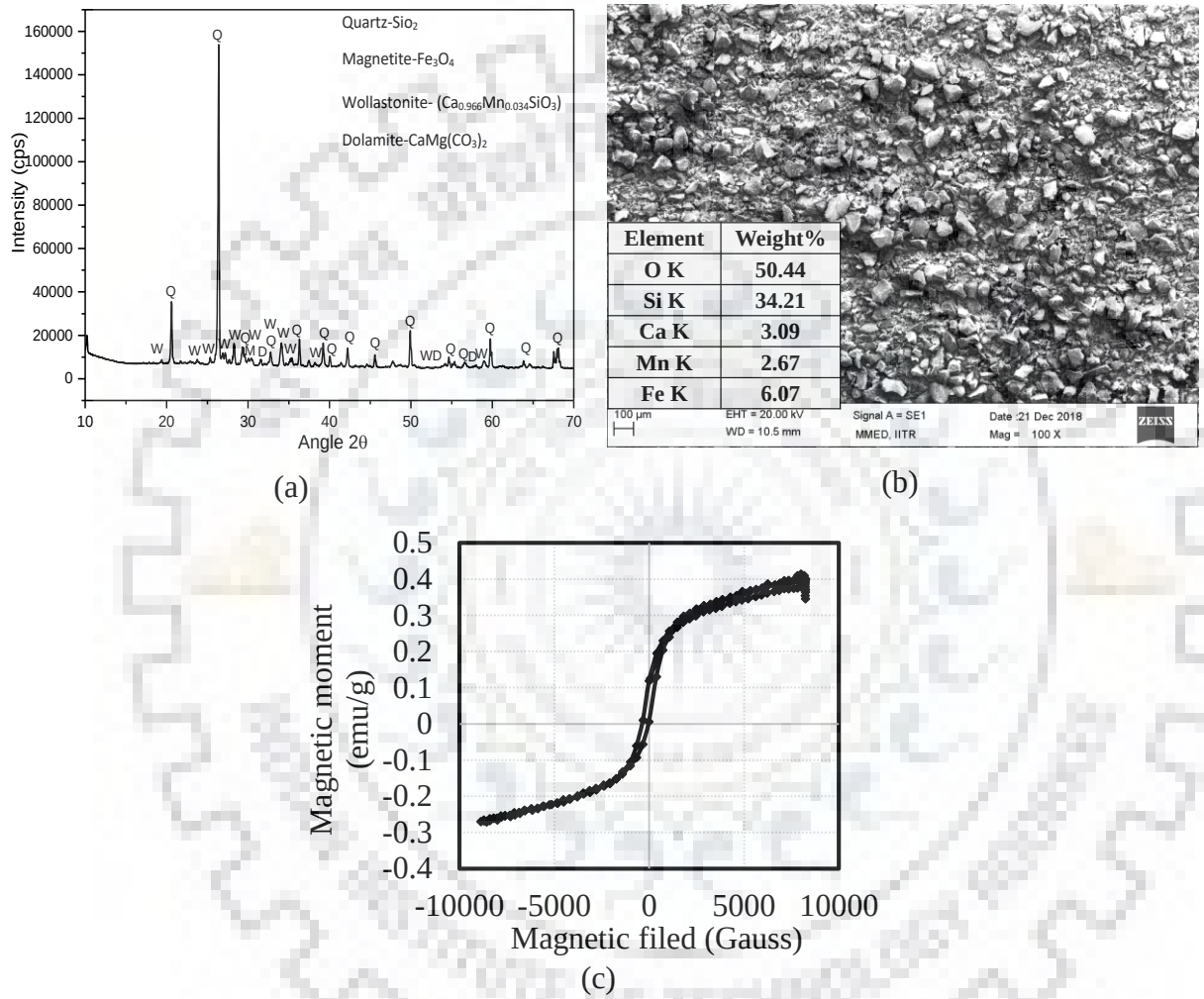

(a) (b) (c)

Figure 4.2.9 (a) XRD analysis (b) SEM- EDAS analysis and (c) VSM analysis of non-magnetic portion obtained through microwave exposure

4.2.3.2 Microwave exposure of banded hematite jasper

4.2.3.2.1 Microwave Exposure

In this route, the ore is exposed to microwave irradiation for a different time and power levels. As a result of microwave exposure, the temperature attained in the sample increases due to the generation of frictional heat caused by the dipole moment of the iron atoms in the hematite phase. It is expected that the internal heat generation helps in the liberation of bonded iron phases as, the selective volume expansion of the quartz phase over hematite phase. It is evident from Fig.

4.2.10a, that microwave power has a significant effect on temperature attained and iron recovery. The effect of sample size on separation efficiency is investigated and the results shown in Fig. 4.2.10b reveals that coarse particles show better separation at lower microwave exposure time compared to fine particles. However, with increasing time the separation of finer particles enhances compared to coarser sizes. However, in 8 min of microwave exposure time, the temperature attained in the coarse fraction is significantly high (853 °C) compared to the finer fraction (360 °C). Thus, it can be concluded that although microwave heating is more effective in a coarser fraction, whereas, the separation of iron-bearing phases from impurities is better in a finer fraction. Fig. 4.2.10c shows variation in iron grade and iron recovery with microwave exposure time up to 14 min. The increasing trend in iron grade with exposure time suggests that microwave exposure improves the separation by selective heating of the hematite phase that consequently weakens the bond between hematite and quartzite. Although iron grade increases linearly with exposure time the iron recovery saturates above 10 min of exposure time. A magnetic concentrate with 57 % iron grade is obtained at 84 % iron recovery in 10 min of microwave exposure.

The assessment of the benefits of microwave exposure was examined through microscopic studies. The optical microscope images of feed and microwave treated product for 10 min are shown in Fig.4.2.11 and 4.2.12 respectively. It is evident from both micrographs that there are massive random cracks in the microwave exposed product compared to feed sample which assists in the liberation of iron values. It is difficult to specify the nature of cracks in terms of a grain boundary or intergranular but nevertheless, the random cracks are clearly observed in SEM micrographs as shown in Fig.4.2.12. Both iron and quartz-rich areas are also marked with the spot analysis. The crushing energy required for microwave treated coarse ore particles is considerably lower than the feed particles. Due to the weakening of the strong bond between the constituent phases which reduces the hardness of ore or increases friability. It is known that quartz undergoes a phase transition at 573°C ($\alpha \rightarrow \beta$) which weakens the banded iron ore matrix due to different coefficient of thermal expansion of hematite and quartzite phase (Tavares and King, 1999). Since in this study, the maximum temperature attained is 525°C, it substantiates the fact that there is no phase change during microwave treatment route. The microwave treatment provides a possible mechanism to induce cracking, particularly between the hematite and the surrounding jasper/quartzite matrix due to differences in microwave absorption characteristics. Also, microwave treatment causes selective heating of iron phases which leads to thermal expansion in grains whereas the rapid quenching results in the development of localized stresses and damage as confirmed by friable nature of microwave treated product.

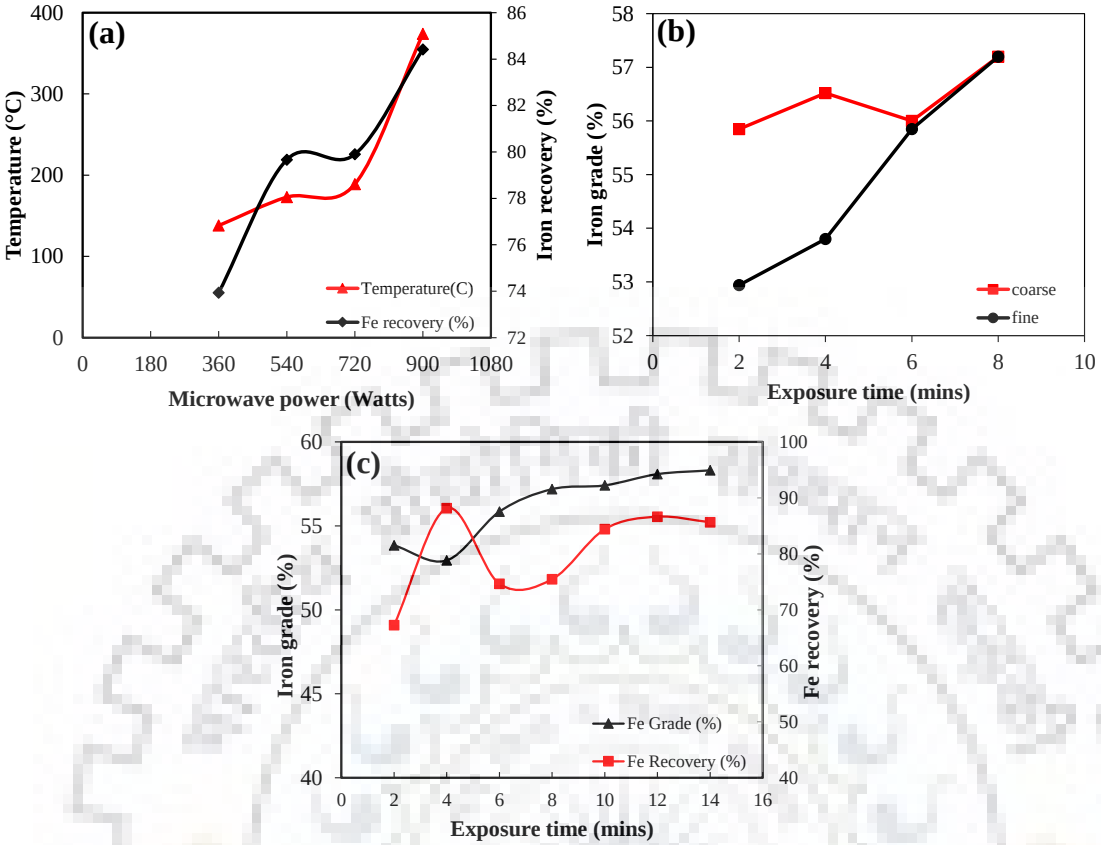

Figure 4.2.10 (a) Effect of (a) microwave power on iron recovery, (b) exposure time on the iron grade for different sizes (c) exposure time on the iron grade and recovery

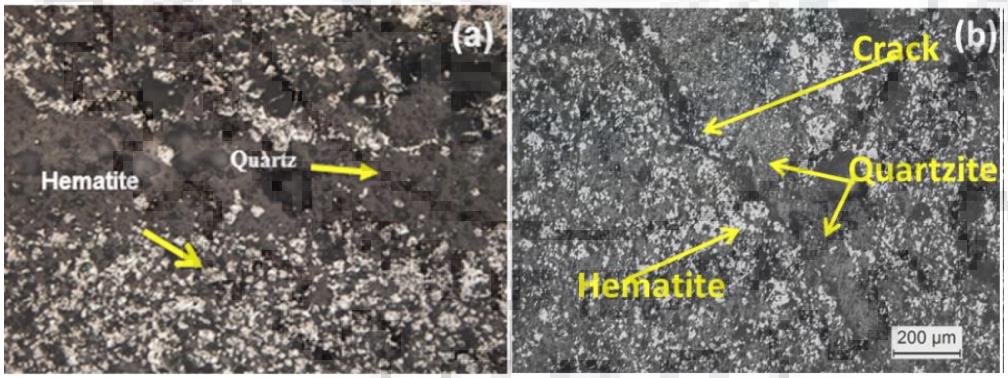

Figure 4.2.11 Optical microscope image of (a) Feed (b) microwave exposed product (10 min)

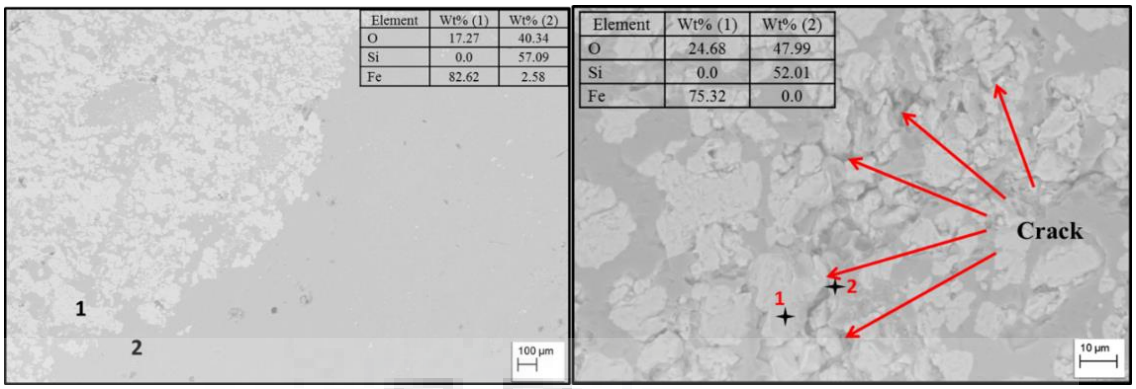

Fig. 4.2.12 SEM micrograph (Electron backscattered mode) of (a) Feed (b) microwave treated product exposure.

The comparison of microwave exposure treatment and magnetic separation process with respect to the overall yield of the magnetic concentrate is shown in Fig. 4.2.13. The yield of the magnetic concentrate in route B remains fairly stable (53-62%) over the complete range of iron grade, however, magnetic yield decreases with increase in iron grade in route A. The conventional route A has lower recovery at higher grades compared to route B. This clearly suggests microwave exposure is beneficial in recovering iron values and can be used as a potential pre-treatment step in the beneficiation process.

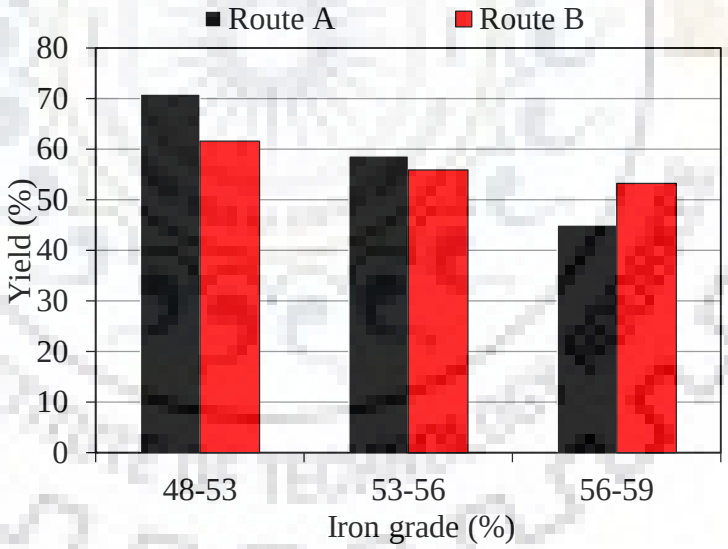

Figure 4.2.13 Variation of concentrate yield with an iron grade for route A and B

4.2.3.2.2 Combined physical beneficiation and microwave treatment

In route C, a three-step beneficiation process is adopted which includes microwave exposure of the magnetic concentrate of 10,000 gauss. The feed material used for microwave exposure in this route possesses a total iron content of 50.6%. Fig. 4.2.14a shows the variation in iron grade and iron recovery with exposure time. The iron grade increases from feed grade of 50.6% to a maximum of 61% for microwave exposure of 10 min. The iron grade of the concentrate increases

significantly at lower exposure time, however, at increased time duration the iron grade saturates ~61%Fe. Fig. 4.2.14b shows the temperature variation attained for different exposure time for feed (route B) and magnetic concentrate (route C). The temperature attained in the concentrate is higher compared to route B for all time intervals. The significant difference in attained temperature attained for both routes suggests that hematite phase present in the ore is susceptible to microwave irradiation and is significant in route C due to higher hematite fraction present in the route C compared to route B. The temperature gradient with respect to time decreases drastically with prolonged exposure and the final temperature eventually saturates above 10 min. The temperature saturation suggests that further time increment may not have any significant improvement in the iron grade. The magnetic concentrate corresponding to 10 min of microwave exposure of WHIMS magnetic concentrate corresponding to 10000 gauss yielded 61% iron grade with 77% iron recovery. For the selection of the optimum route, the iron grade versus iron recovery plot of all the adopted routes (A, B and C) is shown in Fig. 4.2.15. It is evident that route C provides the best grade to recovery ratio under the given experimental conditions. However, for higher recovery, route B is optimal. The conventional beneficiation process i.e., route A is least desirable as it yields the lowest iron grade although with higher recovery.

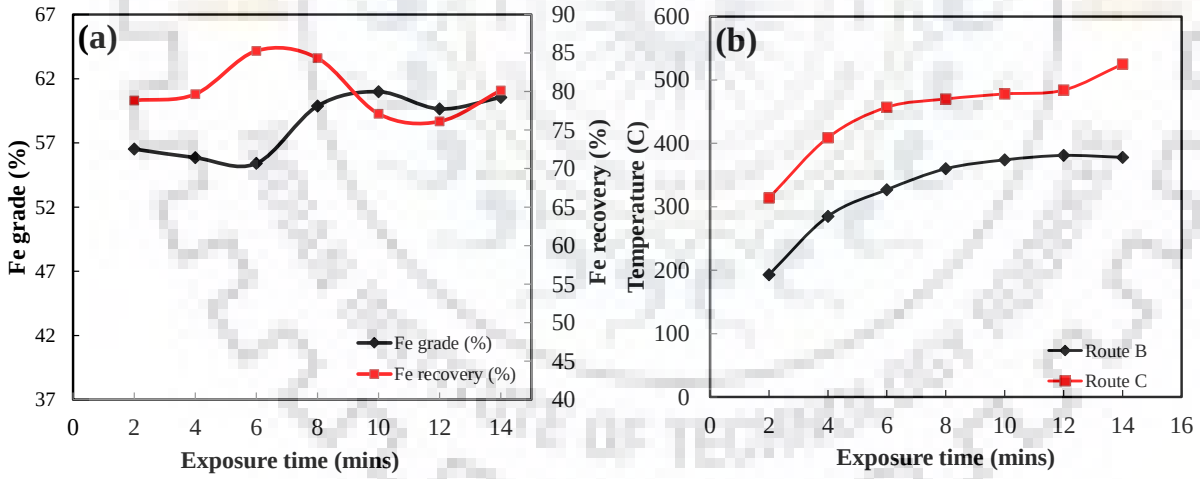

Figure 4.2.14 (a) Variation of Iron grade and recovery with exposure time for route C (b) temperature attained at different exposure times for both routes B and C.

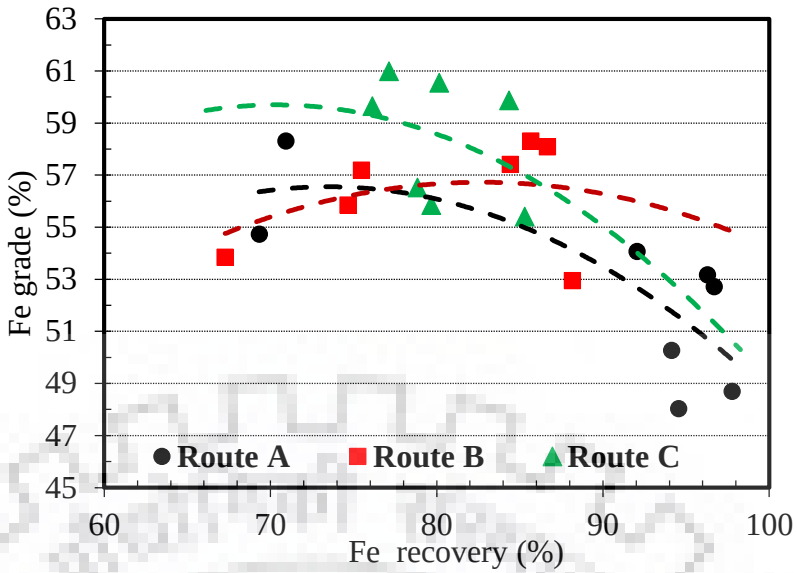

Figure 4.2.15 Iron grade vs. Iron recovery plot for routes A, B, and C.

VSM and XRD analysis were also conducted on the magnetic concentrate on optimal conditions of all the routes A, B and C. The results of VSM analysis are shown in Fig. 4.2.16a in the form of the hysteresis loop. The saturation magnetization of the feed is 5.02 e.m.u/g, Route B: 9.2 e.m.u/g and route C: 8.95 e.m.u/g respectively. However, the increase (with respect to feed) in magnetization route A is lower compared to other routes. The saturation magnetization increases, whereas, the remnant magnetism do not show any significant change. The increase in saturation magnetization implies enrichment of magnetic iron phases in the concentrate. Fig. 4.2.16b shows the XRD plot of the feed and concentrate obtained at optimal conditions of different routes. There is no phase change during the magnetic separation microwave exposure of route B and C. However, the intensity of the quartzite phase decreases, whereas, hematite peak intensity increases for all the routes. The results of VSM and XRD analysis are in agreement with the findings of iron grade and recovery obtained through chemical analysis.

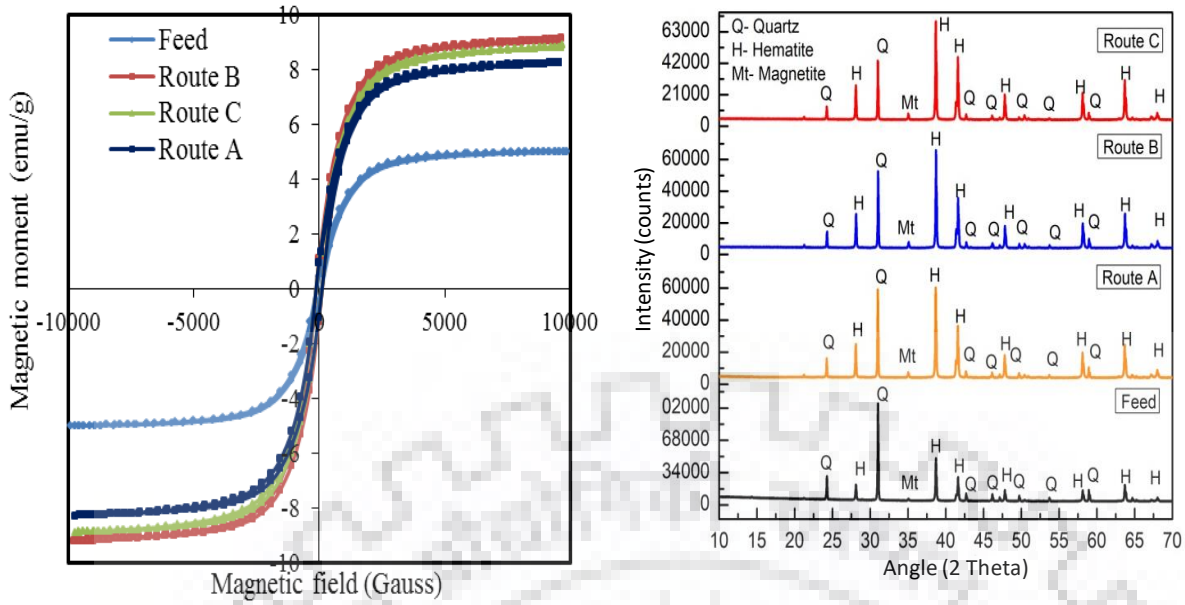

(a) (b)

Figure 4.2.16 (a) VSM plot and (b) XRD plot of the magnetic concentrate at optimized conditions of route A, B, and C

4.2.3.3 Microwave exposure of banded hematite quartzite

The preliminary experiments were carried out for both coarse and fine sizes at the maximum power (900 W). It was found that coarse particles attained a higher temperature compared to finer fraction, however, for the iron grade; the trend was reversed. This is because of liberation issues in the coarse fraction, whereas for a finer fraction, higher heat losses are expected due to the higher surface area. For the sake of convenience and to avoid variations because of particle size, closed size or mono size particles were taken. Owing to the positive response to microwave irradiation, Box Behnken statistical design with three factors was pursued. The factors involved in the design are microwave power, residence time and particle size, whereas iron grade, recovery, and yield were considered as responses. As shown in Table 4.2.3, the yield for all the experiments was confined to 22-29%, grade 48-56% and recovery 37-55% and the temperature attained was between 200-400°C. As there is no phase change in the microwave exposure, the same product is amenable for a blast furnace feedstock. The range of response parameters were determined with corresponding to 95% confidence interval. Means 95% confidence that the mean population value can exist in between upper and lower limit value. The Optimum Fe grade value obtained from the statistical design is almost equal to upper limit obtained through statistical design. Most of the response values were in between the 95% Confidence Interval. But it is observed the response recovery, is having slight variation with optimal value obtained through statistical designed.

The optimal condition for iron grade includes, 540 W, 10 min, and 6.3×4.75 mm, however, limited yield (27%) and iron recovery (50.7%) was achieved. Based on the highest temperature attained and grade, experiments 3, 5 and 6 were subjected to XRD and VSM characterization as shown in Fig. 4.2.17. The XRD analysis revealed that there was no phase change, except that few small peaks of magnetite appeared and are in accordance with saturation values. As the temperature does not exceed 500°C, no phase change was observed as confirmed by XRD and VSM results as shown in Fig 4.2.17.

Table 4.2.3 Experimental design and associated responses.

Expt. No.	Power (W)	Time (min)	Size (mm)	Temp (°C)	Fe_G (%)	Yield (%)	Fe_R (%)
1	720	6	6.3x4.75	261	52.72	24.24	42.59
2	900	14	4.75×3.35	374	50.49	29.55	49.73
3	540	10	6.3×4.75	260	56.30	27.01	50.68
4	720	6	2.38×1.41	319	52.05	31.35	54.39
5	900	10	6.3×4.75	397	51.38	24.12	41.32
6	720	14	6.3×4.75	376	55.40	21.68	40.04
7	900	6	4.75×3.35	297	55.63	26.26	48.69
8	540	14	4.75×3.35	297	50.49	29.27	49.25
9	540	6	4.75×3.35	198	48.48	26.14	42.23
10	720	14	2.38×1.41	370	52.50	26.14	45.74
11	720	10	4.75×3.35	269	54.29	20.57	37.21
12	540	10	2.38×1.41	281	51.83	28.36	48.99
13	720	10	4.75×3.35	288	53.8	20.78	38.16
14	900	10	2.38×1.41	364	50.94	23.89	40.57
15	720	10	4.75×3.35	275	54.79	22.82	40.83
Average (mean)					56.36	71.00	87.48
Standard deviation (s)					4.10	4.96	6.274
(t value*Standard deviation) / Sqrt (sample size)					2.27	2.75	3.47
95% Conversion Interval (95% CI)					56.36 ± 2.27	71 ± 2.75	87.48 ± 3.47

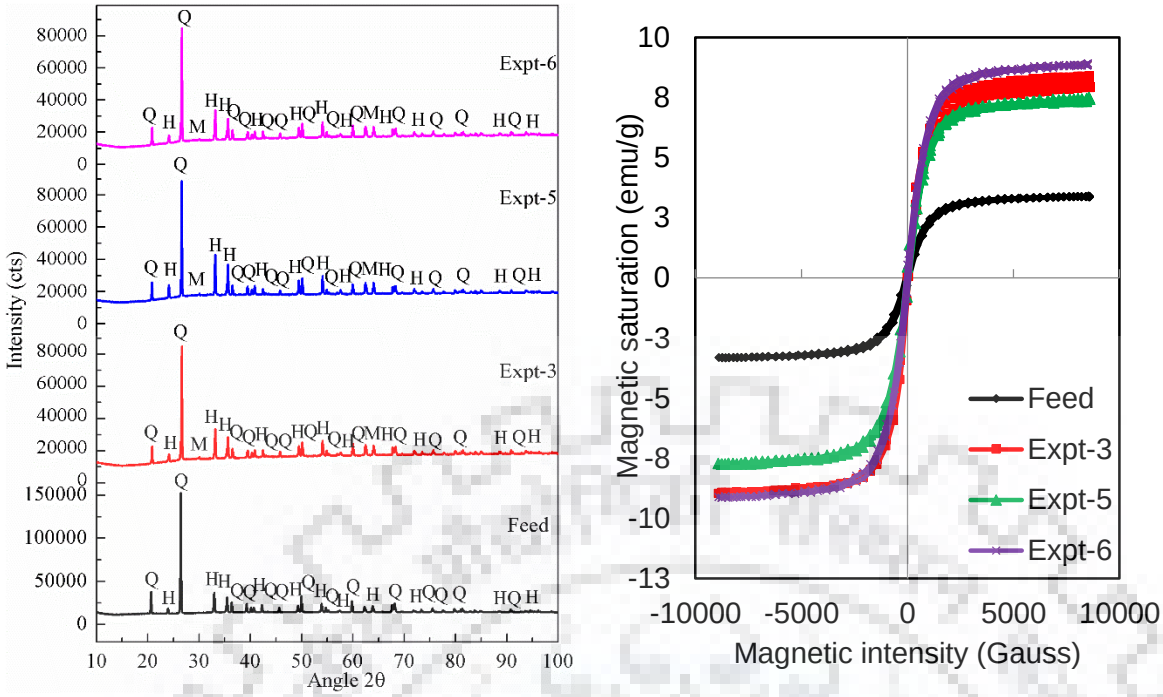

(a) (b)

Figure 4.2.17 (a) XRD plot and (b) VSM plot of the microwave exposed product

Similarly, the ore was subjected to muffle furnace exposure at 500°C to 700°C for 60 min. The iron grade and recovery obtained for the concentrate was~50-60% and 25-65% respectively for both coarse and fine sizes. Iron enrichment was due to the formation of massive random micro cracks in the ore matrix as shown in Fig 4.2.18. It can be seen that significant micro cracks were observed in both microwave and muffle furnace exposed samples because of the different thermal expansion behaviour of quartzite and hematite phase.

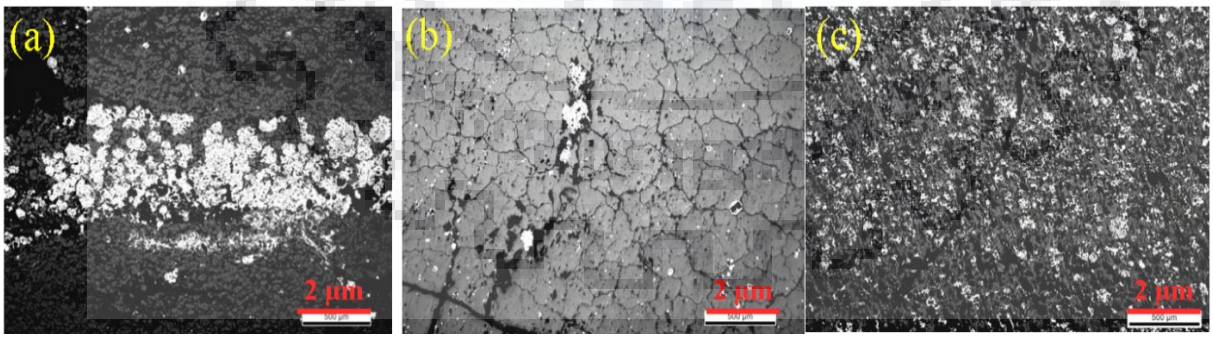

Figure 4.2.18 Optical microscopy of (a) Feed (b) muffle furnace exposed (600°C, 1 h) and (c) microwave exposed (900 W, 10 min)

4.2.4 Reduction roasting of banded iron ores

4.2.4.1 Convectional carbothermal reduction of banded hematite jasper ores

The carbothermal reduction process was pursued to break/unlock the structure. The preliminary experiments were carried out at 500°C, 600ºC and 700ºC for 30 to 90 min at a stoichiometric charcoal dosage of 6 and 9% to delineate the reduction kinetics. However, the reduction of kinetics was not achieved because of the nonlinear trend of grade and iron recovery with temperature and time. This can be attributed to the heterogeneous nature of the BHJ ore and because of the dispersion of impurities throughout the matrix compared to single-phase hematite sample. The iron grade of the magnetic concentrate obtained after reduction is shown in Fig. 4.2.19. The reduction at 600ºC shows better iron grade compared to 700ºC, however, the iron recovery is considerably lower than 700ºC due to a partial reduction of hematite. It is also observed that prolonged reduction leads to a fall in iron grade irrespective of temperature and reductant dosage. Therefore the reduction temperature and range time were selected from 700ºC to 1000ºC, reduction time from 30 to 90 min and reductant dosage as x, 1.5x, 2x where x-denotes the stoichiometric value. Overall the grade is high at low temperatures but the yield and recovery are quite low compared to higher temperatures.

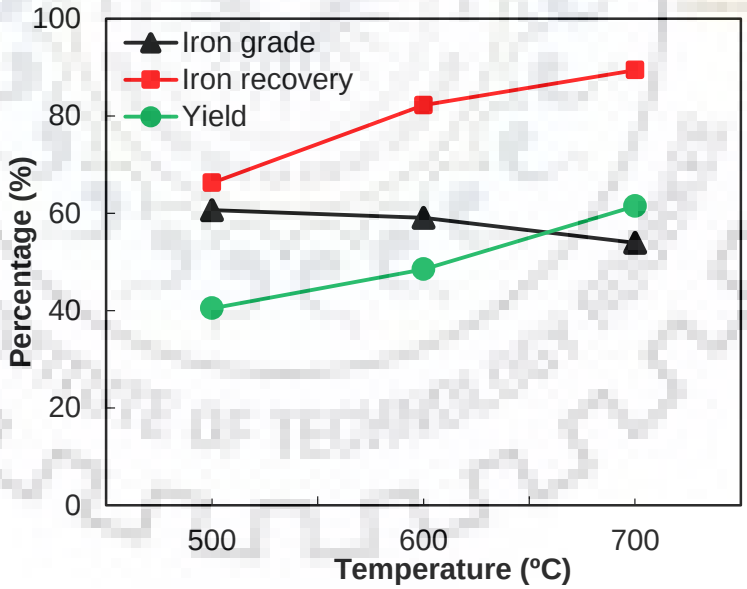

Figure 4.2.19 Effect of reduction temperature and time on iron grade and iron recovery

4.2.4.1.1 Statistical design optimization

The carbothermal reduction process is investigated using a statistical design, Box Behnken method. Temperature, time, and reductant dosage are the main factors and the main objective is to obtain optimal values to maximize iron grade and recovery and evaluating the significant

factor. The boundary values of factors were selected based on the preliminary experiments and are shown in Table 4.2.4. As per the Box-Behnken statistical design, fifteen experiments are conducted including three central points and 12 edge-centered points. All the experimental conditions of the design and the corresponding responses are shown in Table 4.2.5.

Table 4.2.4 Factors and levels of statistical design experiments.

Factor	**Name**	**Unit**	**Coded level values**		
			-1	**0**	**1**
A	Temperature	°C	700	850	1000
B	Time	min	30	60	90
C	Charcoal	%	6	9	12

The experimental values of iron grade and recovery were best-fitted to a modified quadratic model. The statistical parameters i.e., p-value and F-value of the model and individual terms are shown in Table 4.2.6. According to the statistical model, p-value less than 0.05 is desirable for the adequate model. The F value of the modified quadratic model for an iron grade is 6.29 and the p-value is 0.0189 whereas the values for iron recovery are 12.11 and 0.0035 respectively indicating that the models for both iron grade and recovery are statistically significant. In the case of iron grade, temperature, time and temperature^2 are the significant terms, whereas, for iron recovery, temperature and temperature^2 are significant. The empirical formulas or model equation derived from the experimental response for iron grade and iron recovery is, respectively, shown in Eq. (33) and (34). Based on the derived regression equations for iron grade and recovery, the sequence of dominating factors in descending order are shown in Table 4.2.7. As expected, in both cases, the temperature is the dominant factor, whereas, charcoal dosage and reduction of time are less influential factors for both iron grade and iron recovery respectively. The range of response parameters were determined with corresponding to 95% confidence interval. The Optimum Fe grade value obtained from the statistical design slight far away from the upper limit value. Most of the response values were in between the 95% Confidence Interval. Means 95% confidence that the mean population value can exist in between upper and lower limit value.

The actual experimental values were plotted against the model predicted values for both iron grade and iron recovery, shown in Fig.6a and 6b and revealed a good agreement. The contour plots of significant factors for both iron grade and iron recovery are shown, in Fig. 4.2.20a and 4.2.21b respectively. Under given parameters, for obtaining higher iron grade values, lower

temperature and shorter time are recommended irrespective of charcoal dosage, whereas, for high iron recovery values, moderate to low temperature with moderate residence time is favorable.

Table 4.2.5 Experimental design conditions and their respective response.

Run	Factor 1	Factor 2	Factor 3	Response 1	Response 2	Response 3
	Temperature	Time	Charcoal	Grade	Recovery	Yield
	(°C)	(min)	(%)	(%)	(%)	(%)
1	700	90	9	52.9	97.7	72
2	1000	30	9	48.2	21.4	17.3
3	700	30	9	61.2	82	52.3
4	850	30	6	46.5	99.5	83.8
5	700	60	12	52.6	95.7	71.1
6	850	90	6	42.2	99.8	95.7
7	1000	90	9	42	33.2	30.8
8	850	90	12	40.2	94.8	92.1
9	850	60	9	40.9	91.9	87.8
10	1000	60	6	49.8	24.4	19.1
11	850	60	9	42.4	99.5	92
12	700	60	6	51.2	87	66.4
13	850	30	12	44.7	98.7	89.1
14	1000	60	12	48.9	65.7	52.4
15	850	60	9	41	94.6	89.3
Average (Mean)				46.98	79.06	67.41
Std. dev.				5.93	28.78	27.15
(t value*Standered deviation)/Sqrt(sample size)				3.28	15.94	15.04
95% Confidence Interval				46.98 ± 3.28	79 ± 15.94	67.41 ± 15.03

Table 4.2.6 ANOVA for iron grade and iron recovery.

	Iron Grade		Iron Recovery	
Source	F-value	p-value	F-value	p-value
Model	6.29	0.0189	12.11	0.0035
A-Temperature	11.97	0.0135	52.57	0.0003
B-Time	7.73	0.0319	0.6331	0.4565
C-Charcoal	0.1510	0.7110	2.17	0.1914
AB	0.1167	0.7443	0.0336	0.8607
AC	0.1526	0.7096	2.36	0.1756
A^2	30.06	0.0015	36.51	0.0009
B^2	0.6179	0.4617	0.3745	0.5630
C^2	0.2326	0.6467	1.28	0.3013
Lack of Fit	16.67	0.0574	10.89	0.0859

$$Fe_{Grade} = 347.3 - 0.657 \times Temperature - 0.353 \times Time - 0.529 \times (Charcoal\ dosage) + 8.25 \times 10^{-2} \times (Charcoal\ dosage)^2 - 1.28 \times 10^{-3} \times Temperature \times (Charcoal\ dosage) + (3.75 \times Temperature^2 + 13.44 \times Time^2 + 1.12 \times Temperature \times Time) \times 10^{-4}\ (R^2=0.89) \quad (33)$$

$$Fe_{Recovery} = -674.67 + 2.19 \times Temperature + 0.73 \times Time - 26.05 \times (Charcoal\ dosage) + 0.69 \times (Charcoal\ dosage)^2 + 1.81 \times 10^{-2} \times Temperature \times (Charcoal\ dosage) - (1.48 \times Temperature^2 + 3.76 \times Time^2) \times 10^{-3} - 2.16 \times 10^{-4} \times Temperature \times Time\ (R^2=0.94) \quad (34)$$

Table 4.2.7 Impact sequence of factors for iron grade and recovery

Response	First	Second	Third
Iron grade	Temperature	Time	Charcoal dosage
Iron recovery	Temperature	Charcoal dosage	Time

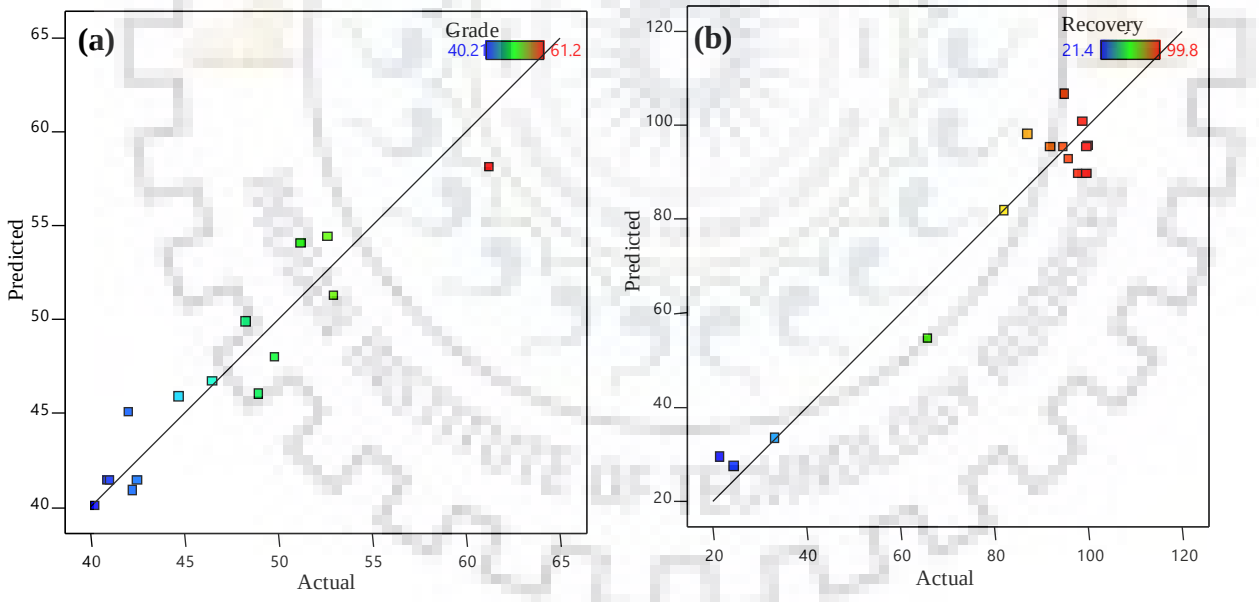

Figure 4.2.20 Predicted vs. actual values of the reduction experiments (a) Iron grade and (b) Iron recovery.

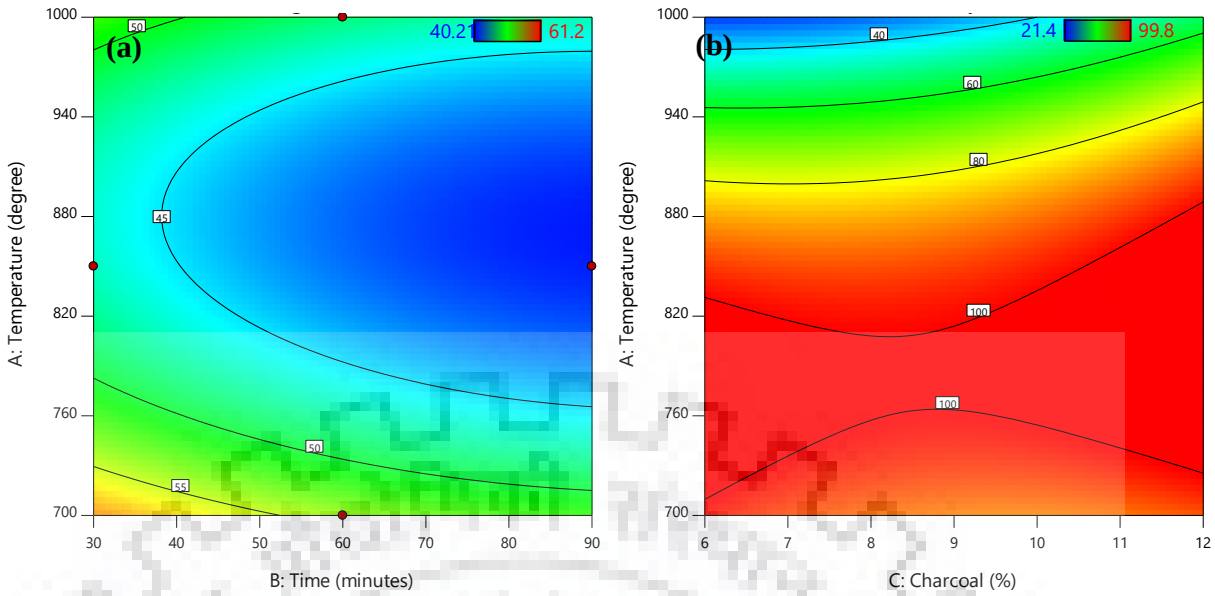

Figure 4.2.21 Contour plots of the significant factors for (a) Iron grade and (b) Iron recovery.

The effect of phase composition on iron grade and recovery of the product is also investigated using the XRD spectra. Fig.4.2.22 shows the XRD analysis of the feed and the magnetic concentrate of experiments 1, 3, 10, 11 and 12. These experiments were selected as they represent each temperature level. It is evident that at lower temperatures, partial reduction of hematite to magnetite occurs and the magnetite fraction increases with prolonged reduction. The substantial presence of quartz phase at a lower temperature indicates that quartzite strongly adheres to the untreated hematite. At higher temperatures, the reduction rate increases leading to an increase in the magnetite phase. At 1000°C, the complete reduction of the magnetite to wustite phase was observed as hematite and magnetite peaks were not observed. However, the presence silica and adequate temperature lead to a reaction between wustite and silica (Eq. 12) resulting in the formation of fayalite "a paramagnetic" phase and causes the ineffective separation resulting in the fall of iron grade, recovery, and yield of the magnetic concentrate. The average iron grade and recovery along with the major iron phases formed during reduction at different temperature levels are shown in Table 4.2.8 to delineate the effect of temperature. It is evident that the phases formed during reduction depend on the reduction temperature and significantly influence the iron grade and recovery of the magnetic concentrate.

The VSM analysis of the feed and the magnetic fractions of experiment 1, 3, 10, 11 and 12 are shown in Fig. 4.2.23. There is a distinct difference in the saturation magnetization of the feed and the reduced sample. The saturation magnetization value increases from 5 to 27 emu/g at reduction conditions of 700°C, 90 min and 9% charcoal. At 700°C with an increase in reduction time, the magnetite fraction in the concentrate increases leading to high saturation values,

whereas, on the other side, the formation of the fayalite phase decreases the magnetization value. Based on the saturation magnetization values and iron grade of the respective magnetic product, it can be inferred that the magnetization value is independent of the iron grade but the presence of iron-bearing phase significantly influences the magnetization value.

Table 4.2.8 Summary of concentrate obtained at different temperatures

Temperature (°C)	Average grade (%)	Average recovery (%)	Average yield (%)	Phases present
700	54.5	90.6	65.4	Hematite, Magnetite
850	42.5	97	90	Hematite, Magnetite
1000	47.2	36.1	30	Fayalite, Wustite

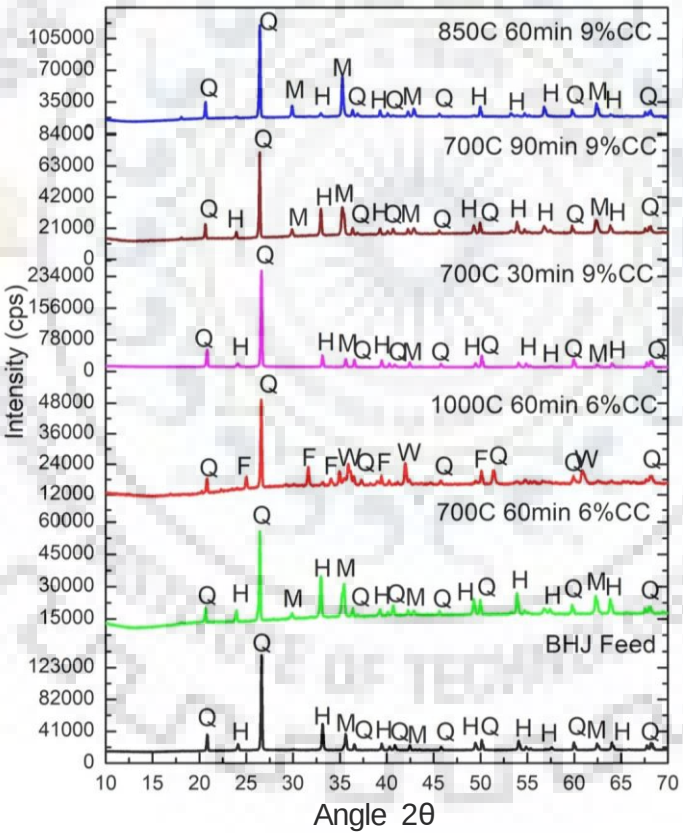

Figure 4.2.22 XRD plot of the feed and magnetic concentrate of different experiments.

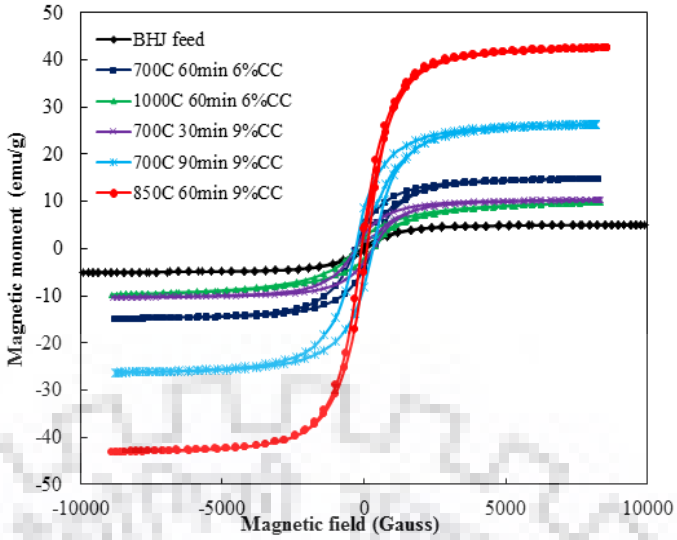

Figure 4.2.23 Hysteresis loop of the feed and magnetic concentrate of different experiments

4.2.4.1.2 Effect of particle size

The influence of particle size on the reduction behavior was investigated at optimal experimental conditions (700°C, 30 min, 9% charcoal). The carbothermal reduction was performed on the closed sizes of 6.3×4.75, 4.75×3.34, 3.34×2.38, 2.38×1, 1×0.5, 0.5×0.312, 0.312×0.2 and 0.2×0.1 mm. The iron grade, recovery, and yield of the magnetic concentrate of different size fractions are shown in Fig. 4.2.24. The geometric mean particle size is considered for the size variation plot along with actual grade, recovery, and yield of the magnetic concentrate. It is expected that the reduction of iron oxide occurs by the diffusion of carbon dioxide-carbon monoxide gas in the underlying matrix at an investigated temperature as solid carbon starts burning above 600ºC leading to the formation of CO-CO_2 gas. The governing factor for diffusion rate is the effective surface area available for diffusion. With the increase in the particle size, the total internal surface area decreases which reduces the diffusion rate. As expected, the iron grade falls with increment in particle size (~61% to ~55%). However, iron recovery and yield values increase with the increase in particle size increases. The ineffective diffusion of gaseous reductant results in only partial reduction of hematite and the unreduced region intimately bonded with the silica also gets trapped in the magnetic concentrate with reduced iron phases. However, the significant fall in the iron grade in the size range of 0.2 to 2 mm is due to the formation of an iron-rich fused mass with a lustrous metallic shine as shown in Fig 4.2.24 and Fig 4.2.25c. It is important to mention that this fraction is ductile in nature and was hand separated using T magnet from the reduced mass. The EDS analysis revealed that the composition is comparable to the direct reduced iron (DRI) formed during the conventional iron ore sintering process and is rich in iron content (~84%) along with carbon (~5.3%), silicon (~3.9%) and oxygen (~6.8%). The optical micrograph

of the same mass suggests the formation of a flake-like structure consisting of martensite structure as shown in Fig.4.2.25 a, b. The elemental mapping of the surface of the fused mass compliments the EDS result and shows that the carbon, silicon, and oxygen are dispersed all over the iron matrix. The XRD analysis of the reduced product corresponding to different sizes indicates that hematite and magnetite are the major iron-bearing phases at all the particle sizes and therefore was not plotted. The XRD analysis of the fused mass indicates the ferrite peaks with some quartz. With the increase in particle size, the iron grade, recovery, and yield, remains fairly stable ~55%,~95% and 70% respectively. However, for finer particle size (minus 75 µm), there was distinct difference in iron grade, recovery and yield and fused mass was not considered in this curve. The average hardness value measured for the fused sample was ~392 HV on a Vickers hardness scale using 10kgf load.

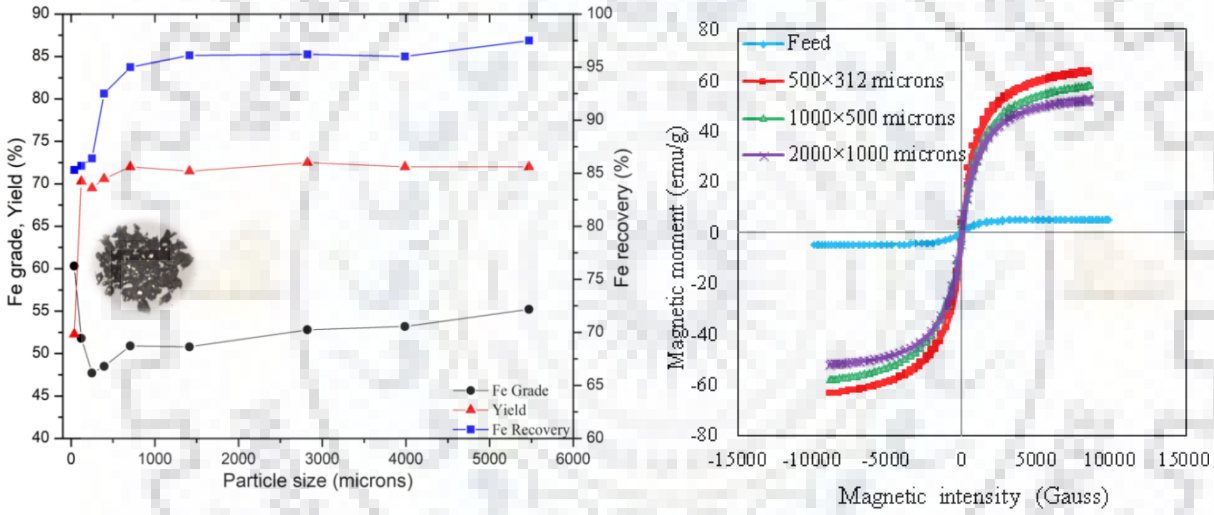

Figure 4.2.24 (a) Effect of particle size on iron grade, recovery, and yield (b) Hysteresis loop of the feed and magnetic concentrate at 700°C, 30 min, 9% Charcoal

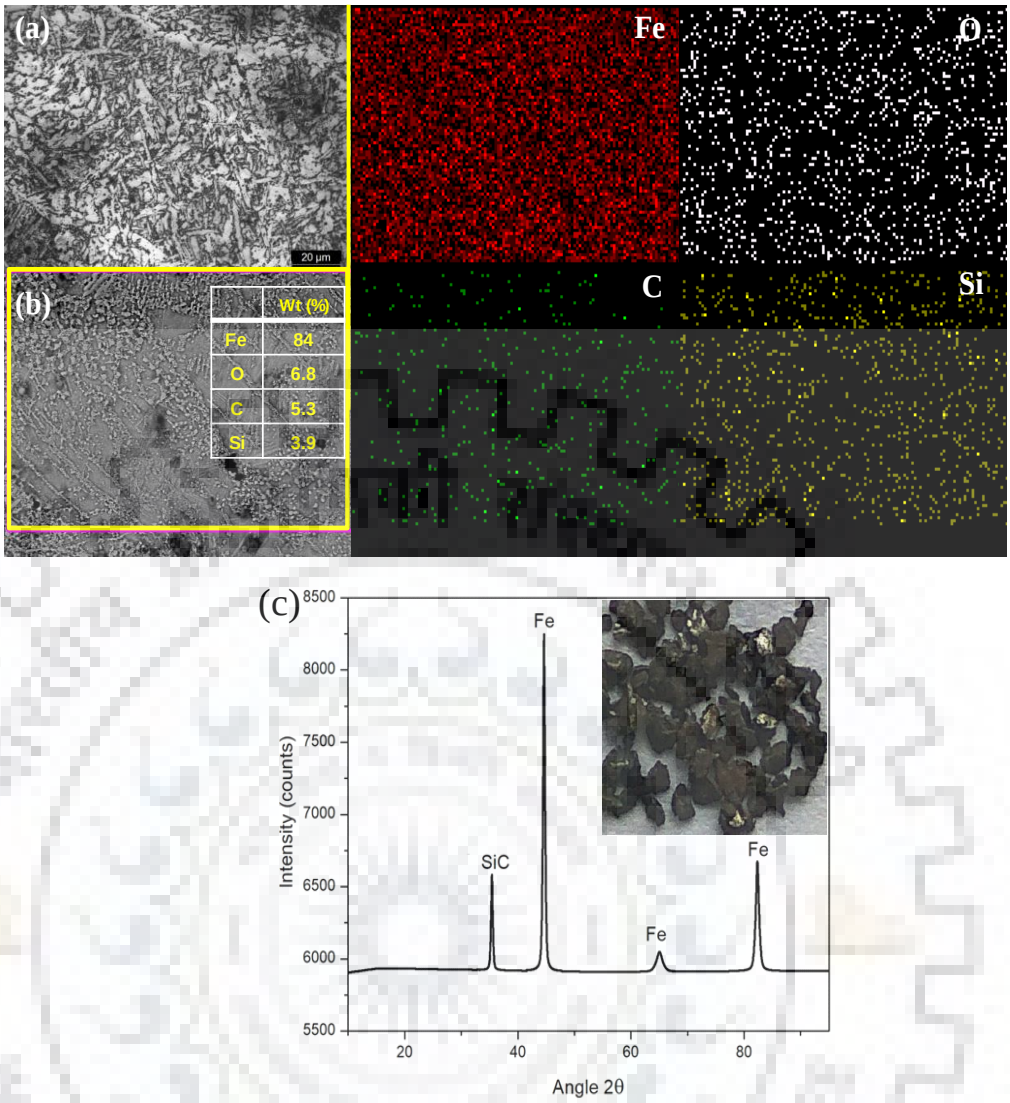

Figure 4.2.25 (a) Optical microscopy and (b) elemental mapping of the fused mass (c) XRD plot of fused mass (700°C, 2000×1000 microns, 9% charcoal, 30 min)

The elemental mapping of the reduced product is shown in the Fig.4.2.26. The distribution of different elements is Fe, Oxygen, silica and, carbon values. The SEM (backscattered image (BSE))–EDAX analysis of as such reduced product reflects the distribution of various transformed phases such as wustite and silicon oxide phases. The highlighted area (1&3) denotes the wustite and area (2&4) denotes the silicon oxide phase. During reduction, hematite is converted to magnetite and further reduced to wustite which is partially converted to ferrite and fayalite (FeO_x).

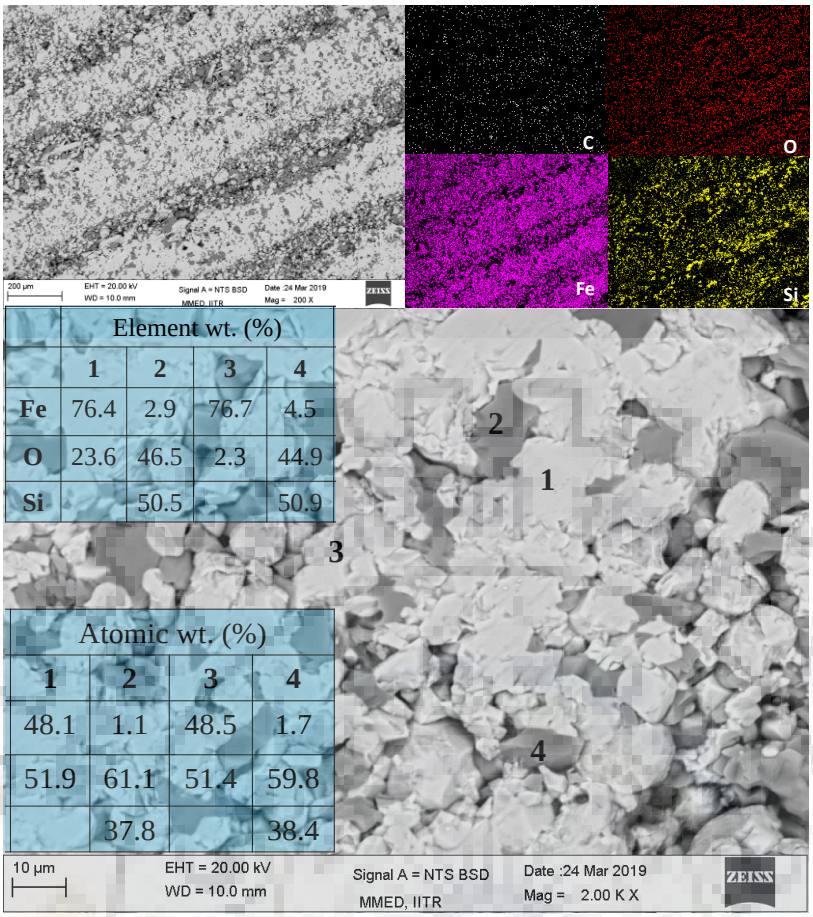

Figure 4.2.26 BSE image EDAX and atomic (%) of reduced product at 700ºC, 30 min and 9% charcoal (1&3. Wustite, 2&4. Silicon-rich phase)

4.2.4.1.3 Reductant evaluation

Considering the cost considerations associated with the use of activated charcoal, alternative carbon sources such as coconut shell (~50% C) and cow dung (~35% C) corresponding to 9% carbon were also investigated for carbothermal reduction. The reduction experiments were conducted at the optimized condition, 700ºC, 30 min, and stoichiometric equivalent carbon (9%). The iron grade-recovery and yield of the magnetic concentrate for different reductants is shown in Fig. 4.2.27 a. As expected, charcoal is the favorable reductant in terms of iron grade but offers low recovery and yield compared to other reductants. The XRD analysis suggests that similar phases were observed in all reductants, however, the quantity of phase fraction is slightly different in the final product. The non-volatile components of alternative reductants also consume a significant amount of thermal energy which decreases the rate of reduction and causes lower iron enrichment.

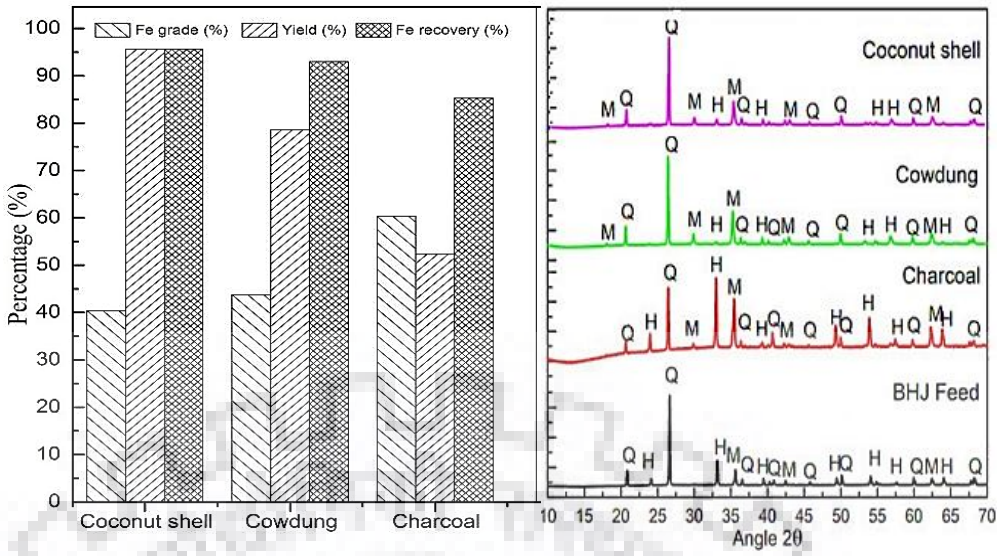

Figure 4.2.27 Reductant variation and XRD analysis at optimal condition (700°C, 30 min, 9% charcoal, minus 75 microns)

4.2.4.2 Microwave carbothermal reduction of banded hematite jasper ore

4.2.4.2.1 Effect of time and charcoal dosage

Fig. 4.2.28 shows the variation in iron grade and recovery with charcoal dosage for an exposure time of 6 and 10 min respectively. In the case of 6 min exposure time, the iron grade initially increases with charcoal dosage and subsequently falls, whereas, in 10 min, the iron grade is confined to small variation. Based on grade and recovery, the optimum carbon dosage is observed as 8% for 6 min whereas for 10 min there is no definite trend. However, the yield of magnetic concentrate initially shows a random trend followed by a steep rise at a higher dosage in both time durations. Fig. 4.2.29 shows the XRD spectra of the magnetic concentrate obtained at different experimental conditions. On the comparison between 6 and 10 min, the lower iron grade at prolonged exposure due to the interaction of iron phases with the quartzite which leads to the formation of fayalite phase as confirmed by the XRD analysis. Also, the lower charcoal dosage leads to the incomplete reduction which explains the initial random trend in iron grade and recovery values in Fig. 4.2.28. The fall in iron grade can be attributed to the formation of ferrite balls which are not accounted in the magnetic concentrate. It is worthwhile to mention that ferrite balls were handpicked and separated using a powerful T-magnet.

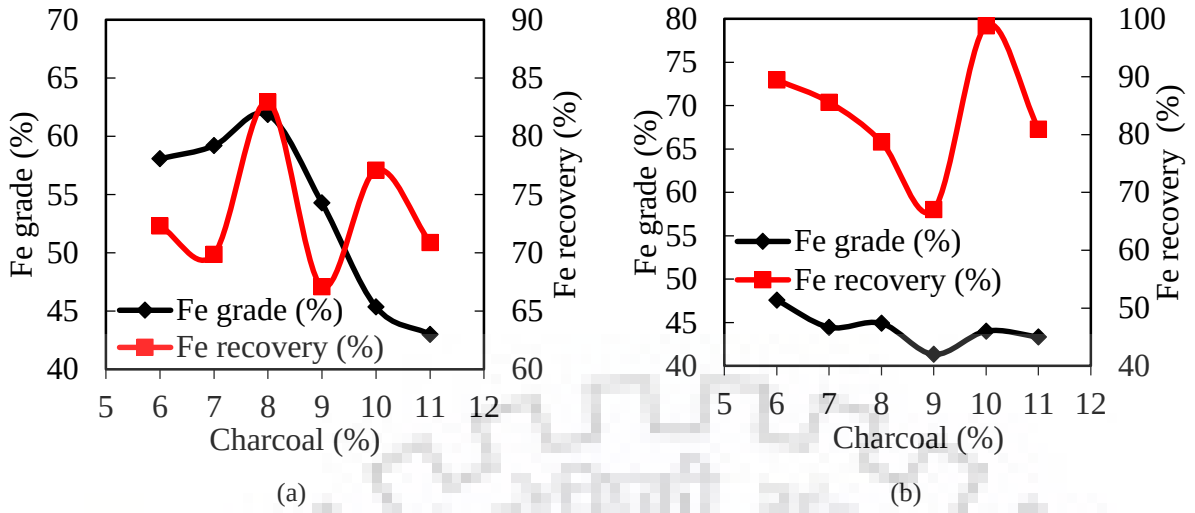

Figure 4.2.28 Effect of charcoal dosage on grade and recovery for (a) 6 min and, (b) 10 min.

The reaction of magnetite to form wustite is undesirable in the context of the magnetizing process as wustite is paramagnetic and therefore will be unresponsive to subsequent low-intensity magnetic separation (Iwasaki and Prasad, 1989). The sufficient amount of bonded silica content in the BHJ ore leads to the easy formation of the fayalite phase. The formation of fayalite suggests that direct reaction between magnetite or wustite and silica as per Eq. 11 and 12 respectively. It appears that magnetite stability is particularly sensitive to changes in reductant addition as magnetite readily undergoes further reduction to form wustite.

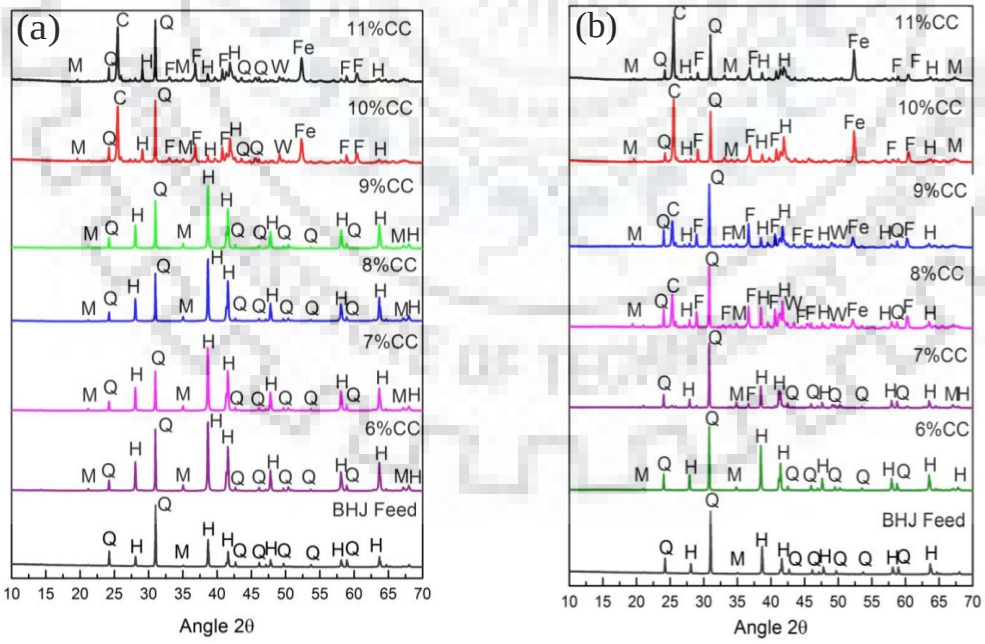

Figure 4.2.29 XRD spectra of microwave reduced magnetic concentrate of BHJ sample for 6 min and 10 min (M- Magnetite, Q- Quartz, H- Hematite, F- Fayalite, C- Cristobalite, Fe- Ferrite).

The quantitative XRD analysis of magnetic concentrate obtained at varying charcoal dosage for 10 min exposure for different time intervals at 11%C is shown in Fig. 4.2.30 (a & b). The

formation of fayalite, wustite, ferrite, and cristobalite occurs above 9% charcoal for 6 min, whereas, in the case of 10 min reduction; wustite ferrite, cristobalite, and fayalite occurred above 7% charcoal. It can be seen that with an increase in charcoal dosage the hematite phase fraction reduces drastically from 54.5% to 12.2%. A stepwise sequential of iron oxide reduction can be observed with an increase in charcoal dosage. The hematite initially reduces to magnetite at 6 and 7% charcoal and the magnetic fraction comprises mainly two iron phases. With the increase in charcoal dosage, wustite formation is observed along with fayalite ($2FeO.SiO_2$) phase which is complemented by a decrease in hematite fraction, and ferrite formation is also initiated. With further increase in charcoal dosage, the ferrite phase increases, whereas, the hematite phase decreases. The quartzite impurities were trapped in the magnetic concentrate in the form of cristobalite and it can be inferred that cristobalite formation restricts the fayalite formation. Also, the wustite fraction increases with a decrease in the fayalite fraction depicting that the wustite phase interacts with the quartz to form fayalite. The decrease in Fe grade and Fe recovery of the magnetic concentrate with an increase in charcoal dosage is due to the formation of ferrite balls.

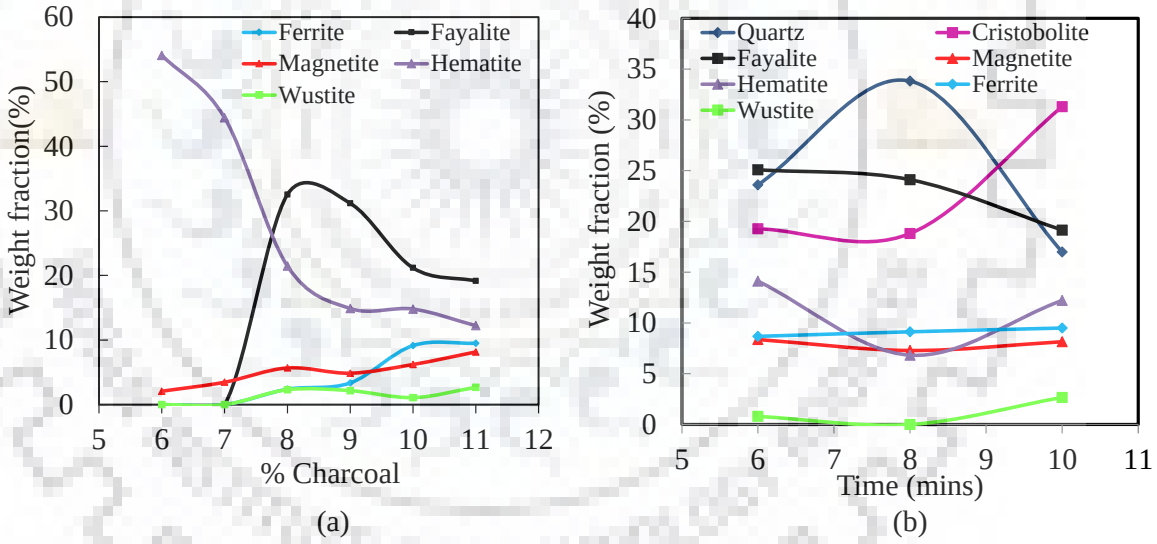

Figure 4.2.30 Quantitative XRD analysis of phase fraction for (a) different charcoal dosage at 10 min reduction time and, (b) different exposure time at 11% charcoal dosage.

Surprisingly, at the higher charcoal dosage, the formation of metallic spherical balls of size 1±0.5 mm is observed in the product. The actual photograph of the reduced product showing the metallic balls and the optical micrograph of a typical metallic ball is shown in Fig. 4.2.31. The micrograph clearly reveals the retained austenite and martensitic iron phase in the ball due to rapid cooling during water quenching post-reduction. The average hardness value recorded on the Vickers hardness scale for ferrite ball is around 302 HV indicating low carbon martensitic product. The balls formed during the experiment are separated from the product and it is not

accounted for in the magnetic concentrate. The elemental mapping of the reduced product containing ferrite balls is shown in Fig. 4.2.31. It can be clearly seen that the ball surface comprises iron which complements the optical microscopy observation whereas the surrounding area consists of segregation of silica and iron values.

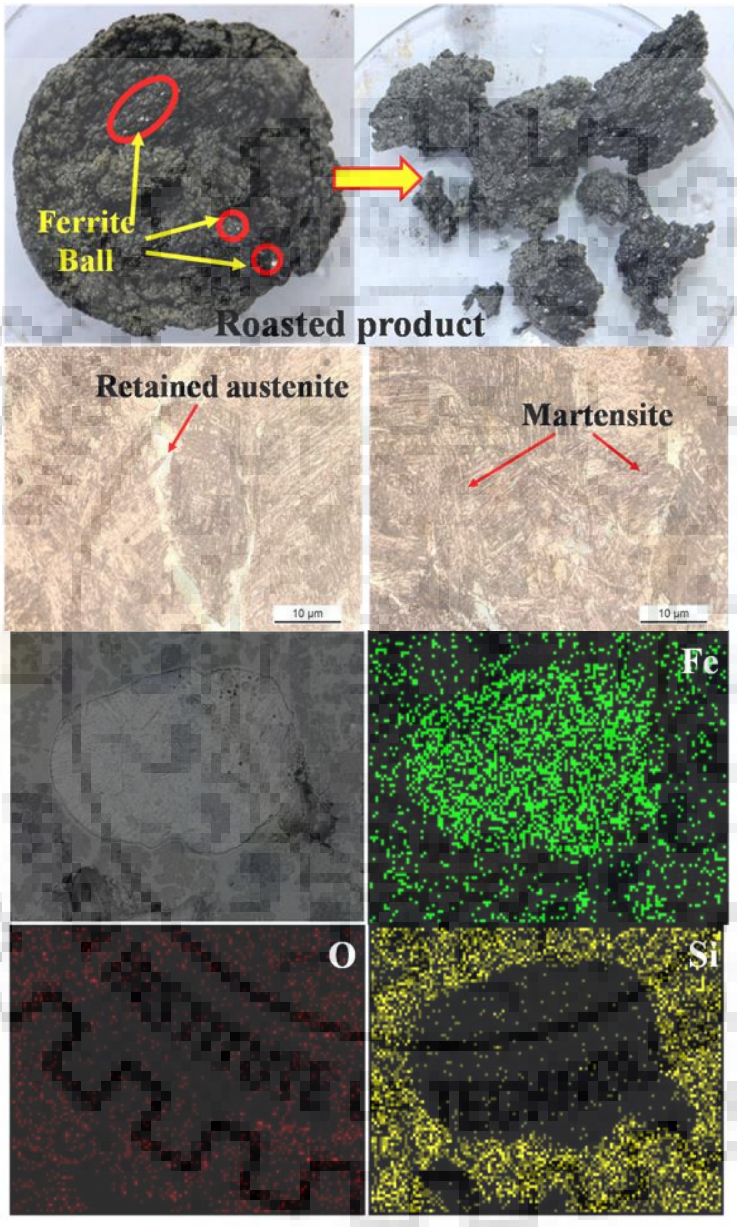

Figure 4.2.31 Photograph of the reduced product with enriched metallic balls, an optical micrograph of the ball, and the elemental mapping of the reduced product

Next, the magnetic characteristic of the concentrate was evaluated using VSM. The hysteresis loop obtained from the VSM analysis of the feed, magnetic, non-magnetic and ferrite balls obtained at 11% C, 10 min and are shown in Fig. 4.2.32a. The saturation magnetization of the material depends upon the phase fraction of the material. The saturation magnetization of feed is

5.02 emu/g, whereas, the magnetic and non-magnetic product is 32.87 and 0.86 emu/g respectively. The significant increase in the magnetization can be due to the occurrence of magnetic iron phases. It is known that the pure iron at room temperature possesses a magnetization of 217.6 emu/g (Crangle and Goodman, 1971). The ferrite balls formed during carbothermal reduction has a magnetization of 190.4 emu/g and based on the magnetization property the purity of ferrite balls is approximately 88%. Fig. 4.2.32b shows the saturation magnetization of the magnetic concentrate at different charcoal dosage for different microwave reduction times. It can be observed that the saturation magnetization values increases with the charcoal dosage for both time durations. However, a considerable increase in the values above 9% C is observed is attributed to the formation of magnetite and ferrite phase.

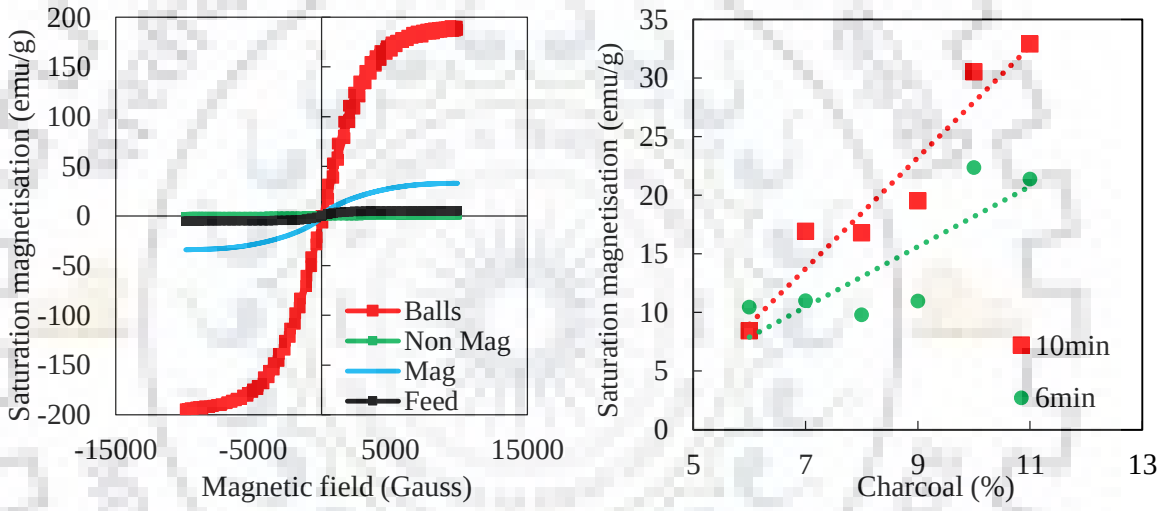

Figure 4.2.32 a) Hysteresis plot of the feed and the product (Magnetic, Non-magnetic and balls) at 11%C for 10 min exposure time and b) Magnetic susceptibility of the magnetic concentrate.

4.2.4.2.2 Effect of microwave power and cooling method

The effect of microwave power on the iron grade and recovery was investigated at 360, 540 and 720 W for 10 min at 11% charcoal dosage as shown in Fig. 4.2.33a. The iron grade shows a decreasing trend from ~55% at 360W to ~44% at 900 W, whereas, iron recovery initially increases and subsequently falls. The formation of ferrite balls i.e., accumulation of iron values at higher microwave power (900 W) leads to a deficiency of iron values in the magnetic product and the occurrence of fayalite phase further leads to falling off in iron grade at higher power. It can be observed that iron grade significantly falls with microwave power because of the formation of magnetic phases such as ferrite ball observed at 900 W. The optimal condition based on ferrite ball formation is at 900 W, however, with grade perspective optimal microwave power of 360W yields a suitable concentrate (55% Fe_G, 60% Fe_R with 40% yield). Based on the

systematic investigation of influential factors such as time and charcoal dosage, towards the ferrite ball formation, next the effect of the cooling method post-reduction was pursued. These experiments were conducted at 10 min reduction time and 11% charcoal dosage to evaluate the response of the cooling method on the formation of different iron phases. As shown in Fig. 4.2.33b, it is observed that there are not many changes in the iron phases except slight variation in peak intensity. The non-lid with quenching cooling method is found appreciate for ferrite formation with respect to peak intensity.

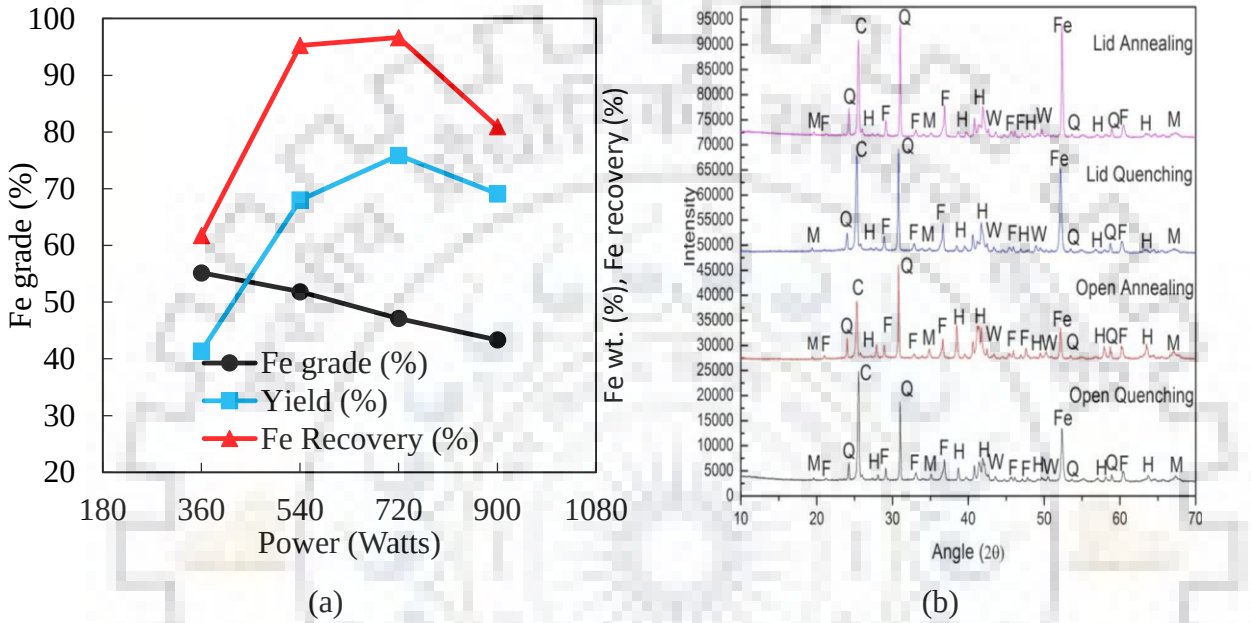

(a) (b)

Figure 4.2.33(a) Effect of microwave power on iron grade, yield, and recovery (10 min, 11% charcoal) (b) XRD analysis of magnetic concentrate at 10 min, 11% charcoal for different cooling environments.

4.2.4.2.3 Design optimization of BHJ through microwave reduction

The carbothermal reduction was pursued using a Taguchi statistical design in a variable power microwave environment. The experimental parameters investigated are microwave power, exposure time and charcoal dosage. The experimental conditions and the response of iron grade and recovery of the Taguchi L_9 orthogonal design are listed in Table 4.2.9. The responses were analyzed using Signal to Noise (SN) ratio with maximum optimization criterion, implying higher the value the better is the response. The range of response parameters were determined with corresponding to 95% confidence interval. Means 95% confidence that the mean population value can exist in between upper and lower limit value.

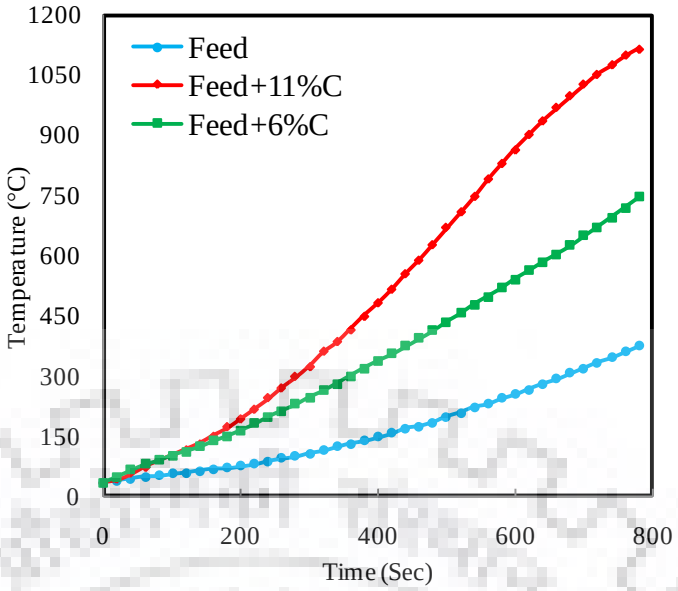

Figure 4.2.34 Time-temperature plot of feed-charcoal mixture in a microwave furnace (800 W).

Table 4.2.9 Experimental design conditions and associated responses.

Expt.	Time (min)	Reductant (%)	Power (W)	Temp. (°C)	Grade (%)	Recovery (%)	Yield (%)
1	8	6	540	403	58.45	68.81	43.56
2	10	6	720	482	58.75	67.91	42.76
3	12	6	900	659	60.87	74.37	45.2
4	8	9	720	638	61.67	73.44	44.04
5	10	9	900	855	55.85	85.44	56.6
6	12	9	540	851	53.84	73.7	50.7
7	8	12	900	>1100	49.15	89.32	67.2
8	10	12	540	>1100	51.38	82.92	59.7
9	12	12	720	>1100	42.5	77.5	67.5
Average (mean)					54.72	77.05	53.03
Standard deviation (s)					5.86	6.98	9.48
(t value*Standard deviation)/Sqrt(sample size)					4.51	5.36	7.29
95% Confidence Interval (95% CI)					46.98 ± 3.28	79 ± 15.94	67.41 ± 15.03

$$\mathrm{Fe_{Recovery}}\ (\%) = \frac{(\mathrm{Fe_{Grade}\ X\ Weight})_{\mathrm{magnetic}}}{(\mathrm{Fe_{Grade}} \times \mathrm{Weight})_{\mathrm{feed}}} \times 100 \qquad (35)$$

$$\mathrm{Yield}\ (\%) = \frac{\mathrm{Weight_{magnetic}}}{\mathrm{Weight_{Total}}} \times 100 \qquad (36)$$

It can be observed from Table 4.2.35 that increasing reductant dosage leads to an increase in temperature, decreasing grade, and higher iron recovery. The iron grade varies between 42.5 and 61% Fe, whereas, for iron recovery, the range is confined to 67 to 90%Fe. The plot of means of individual factors of the L_9 statistical design for iron grade and recovery are shown in Fig. 6a and 6b respectively. For the iron grade, it can be seen, that on increasing the exposure time and

reductant dosage, initially the SN ratio increases slightly and on boundary condition, it falls below mean value. However, the factor power shows an opposite trend and the SN ratio increases considerably at a maximum power of 900 W. For iron recovery, on increasing the time from low to middle level, the SN ratio increases and on further increases to the maximum level the value decreases significantly and falls below the mean value. This can be attributed to the occurrence of fayalite at higher time and magnetite at lower time intervals. The factor power shows a similar trend as in iron grade, whereas, the SN ratio shows an increasing trend with reductant dosage. Higher charcoal dosage leads to increased absorption of microwaves resulting in high temperature. It is observed that the charcoal dosage is the most influential factor and time is the least influential factor for both iron grade and recovery over the examined range. Surprisingly the ferrite ball formation was also observed in two design experiments (Expt. 7 and 9).

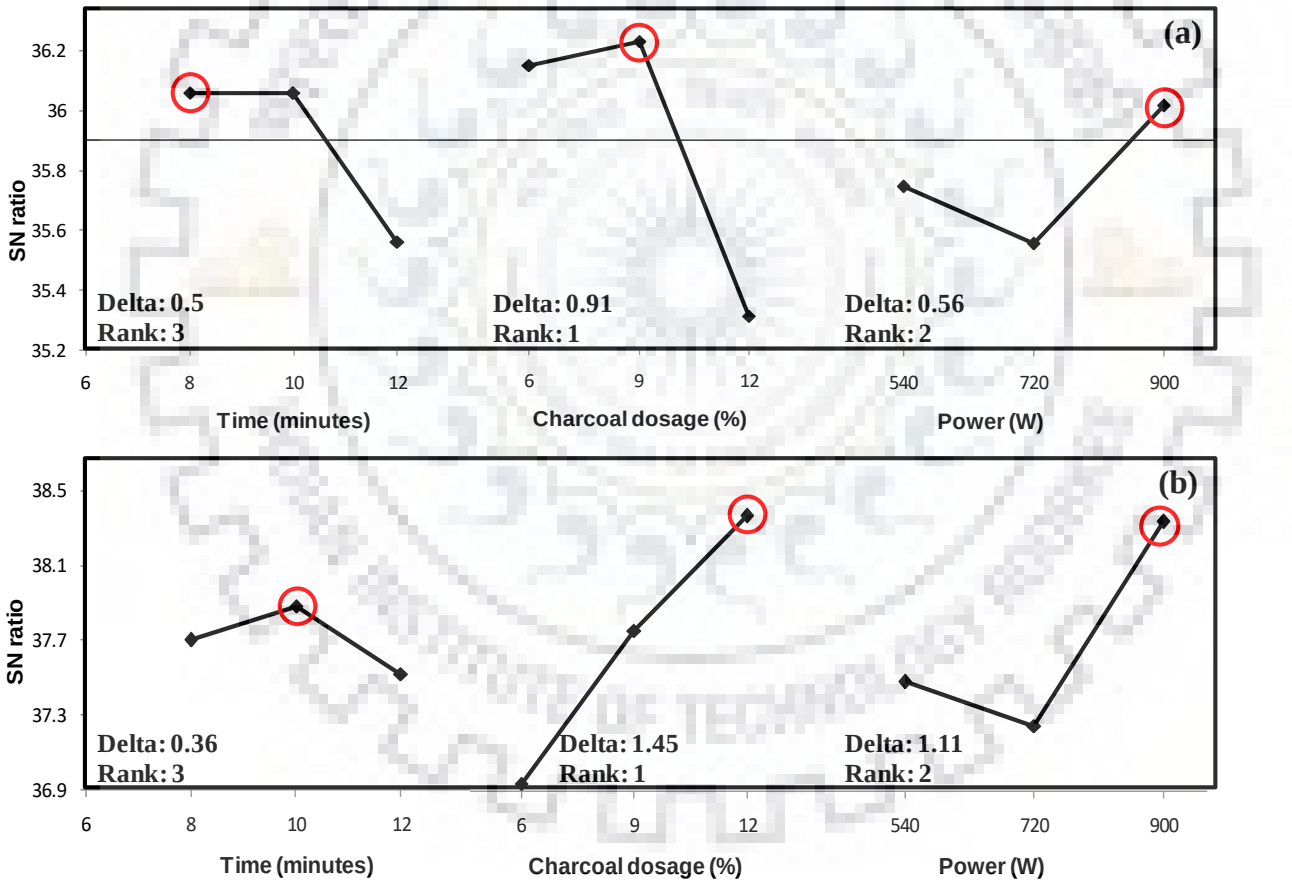

Figure 4.2.35 Main effects plot of SN ratios for (a) iron grade and (b) iron recovery; at optimum condition (8 min, 9% charcoal, and 900 W) for maximizing recovery.

Fig. 4.2.36 and 4.2.37 show the contour plots for iron grade and recovery with significant experimental factors based on delta values. It is evident that low charcoal dosage is favorable for the high iron grade with the moderate power of 540 to 800 W. It is observed that the iron grade

falls from ~ 60% at 6% charcoal to ~ 42% at 12% charcoal. High charcoal dosage leads to an increase in the attained temperature resulting in the formation of fayalite phase as confirmed by the XRD analysis. Fayalite phase formation leads to an accumulation of quartzite values in the magnetic concentrate and thereby decreasing iron grade. Lower exposure time and charcoal dosage are desirable for the higher iron grade as shown in Fig.7b.The presence of quartzite impurities in the feed leads to interaction between the iron phase and impurities during prolonged exposure at high temperature. The effect of reductant dosage and power on the iron recovery in the magnetic concentrate is shown in Fig. 8. The recovery value increases from approximately 68% to 89% diagonally in the graph. The temperature attained at different power levels shows considerable difference i.e., 400°C and 1200°C respectively. This indicates that at lower temperature there is no variation in the iron phase hence, resulting in lower iron recovery whereas at a moderate temperature the formation of magnetite and ferrite phase leads to iron enrichment in the concentrate. Fig. 8b shows the variation of iron recovery with power and time and it can be observed that higher recovery is achieved at high microwave power and low time.

The regression equation derived for iron grade and recovery based on experimental response with all the factors is shown in Table 4.2.10. The statistical fit "R^2" for both the equations indicate the adequateness of the derived model. The optimal condition for maximizing iron grade is determined according to the statistical main effect plot (Fig. 6, marked as a circle); 900 W, 9% charcoal, and 8 min and for iron recovery; 900 W power, 12% charcoal, and 10 min. The obtained magnetic concentrate consists of ~50.5%Fe, ~67.5% recovery at a yield of 49.5% along with the formation of ferrite balls. It is important to mention that grade varies considerably due to the formation of paramagnetic phases (such as Wustite (W), Fayalite (F)), and does not follow the linear trend as reflected by low R^2 value.

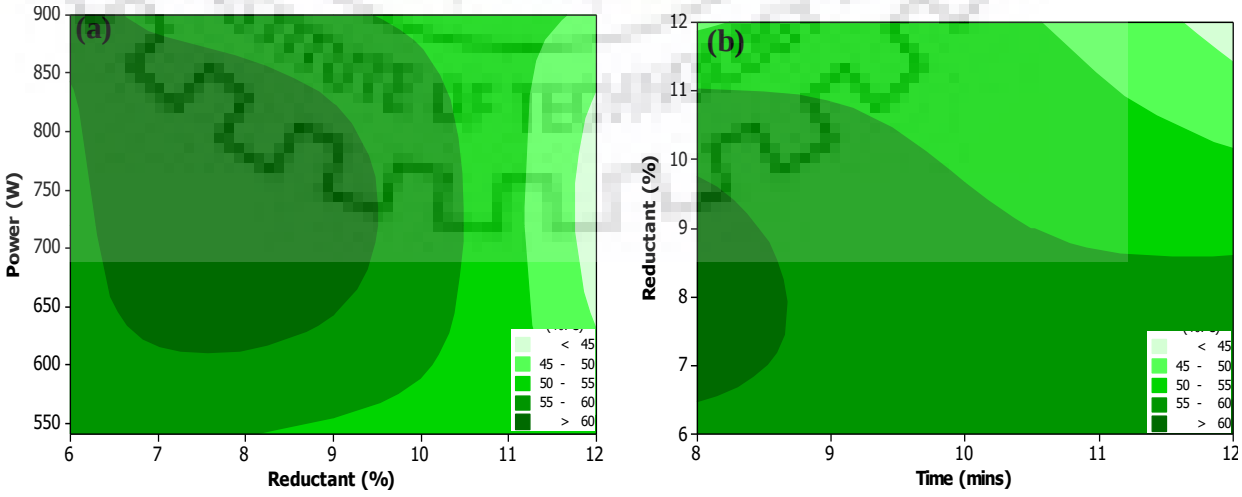

Figure 4.2.36 Contour plots for the iron grade with (a) reductant and power, (b) time and reductant.

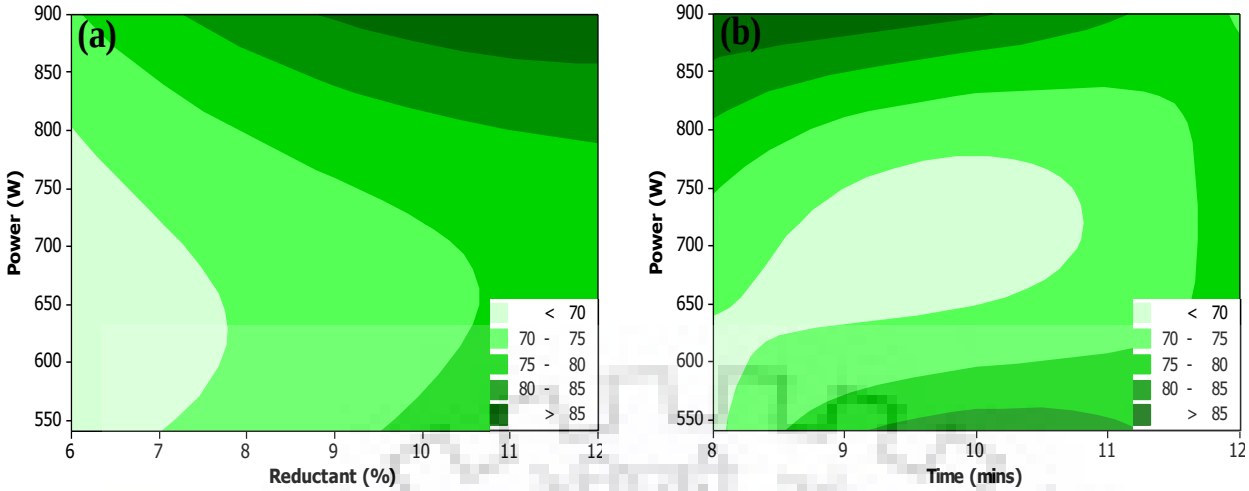

Figure 4.2.37 Contour plots for iron recovery with (a) reductant and power (b) time and power.

Table 4.2.10 Regression equation for iron grade and recovery based on statistical design.

Response	Equation
Iron Grade	Fe_{Grade} = 80.8 - 1.01×Time - 1.95×Reductant + 0.0020×Power (R^2=0.74) (37)
Iron Recovery	$Fe_{Recovery}$ = 46.9 - 0.500×Time + 2.15×Reductant + 0.0219×Power (R^2=0.79) (38)

The XRD plot of the magnetic concentrate with highest and lowest iron grade concentrates are shown in Fig. 4.2.38. At reduction conditions of 720 W, 8min, and 9% C, hematite was the major iron-bearing phase along with the magnetite. It is important to mention that there was no significant phase change at this condition, however, the iron grade increases to ~62%. The iron enrichment can be attributed to the effective separation between the strongly bonded iron and quartzite phase. The microwave irradiation results in selective heating of iron phases which weakens the underlying bond with impurities. It is observed that the temperature was increased to approximately 650°C only and also the shorter duration of exposure was not sufficient for complete reduction of hematite to magnetite. However, the hematite phase leads to lower iron recovery and yield of the magnetic concentrate as hematite phase is paramagnetic. On increasing the charcoal dosage and exposure time, the temperature rises above 1000°C leading to the formation of fayalite and ferrite phase as revealed by XRD analysis. At conditions of 900 W, 8min and 12%C, the iron grade increases to ~49% with a recovery of ~90%. The XRD plot shows that hematite is partially reduced to magnetite, fayalite and ferrite phase. The formation of fayalite phase leads to accumulation of quartz which reduces the iron grade whereas the formation of ferromagnetic phases such as magnetite and ferrite significantly increases the iron recovery. On reducing the charcoal dosage to 6% and increasing the exposure time at the same

power, it is observed that the temperature was restricted to 650°C resulting in no phase change. It was observed that the quartz phase transforms into cristobalite phase above 650°C. The hematite present in the feed was partially reduced to magnetite leading to morphological alteration of the ore resulting in enhanced separation of iron phase from the impurities. The peak intensity of the quartz phase decreases significantly which leads to corresponding enrichment of hematite and magnetite phases in the product. Fig. 4.2.39 shows the variation in grade-recovery and yield values with the attained temperature. It was observed that the occurrence of hematite and magnetite phases leads to iron enrichment, however, it leads to poor recovery and yield. However, above 750°C, the formation of fayalite phase leads to falling in iron grade although the recovery and yield increases due to structural breakdown of matrix leading to better separation.

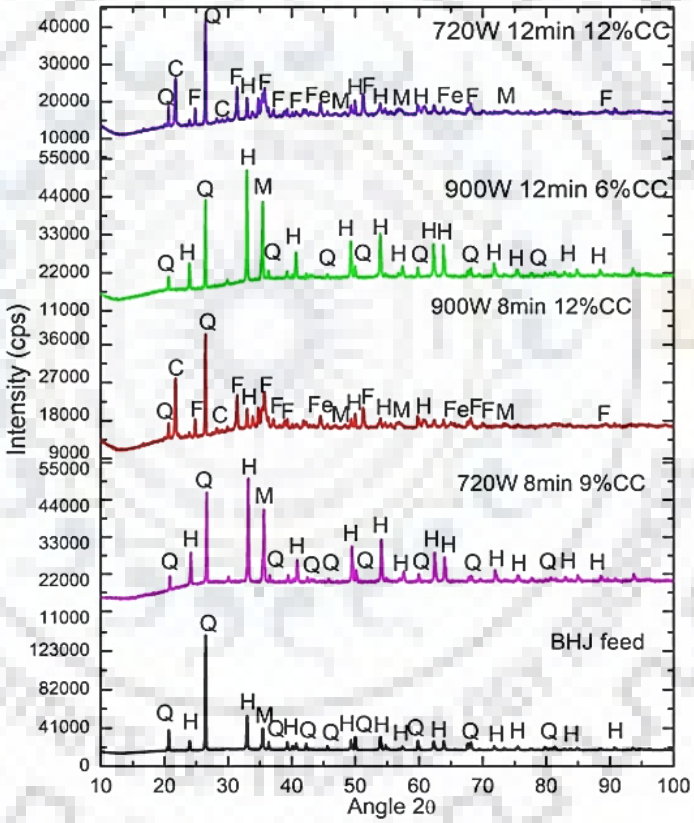

(Q - Quartz, H – Hematite, M – Magnetite, F – Fayalite, C – Cristobalite, Fe – Ferrite)

Figure 4.2.38 XRD plot of the feed and magnetic concentrate of selected experiments.

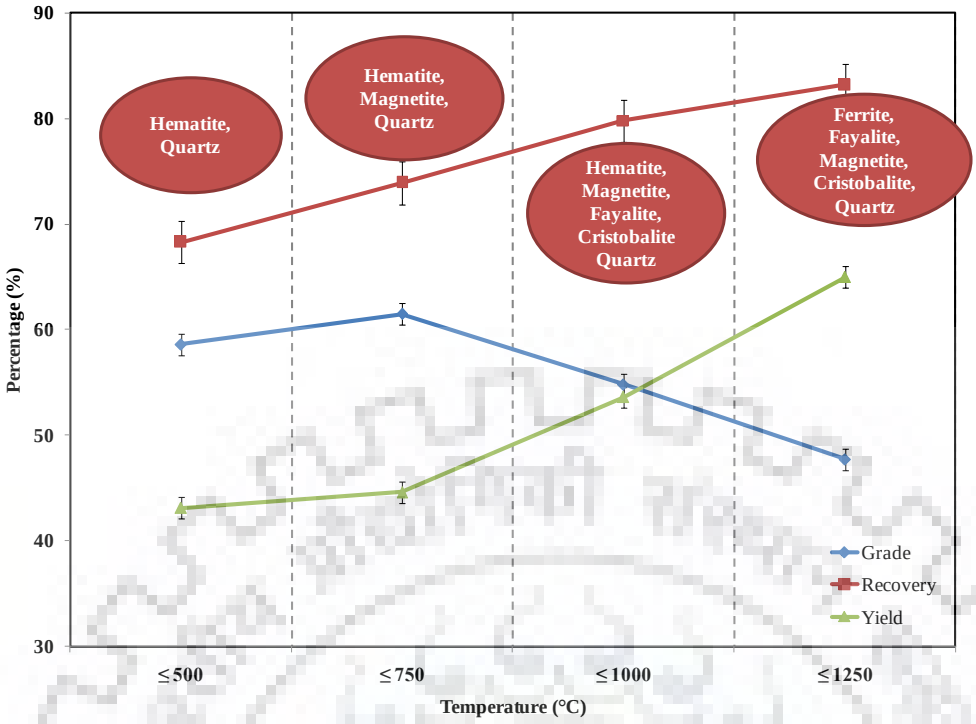

Figure 4.2.39 Variation of iron grade, recovery, and yield of magnetic concentrate with temperature.

Next, an attempt has been made to study the effect of particle size during carbothermal reduction. Therefore, the experiments were conducted at optimal condition (900 W, 8 min) for closed sizes of 312×200, 200×100 and 100×75 microns to nullify the size effect for heat changes. Fig. 4.2.40 shows the corresponding iron grade, recovery, and yield of the magnetic concentrate. As expected, iron grade and yield decrease with increase in particle size. It is known that the reduction takes place primarily due to gaseous diffusion of carbon dioxide-carbon monoxide gas in the iron phase matrix and the rate of diffusion depends upon the contact area. Therefore, at coarse particle size the effective total surface area of particles decreases resulting in limited diffusion and hence limited reduction. It is expected at coarser particle size, the iron grade should improve due to selective heating of hematite phase in a bonded structure, but due to the fine dissemination of Jasper/quartzite phase in the hematite matrix, the grade does not increase as expected. As expected, at all particle sizes, same phases (Quartz, Cristobalite, Magnetite, Fayalite, Ferrite) were formed as shown in Fig. 4.2.41a, thereby suggesting that there is a negligible effect of particle size. The photograph of the reduced product containing ferrite balls at the optimal condition is shown in Fig. 12b. However, the weight of formed ferrite ball decreased with increase in particle size and no ball formation was observed in 312x 212 microns respectively.

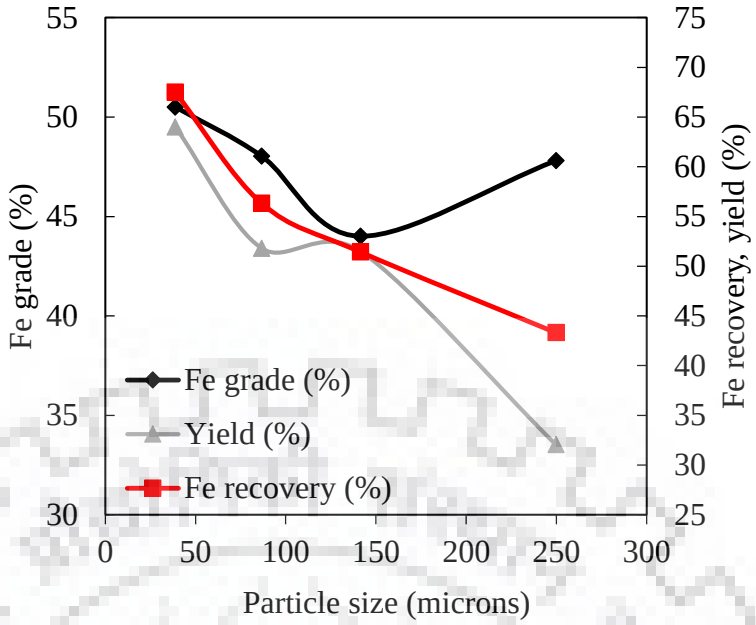

Figure 4.2.40 Effect of particle size on iron grade, recovery, and yield of magnetic concentrate (900 W, 8 min, and 9% charcoal).

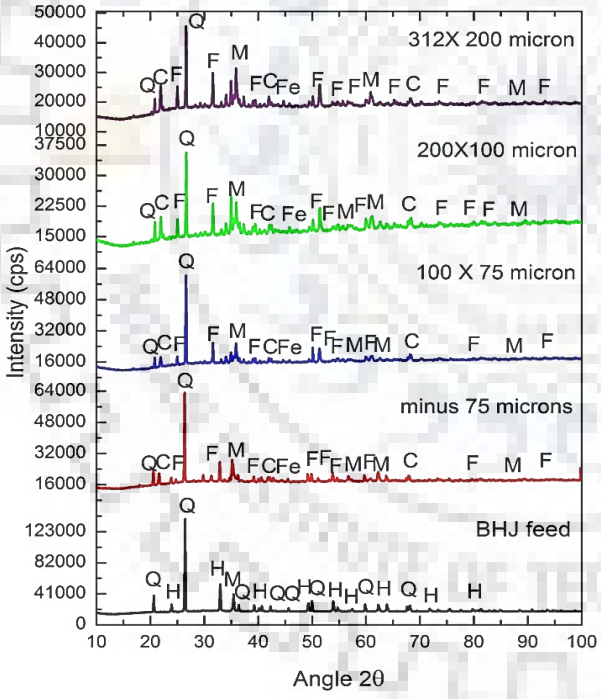

(Q - Quartz, H – Hematite, M – Magnetite, F – Fayalite, C – Cristobalite, Fe – Ferrite)

Figure 4.2.41a XRD plot of different particle size concentrates at 900 W 8 min and 9% charcoal

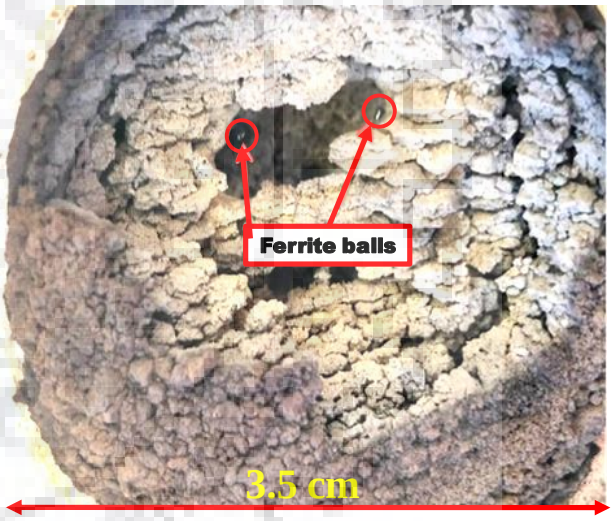

Figure 4.2.41b Photograph of the reduced product at the optimum condition level

The morphology of the magnetic concentrate obtained at different experimental conditions was studied using SEM attached with EDS. The elemental analysis of the magnetic concentrate of experiment 1 and 2 shows iron grains associated with oxygen and the ratio indicates the presence of hematite phase. This can be also confirmed as the attained temperature does not exceed 500°C and hence, no phase change was expected. The micrograph of the magnetic concentrate (experiment 3) indicates the occurrence of magnetite along with hematite phase as shown in Fig. 4.2.42. In the experiments with an attained temperature above 1000°C, the formation of ferrite balls was observed and the corresponding ferrite flake formation from the magnetite or wustite phase is shown in Fig. 4.2.42c. It is important to mention that a considerable quantity of ferrite balls was formed (approximately 3-4% with respect to total mass) when the attained temperature exceeds ~1100°C. Fig. 4.2.41d shows the micrograph of a typical ferrite ball formed during experiment 7 with radii of 50±10 microns. The EDS analysis of the same indicates 5.77% carbon and 89-90% Fe which is close to Fe-C eutectic composition. It is expected that with sufficient carbon, the melting point of iron decreases and the localized melting occurs resulting in the formation of ferrite balls.

Fig. 4.2.43 shows the hysteresis loop of the feed sample and the corresponding magnetic concentrates of various experiments. As expected, the occurrence of the ferrite phase in the concentrate leads to an increase in the saturation magnetization. The saturation magnetization value increases from 5.02 to 24 emu/g for the experimental condition of 720 W, 12 min and 12% C with ferrite, fayalite, and magnetite as the major phases. The concentrate containing magnetite and hematite phase-only shows slight increment in the magnetization value (8.63 and 9.11 emu/g). The four-fold increase in the magnetization can be attributed to the formation of magnetic iron phases. The ferrite balls formed during carbothermal reduction showed magnetization of 153.61 emu/g and reflects purity of 70.59%.

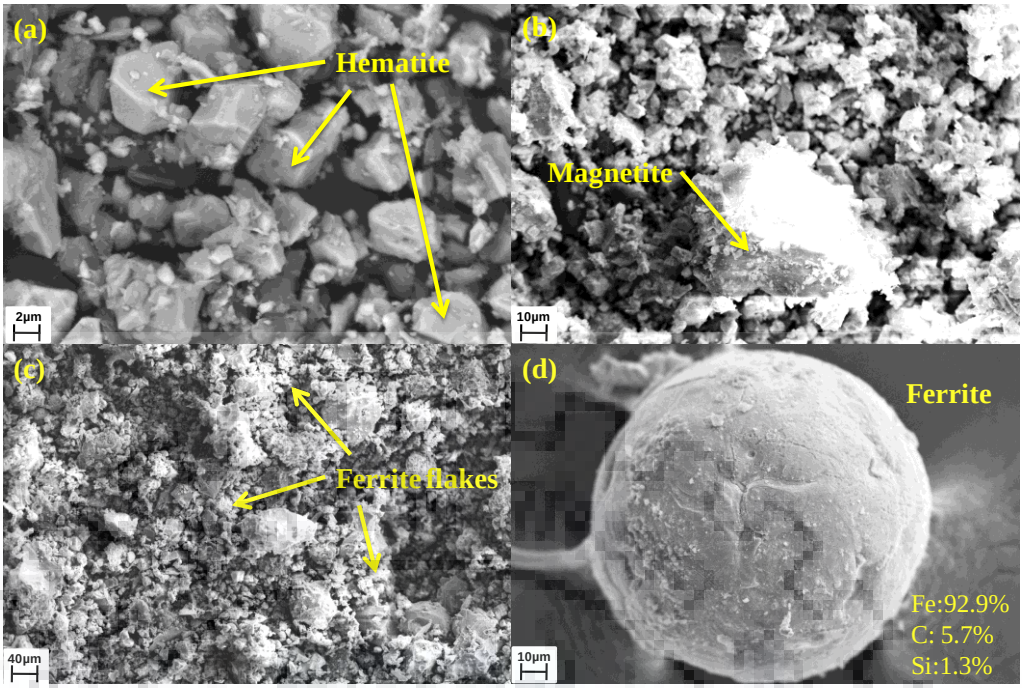

Figure 4.2.42 SEM image of the magnetic concentrate of experiment 900 W 8 min 12% charcoal.

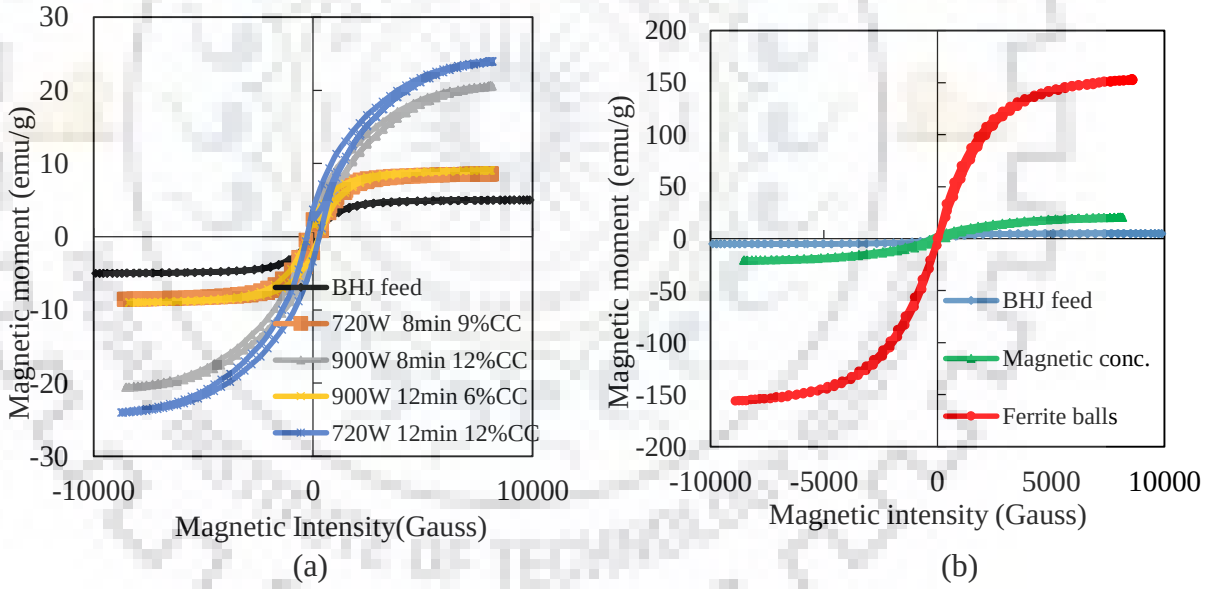

Figure 4.2.43 Hysteresis loop of the (a) feed and the magnetic concentrate of different reduction conditions, (b) feed, and concentrate and ferrite ball corresponding to 900 W, 8 min, 12% C.

The BSE image, elemental and atomic weight percentage for the reduced product at 900 W, 8 min and 12% charcoal is shown in Fig. 4.2.44. It reflects the distribution of various phases such as fayalite, ferrite, and Cristobalite. The highlighted area (1) denotes the ferrite and is associated with the fayalite ($FeO.SiO_2$). During reduction, wustite is partially converted to ferrite and fayalite ($FeO.SiO_2$) and the ferrite phase is seen in close association with fayalite phase in the underlying phase matrix and point 2 reflects the composition of ferrosilicon. The reduced product

of 900 W, 8 min and 9% charcoal (optimum condition obtained from the main effect plot) is shown in Fig. 4.2.45. Reflects points 1&2 ferrite, points 3 to 5, 7 to 8 and 6&9 denotes ferrite, fayalite, and cristobalite respectively.

Similarly, BSE analysis was conducted for optimum condition experiment 900 W, 10 min 12% charcoal as shown in Fig. 4.2.46. It reflects different points, 2 ferrites, 6&7. Ferro silicon 1&5 fayalite, 4. Cristobalite, 3. Cementite based on their atomic weight percentage.

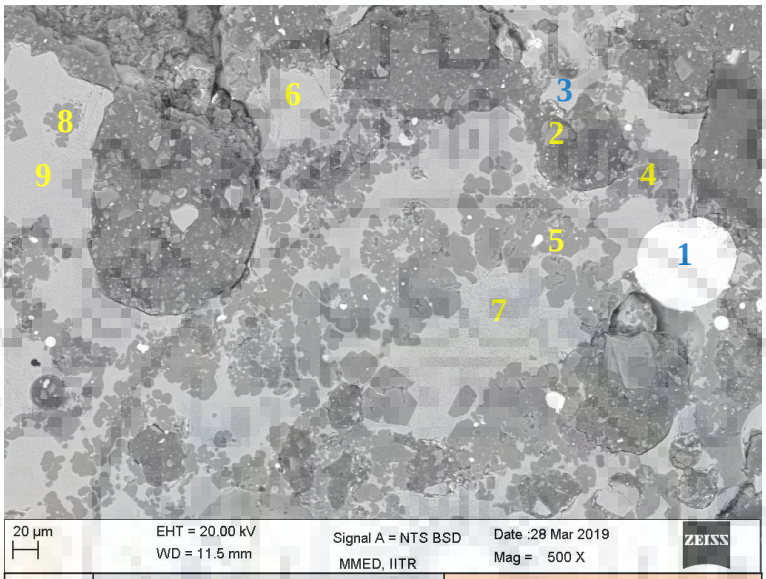

	Element wt. (%)				Atomic wt. (%)			
	Fe	**O**	**C**	**Si**	**Fe**	**O**	**C**	**Si**
1	100				100			
2	50.8	25.4		23.8	27.2	47.4		25.4
3	48.4	25.8	5.4	20.2	23.7	44.2	12.4	19.7
4	23.3	36.7	6.8	33.1	9.3	51.4	12.8	26.4
5	1.5	43.9	8.2	46.3	0.5	53.7	13.4	32.3
6	48	27.1		24.8	25	49.3		25.7
7	49.2	26.3		23.8	25.9	48.4		25
8	1	43.7	8.2	47	0.3	53.5	13.9	32.8
9	48.9	27.2		23	25.5	49.6		24

Figure 4.2.44 BSE image EDAX and atomic (%) of reduced product at 900 W, 8 min and 12% charcoal (1. Ferrite, 2. Ferro silicon 3, 6, 7&9. Fayalite, 4, 5&8. Cristobalite)

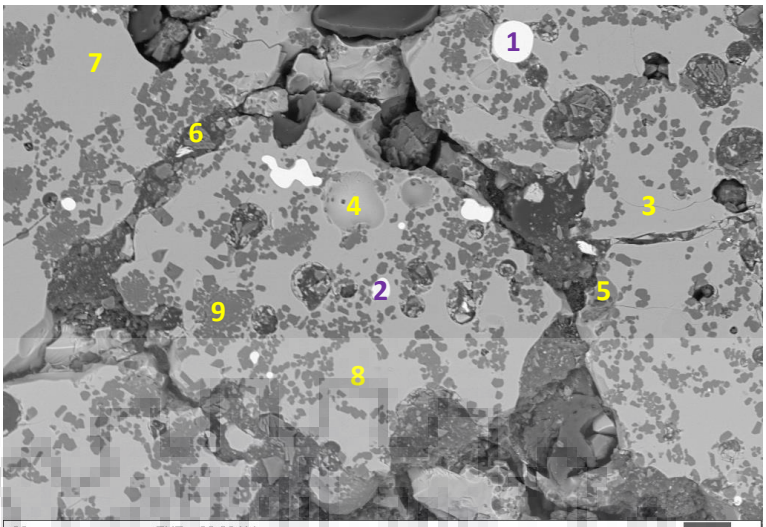

Point No.	Element wt. (%)				Atomic wt. (%)			
	Fe	O	C	Si	Fe	O	C	Si
1	100				100			
2	100				100			
3	48.1	31.9		19.9	24.2	55.9		19.9
4	49.7	30.1		20.2	25.5	53.9		20.6
5	73.9	15.1		10.8	49.8	35.6		14.5
6			27.6	72.4			47.1	52.9
7	47.9	31.2		20.8	24.2	54.9		20.9
8	47.3	31.8		20.9	23.7	55.5		20.8
9	2.2	48.6		49.2	0.8	62.9		36.2

Figure 4.2.45 BSE image EDAX and atomic (%) of reduced product at 900 W, 8 min and 12% charcoal (1&2. Ferrite, 2.Ferro silicon 3 to 5 & 7 to 8 Fayalite, 6&9. Cristobalite)

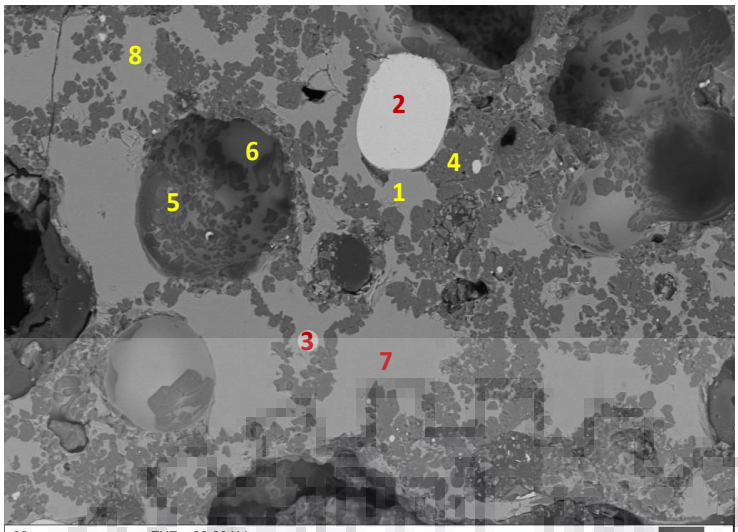

Point No.	Element wt. (%)				Atomic wt. (%)			
	Fe	O	C	Si	Fe	O	C	Si
1	47.9	32.2		19.8	23.9	56.3		19.7
2	100				100			
3	96.8		3.2		86.6		13.3	
4	1.2	48.2	8.8	41.7	0.4	57.3	14	28.3
5	48.7	30.2		21	24.8	53.8		21.3
6	46.7	33.1		20.1	23.1	57.1		19.7
7	48.2	32		19.8	24.2	56.1		19.7

Figure 4.2.46 BSE image EDAX and atomic (%) of reduced product at 900 W, 10 min and 12% charcoal (2. Ferrite, 6 & 7. Ferrosilicon 1&5 Fayalite, 4. Cristobalite, 3. Cementite)

4.2.5 Conventional and microwave carbothermal reduction of banded hematite quartzite

Standard reduction kinetics experiments were pursued at 6, 9, and 12% charcoal at different temperature and time to determine the activation energy as shown in Fig. 4.2.47. As expected, the iron grade and recovery of the magnetic concentrate decreases with an increase in temperature; however, no trend of reaction progress was observed with time. This can be attributed to the heterogeneous nature of the sample. It can be deduced, that iron enrichment (grade) was better at a lower temperature (600°C) compared to a higher temperature (800°C). Since reduction kinetics was not delineated from the data, a statistical design was investigated to evaluate optimal conditions for obtaining a pellet grade concentrate. The factors involved in the statistical design were temperature, charcoal, and time and particle size with the iron grade, recovery, and yield as process responses shown in Table 4.2.11. The range of response parameters were determined with corresponding to 95% confidence interval. The Optimum Fe grade value obtained from the statistical design slight far away from the upper limit value. Most of the response values were in between the 95% Confidence Interval. Means 95% confidence

that the mean population value can exist in between upper and lower limit value. It is also observed the response recovery, is having slight variation with optimal value obtained through statistical designed.

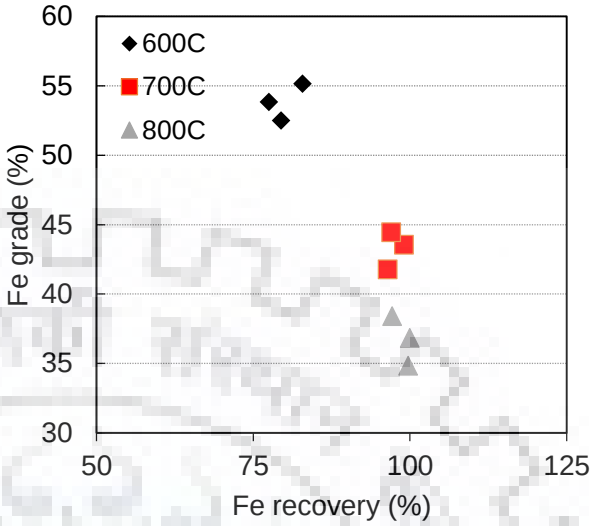

Fig. 4.2.47 Kinetics plot for iron grade and recovery in a conventional reduction

Table 4.2.11 Taguchi L_9 statistical design and associated responses

S.No.	Temp. (°C)	Charcoal (%)	Time (min)	Particle size (µm)	Fe_G (%)	Fe_R (%)	Yield (%)
1	500	6	30	minus 75	53.62	46.96	26.28
2	500	9	60	150×75	57.64	68.52	35.67
3	500	12	90	312×150	52.28	60.33	34.62
4	650	6	60	312×150	50.49	100.55	59.75
5	650	9	90	minus 75	48.03	85.90	53.65
6	650	12	30	150×75	51.83	96.66	55.95
7	800	6	90	150×75	45.57	96.39	63.45
8	800	9	30	312x150	42.45	97.81	69.13
9	800	12	60	minus 75	37.98	95.49	75.43
Average (mean)					48.88	83.18	52.66
Standard deviation (s)					5.71	18.49	15.91
(t value*Standard deviation)/Sqrt(sample size)					4.392497898	14.22	12.23
95% Confidence Interval (95%CI)					48.88 ±4.39	83.18 ± 14.21	52.91 ± 12.22

Lower temperature (500ºC) yielded optimal concentrate with Fe_G of 57.6%, Fe_R of 68.54%, and a yield of 35.6%. The VSM results of different experiments shown in Figure 4.2.48 are in agreement with the iron grade-recovery and XRD results. At a lower temperature, dominant phases were hematite, magnetite, & quartz, whereas, wustite, hematite, magnetite & quartz were

dominant phases at a higher temperature. The formation of wustite phase at higher temperature leads to loss of iron values as wustite is paramagnetic.

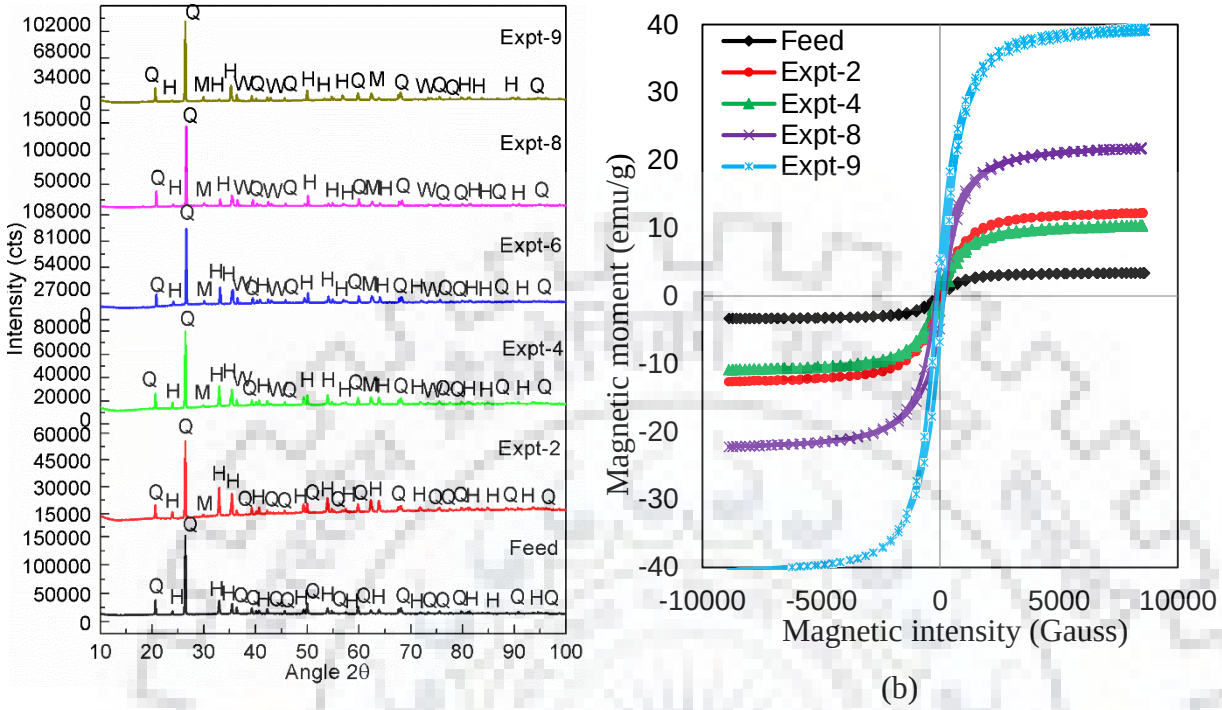

Figure 4.2.48 (a) XRD (b) VSM plots for the optimal condition in a muffle furnace reduction.

4.2.5.1 Microwave carbothermal reduction

Preliminary experiments revealed that the heating rate and residence time influence the reduction process. Fig. 4.2.49 shows the time-temperature plot for the feed and mixture (feed and charcoal) at different dosages in a microwave furnace (maximum power 800 W). It can be seen that during microwave exposure; ~400°C was achieved in 12 min and~1100°C in 12% carbon. Initially, the heating rate increases slowly, followed by a steep slope, which subsequently saturates. The variation in the heating rate is due to phase transformation during microwave irradiation. Carbon is an excellent microwave absorber that leads to an initial increase in the heating rate, and this was confirmed by different heating rates of feed and mixture samples. As the temperature increases, carbon reduces the hematite phase and converts it into the magnetite phase, leading to increased absorption of microwaves. As soon as the carbon in the system exhausts along with the magnetite transformation to wustite, the heating rate decreases and temperature eventually saturates. The average heating rate during microwave reduction was approximately 85 °C/ min compared to 10 to 20 °C/ min in a muffle furnace. The heating rate was significantly faster in 12% C due to the transformation of the hematite phase in a relatively shorter duration. It can be observed that within 8 min the heating rate was steady, and therefore, the statistical design

(Taguchi L-9) experiments were conducted for 8-12 min, charcoal dosage 6-12% and 540-900 W power.

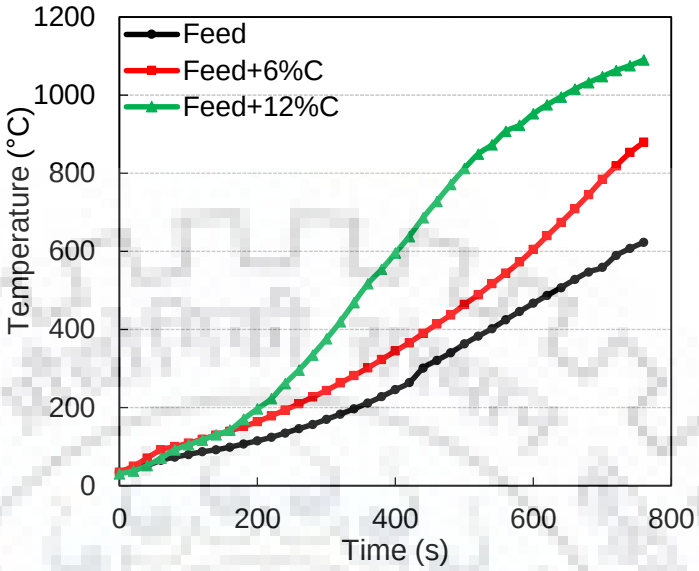

Figure 4.2.49 Time-temperature plot for feed and charcoal mixture during microwave exposure (800 W, minus 75 microns).

The presence of bonded silica in the BHQ ore leads to an easy formation of the fayalite phase suggesting direct reaction between magnetite/wustite and silica. In most of the design experiments, the high temperature was attained except for Expt. 1. A huge blue flame was observed and higher the charcoal dosage, faster the flame was attained during the experiments as shown in Table 4.2.12. The range of response parameters were determined with corresponding to 95% confidence interval. The Optimum Fe grade value obtained from the statistical design slight far away from the upper limit value. Most of the response values were in between the 95% Confidence Interval. Means 95% confidence that the mean population value can exist in between upper and lower limit value. It is also observed the response recovery, is having slight variation with optimal value obtained through statistical designed.

Based on design results; the optimal conditions were Fe_G of 57.6%, Fe_R of 47%, a Yield of 24% (without ball formation) and Fe_G of 44.7%, Fe_R of 82%, a Yield of 55% (with ball formation). It was observed that the hematite and quartzite phases were disappeared along with the formation of new phases such as cristobalite, magnetite, and fayalite. In Expt. 8 and 9 iron-rich/ ferrite balls were observed with the naked eye and to facilitate separation, a handful T-magnet (fixed intensity~1500 Gauss) was used. Balls were primarily of pure iron composition and their purity cannot be evaluated using chemical titration procedure, and hence were not considered.

Considering that most of the experiments yielded a high temperature along with the formation of wustite, fayalite, and cristobalite phases, the main effect plot of parameters was not pursued. The hysteresis loop obtained from the VSM analysis of the feed, magnetic, non-magnetic and ferrite balls for 900 W 12% C, 10 min is shown in Fig 10c. The saturation magnetization of feed was 5.02 emu/g whereas the magnetic, non-magnetic product and ferrite ball was~30, 0.86 and 202 emu/g respectively suggesting a purity of~93% for the ball. After separation of the balls from the magnetic concentrate, the concentrate showed the highest magnetic saturation for an optimal condition 900 W, 12% C, 10 min, and all the fractions were subjected to XRD analysis as shown in Fig. 4.2.50d. The formation of fayalite, cristobalite, and quartz phases were observed in magnetic and nonmagnetic fractions, whereas pure ferrite phase was observed in the ball.

Table 4.2.12 Experimental design and associated responses.

S. No.	Power (W)	Charcoal (%)	Time (min)	Particle size (μm)	Temp. (°C)	Ball formation	Fe_G (%)	Fe_R (%)	Yield (%)
1	540	6	8	-75	383	X	57.64	47.16	24.54
2	540	9	10	150×75	>1100	X	46.47	73.72	47.59
3	540	12	12	312×150	>1100	X	46.02	62.52	40.76
4	720	6	10	312×150	>1100	X	51.16	63.56	37.27
5	720	9	12	-75	917	X	46.91	72.77	46.54
6	720	12	8	150×75	>1100	X	54.73	72.67	39.83
7	900	6	12	150×75	>1100	X	54.29	65.60	36.25
8	900	9	8	312×150	>1100	√	55.85	54.48	29.26
9	900	12	10	- 75	>1100	√	44.68	82.72	55.54
Average (mean)							50.86	66.13	39.73
Standard deviation (s)							4.64	10.19	8.93
(t value*Standard deviation)/Sqrt(sample size)							3.57	7.83	6.86
95% Confidence Interval (95%CI)							50.86 ±3.57	66.13 ±7.83	39.73 ±6.86

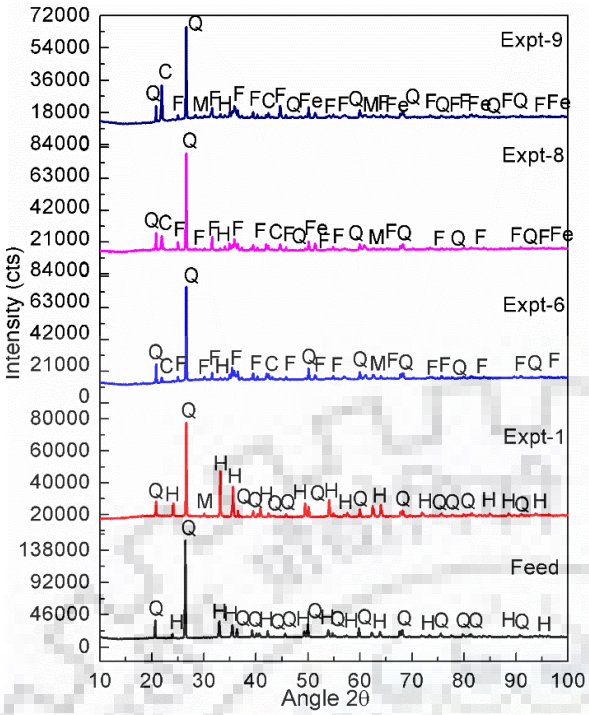

Q-quartz, H-hematite, M-magnetite, C-cristobalite, F-Fayalite and Fe- Ferrite

(a)

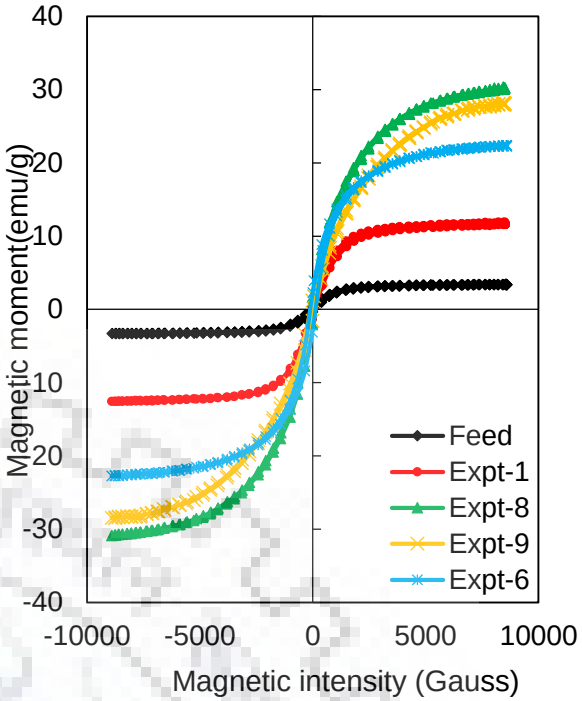

(b)

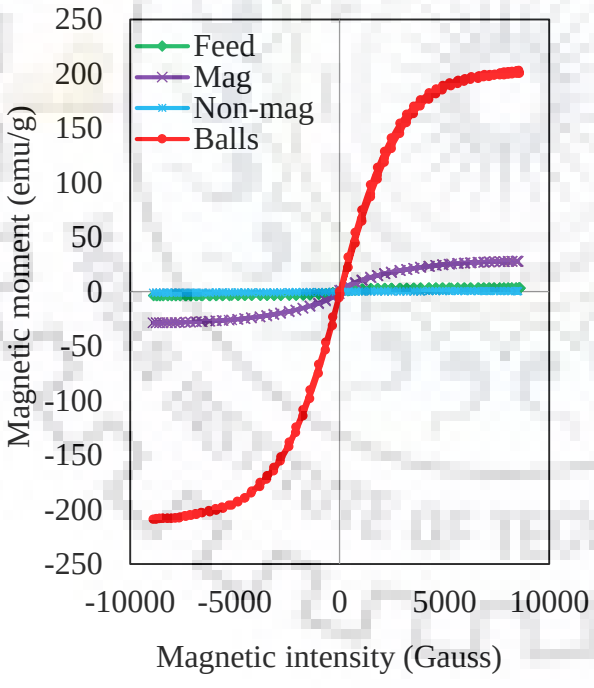

(c)

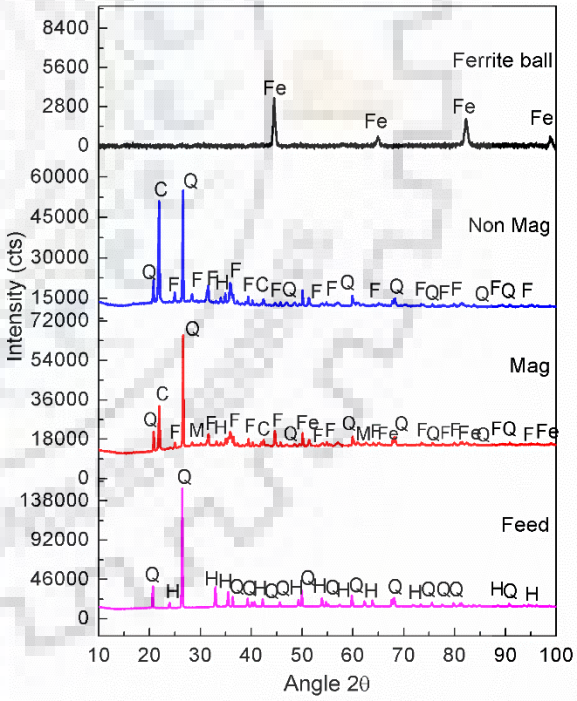

(d)

Figure 4.2.50 Characterization of selected experiments (a) XRD plot (b) VSM plot; Products of Expt-9 (c) VSM plot (d) XRD plot

At higher charcoal dosage, i.e., 9% to 12% the formation of iron-rich/ferrite balls of size 1±0.5 mm was observed in the reduced product. The scanning electron micrograph, elemental mapping,

and optical micrograph are shown in Fig 4.2.51(a, b, c) respectively. It can be seen that the composition of the ball comprises 92% Fe and~6% C. The optical micrograph of the ferrite ball reveals retained austenite and martensitic iron phase due to water quenching post reduction. The average hardness for the iron ball was around 250 HV, indicating low carbon martensitic product. The XRD plot shown in Fig. 4.2.51d depicts pure ferrite phase with a bcc structure. The effect of particle size on ferrite ball formation was also investigated as shown in Fig 4.2.51e. It was found that fine particle size resulted in a coarse ferrite ball with higher saturation magnetization. The similar iron grade was observed for different sizes; however, the ball weight was found to decrease with increasing particle size. The BSE image, elemental and atomic weight percentage for the reduced product at 900 W, 8 min and 12% charcoal is shown in Fig. 4.2.52. It reflects the distribution of various phases such as fayalite, ferrite, and Cristobalite. The highlighted area (1&2) denotes the ferrite and is associated with the fayalite ($FeO.SiO_2$). During reduction, wustite is partially converted to ferrite and fayalite ($FeO.SiO_2$) and the ferrite phase is seen in close association with fayalite phase in the underlying phase matrix.

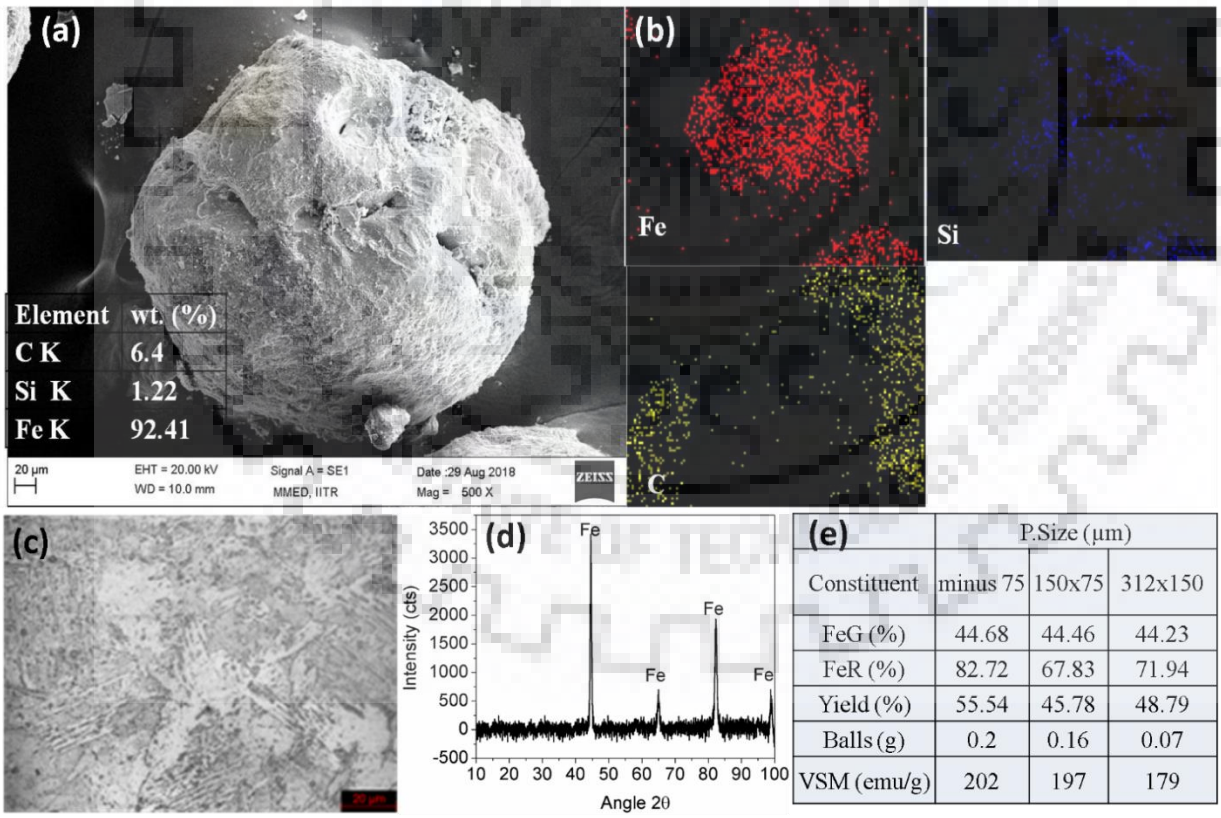

(e)	P.Size (µm)		
Constituent	minus 75	150x75	312x150
FeG (%)	44.68	44.46	44.23
FeR (%)	82.72	67.83	71.94
Yield (%)	55.54	45.78	48.79
Balls (g)	0.2	0.16	0.07
VSM (emu/g)	202	197	179

Figure 4.2.51 Ferrite ball observed at 900 W, 12% C, 10 min, minus 75 µm (a) Scanning electron micrograph (b) elemental mapping (c) Optical microstructure (d) XRD plot (e) Effect of particle size

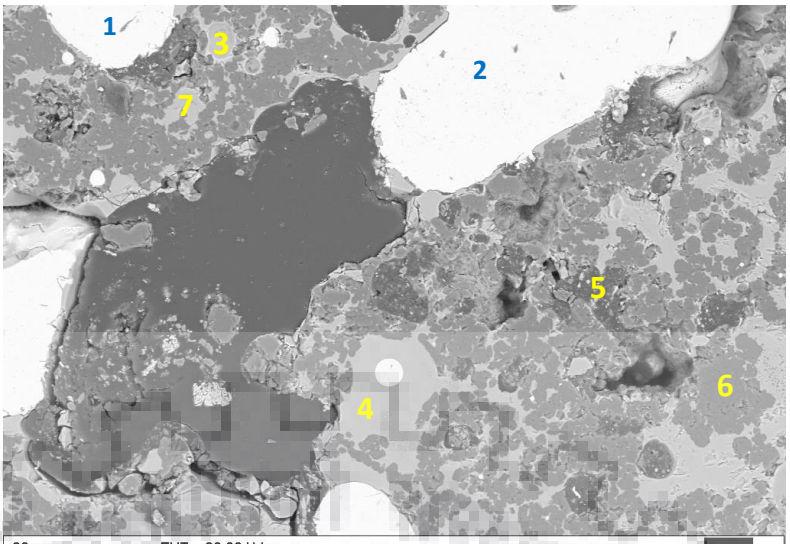

Point No.	Element wt. (%)				Atomic wt. (%)			
	Fe	O	C	Si	Fe	O	C	Si
1	100				100			
2	100				100			
3	52.1	26.9		20.9	27.8	50		22.2
4	47.7	25.4	7.5	19.3	22.8	42.3	16.6	18.3
5	1.8	41.1	11.1	45.9	0.6	49.8	17.9	31.6
6	1	42.8	7.7	48.3	0.3	52.9	12.7	33.9
7	48.2	25.4	7.2	19.2	23.1	42.5	16	18.3

Figure 4.2.52 BSE image EDAX and atomic (%) of reduced product at 900 W, 10 min and 12% charcoal (1&2. Ferrite, 3, 4&7. Fayalite, and 5&6. Cristobalite

The effect of charcoal dosage at 900 W and 10 min was evaluated as shown in Fig. 4.2.53. The variation in iron grade, recovery, ball weight, saturation magnetization, and hardness values was investigated for an exposure time of 10 min. The iron grade-recovery was almost constant ~47% Fe and 90% due to the ball formation and saturation magnetization was also confined to ~ 180-200 emu/g. The overall iron grade and recovery of different routes adopted in this study are shown in Fig. 4.2.54. It can be seen that physical separation i.e., both magnetic separation and spiral separation lack iron grade and recovery, whereas microwave reduction offers ~ 60% Fe grade with 75% recovery. It should be noted that overall carbothermal reduction offers higher recovery than exposure alone. Based on the results obtained in this study at 900 W, it is expected that a high power microwave may yield a similar product approaching pig iron composition (Fe% ~90 to 95%). Implementing the microwave processing at a commercial scale is halted primarily due to high initial capital investment, limited depth penetration of microwaves, variation in dielectric properties of material with temperature, and the uncertainty of process efficiency regarding conversion of electric power to microwave power at different frequencies (Lab scale 2.45 GHz and Industrial 915 MHz).

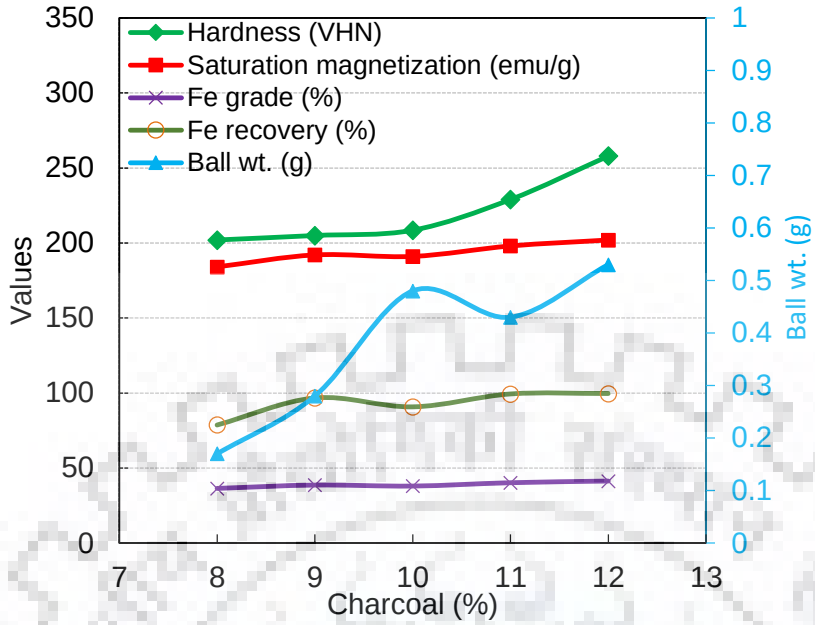

Figure 4.2.53. Variation of Fe grade, recovery and ball quality parameters of microwave reduced sample at 900 W 10 min, 8-12% charcoal

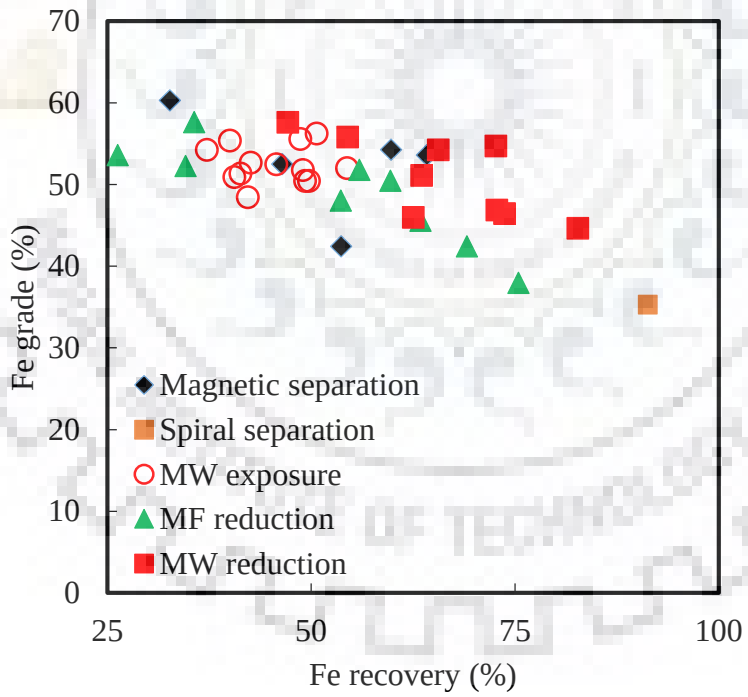

Figure 4.2.54 Iron grade-recovery curve for all the processes adopted in the study

CHAPTER 5
CONCLUSIONS

In this study the upgradation of banded iron ores was investigated. In the first part, these ores were grounded with ball mill system and compression testing machine for the feed and alternative treated samples followed by magnetic separation. In the second part, ores are subjected to carbothermal reduction for the effective separation of iron values from impurities followed by low intensity magnetic separation.

The detailed comminution investigations of banded iron ores were performed in dry and wet grinding ball mill system, intended to determine the breakage parameters such as selection function and breakage function of ores (BHQ, BHJ, and BMQ) of varying hardness and energy consumed during comminution studies by maintaining constant volume feed rate. An 11.5×10 inches batch ball mill was used for experimental studies, at a fixed operating condition of critical speed ~60 rpm. The cumulative breakage parameters and the specific rate of breakage were determined of banded iron ores of different mono-sizes, short grinding times in batch open grinding systems. The banded hematite jasper is found harder to process than banded hematite quartzite and banded magnetite quartzite.

Thermal treatment followed by quenching of banded iron ores produced a massive amount of random cracks due to induced thermal stresses and produced more fines (below 100 microns) than feed. Thermal treatment followed by rapid quenching caused to increase in P_{50} size for all the different monosizes. Pre-treatment also led to a decrease in specific rate of energy for the same amount of fines production. The intensity of random cracks developed was increased along with increasing particle sizes, thus reduces the grinding rates for liberation size. But the pre-treated samples don't show any positive effect on downstream magnetic separation for the enrichment of iron values in magnetic concentrate.

Compression testing mode was more efficient than ball mill grinding with respect to particle size distribution and fineness due to significant micro-cracks. Also, the specific energy is significantly less for the same fineness levels. In pre-treated samples (thermal and microwave), micro-cracks were observed which does not significantly affect downstream operation i.e., magnetic separation. Finally, compression mode is found better compared to ball mill with reference to finer particle size distribution at lower specific energy values. Based on the batch grinding behavior with different comminution alternatives, thermal treatment followed by quenching was found a suitable treatment option.

The banded magnetite phase is receptive to microwaves, which significantly aids in the liberation of iron values. The formation of significant random cracks during microwave treatment assisted the release of iron values from the matrix as explained by enhanced grade values. Under optimal conditions of 720 W, 6 min and particle size minus 75 µm, concentrate with 60.1% Fe, 99% Fe recovery at 71% yield was achieved in a single step. The saturation magnetization for feed and magnetic concentrates is 44 and 63 emu/g respectively and the magnetization value saturates with an increase in residence time. It is concluded that the iron enrichment occurs as confirmed by chemical analysis and magnetic saturation values, however, XRD analysis proved to be inconclusive in observing any phase changes. The single-step microwave exposure including magnetic separation at 1000 Gauss only provides significant up-gradation and holds strong potential to be used as a pre-treatment step for the beneficiation of similar iron ores.

The conventional magnetic separation and spiral concentration technique are found to be ineffective to beneficiate BHJ/BHQ ore. The microwave exposure of BHJ provides significant enrichment and can be used as a pre-treatment step in the beneficiation of similar low-grade iron ores. The yield of the magnetic concentrate of route B remains fairly stable (53-62% yield) over iron grade range however magnetic yield decreases with increase in iron grade of route A. The conventional route A has a lower recovery at higher grades compared to route B whereas route C provides the best grade to recovery ratio (A: Magnetic separation, B: Microwave exposure, and C: Microwave exposure for magnetic concentrated samples). Under optimal conditions, an iron-enriched concentrate with 61% Fe, 85% Fe recovery at 50% yield can be achieved from BHJ feed ~38% Fe without any chemical additive. There is no phase change after the microwave exposure in the adopted routes, however, the generation of significant micro-cracks enhances the separation. The designed pre-treatment process for BHJ ore beneficiation without incorporation of any reductant ore chemical additive seams promising for such low-grade iron ores.

The microwave exposure of BHQ via statistical design yielded an optimal condition of 540 W, 10 min, and 6300×4750 µm, a concentrate with Fe_G of 56.30%, Fe_R of 50.68% and a yield of 27.01%. Similarly, muffle furnace exposure was carried out at 500 to 700°C for 60 min and concentrate with Fe_G of 59%, Fe_R of 24.8% and a yield of 12.5% was observed along with microcracks. It can be seen that significant microcracks were observed in both microwaves and muffle furnace exposed samples because of the different thermal expansion behavior of quartzite and hematite phase.

Therefore, the microwave irradiation of BMQ iron ore helped in huge enrichment of iron values, but microwave irradiation of BHQ/BHJ yield a significant amount of iron enrichment but the process yield obtained was approximately 50% and 25% in BHJ and BHQ respectively. To

improve further enrichment of Fe grade, recovery and mostly the process yield values, the carbothermal reduction was performed in a muffle furnace and microwave furnace.

The carbothermal reduction was performed through conventional route and microwave carbothermal route with stoichiometric reductant dosage.

Muffle furnace reduction of BHQ ore was pursued through standard reduction kinetics experiments and also Taguchi L-9 statistical design. As expected the iron grade and recovery of the magnetic concentrate decrease with an increase in temperature, however, no such definite trend of reaction progress was observed with time to delineate activation energy at 6, 9, and 12% charcoal (stoichiometry). This can be attributed to the fact that BHQ sample is of heterogeneous nature due to the dispersion of quartzite in the hematite matrix. It can be deduced, that iron enrichment (grade) was better at a lower temperature (600ºC) compared to a higher temperature (800ºC). In the lieu of optimization of process parameters, Taguchi L-9 statistical design at an optimal concentrate (at 500ºC, 9% charcoal, and 60 min) of Fe_G of 57.6%, Fe_R of 68% and a yield of 35.7% was obtained and also both cooling method and particle size does not have a significant effect on process response, however; the iron enrichment was in accordance with optimal condition results.

Similarly, the carbothermal reduction was also evaluated using Box Behnken statistical design and was found effective for the up-gradation of low-grade BHJ ore. The temperature was found as the significant factor for the optimization of both iron grade and recovery. At higher temperature, the formation of fayalite and wustite deteriorates the iron grade-recovery as they report to a nonmagnetic fraction. Under optimal conditions (700ºC, 30 min, 9% charcoal, minus 75 microns size) a concentrate (Fe_G of 61.2%, Fe_R of 82%, and a Yield of 52%) was obtained. Coarser particle size and alternative reductants do not have a significant effect, however, the fused fraction consisting of ~ 85% Fe with retained austenite and martensitic iron phases was obtained up to 2 mm particle size. The BSE micrograph and their atomic percentage reveals that the dominant phases such as wustite and silicon oxide were formed during muffle furnace reduction.

In the context of searching for a better route, the carbothermal reduction was also performed in the microwave oven for the first time to treat low-grade iron ores. The preliminary experiments conducted for 6-10% charcoal dosage for two residence time intervals i.e., 6 and 10 min. The ferrite balls were observed within 6-10 min at 8% and above charcoal dosage at a microwave power of 900 W. It is found that a small fraction of microwave irradiated BHJ ore-charcoal mixture was rapidly smelted to produce ferrite balls. The iron grade falls at prolonged exposure due to the interaction of iron phases with the quartzite due to the formation of fayalite. The

formation of fayalite, wustite, ferrite, and cristobalite occurs above 9% charcoal for 6 min, whereas, at 10 min; wustite ferrite, cristobalite, and fayalite occurred above 7% charcoal. The preliminary experiments conducted in microwave furnace revealed that during the short duration of microwave exposure, a temperature of ~ 400°C and ~1100°C was achieved for feed and charcoal mixture respectively. The microwave carbothermal reduction of low-grade BHJ ore shows promising potential for recovery of associated iron values. The optimal condition 720 W power, 9% charcoal and 8 min based on Taguchi L_9 statistical design yielded a magnetic concentrate having ~61.6% Fe, ~73.4% recovery at a yield of 44% and can be used for pellet making industry. Similarly, the experimental condition 900 W power, 12% charcoal, and 8 min yielded a magnetic concentrate with ~ 49.1% Fe, ~89.3% recovery at a yield of 59.7% along with the significant amount of ferrite balls with a saturation magnetization of ~153 emu/g. The BSE image, elemental and atomic weight percentage for the reduced product at 900 W, 8 min and 12% charcoal, reflects the distribution of various phases such as fayalite, ferrite, and Cristobalite. However, another optimal condition derived from main effect plot was 900 W power, 9% charcoal and 8 min yielded a magnetic concentrate with ~50.5% Fe, ~67.5% recovery at a yield of 49.5% along with the formation of ferrite balls with a saturation magnetization of ~101 emu/g. It is important to mention that the ferrite ball magnetic concentrate comprises ferrite, fayalite and magnetite phases. The average hardness value recorded on the Vickers hardness scale for ferrite ball is around 302 HV indicating low carbon martensitic product. The morphology of the concentrate obtained indicates the sequential reduction of hematite to ferrite in a sequence: $Fe_2O_3 \rightarrow Fe_3O_4 \rightarrow FeO \rightarrow Fe$ and the extent of reduction depending upon the attained temperature. The elemental analysis of ferrite ball indicates the presence of the approximately eutectic composition of Fe-C (~5% C) that may lead to a lowering of the melting point of iron and localized ball formation.

Similarly, the microwave carbothermal processing of low-grade BHQ iron ore (Fe ~31%) was also investigated. The statistical design was yielded Fe_G of 57.6%, Fe_R of 47% and a Yield of 24% at optimum condition 540 W, 8 min, 6% charcoal and particle size minus 75 μm. Optimal condition 900 W, 12% charcoal, 10 min, the next percentage of charcoal was varied from 6-12% C and it was seen that ball formation started after 8% carbon and significant balls were observed at 10 to12% C. The optical micrograph of the ferrite ball clearly reveals the presence of retained austenite and martensitic iron phase due to water quenching post-reduction. The BSE image and elemental and atomic weight percentage for the reduced product at 900 W, 8 min and 12% charcoal, reflects the distribution of various phases such as fayalite, ferrite, and Cristobalite. During reduction, wustite is partially converted to ferrite and fayalite ($FeO.SiO_2$) and the ferrite

phase is seen in close association with fayalite phase in the underlying phase matrix. The average hardness value of the ferrite ball is around 250 HV indicating low carbon martensitic product with a saturation magnetization of 202 emu/g with a purity of approximately 93%. It can be observed that iron grade significantly falls with microwave power because of the formation of strong magnetic ferrite phase observed at 900 W. The key difference in reduction behavior of microwave and muffle furnace includes the wustite formation in conventional reduction whereas in microwave reduction fayalite formation was dominant and the formation of ferrite balls. It is strongly believed that the results of this study can provide some key insights for researchers for the application of microwaves in the enrichment of low-grade iron ores. The overall conclusion can be summarized as following Fig. 5.1. The increase in charcoal dosage and increasing in reduction residence time in microwave doesn't show any increase in Fe grade in magnetic concentrate. The cooling effect and increase in sample quantity also don't give any promising results. It may be further improvised by reducing at controlled atmosphere and at high power i.e., more than 900 W.

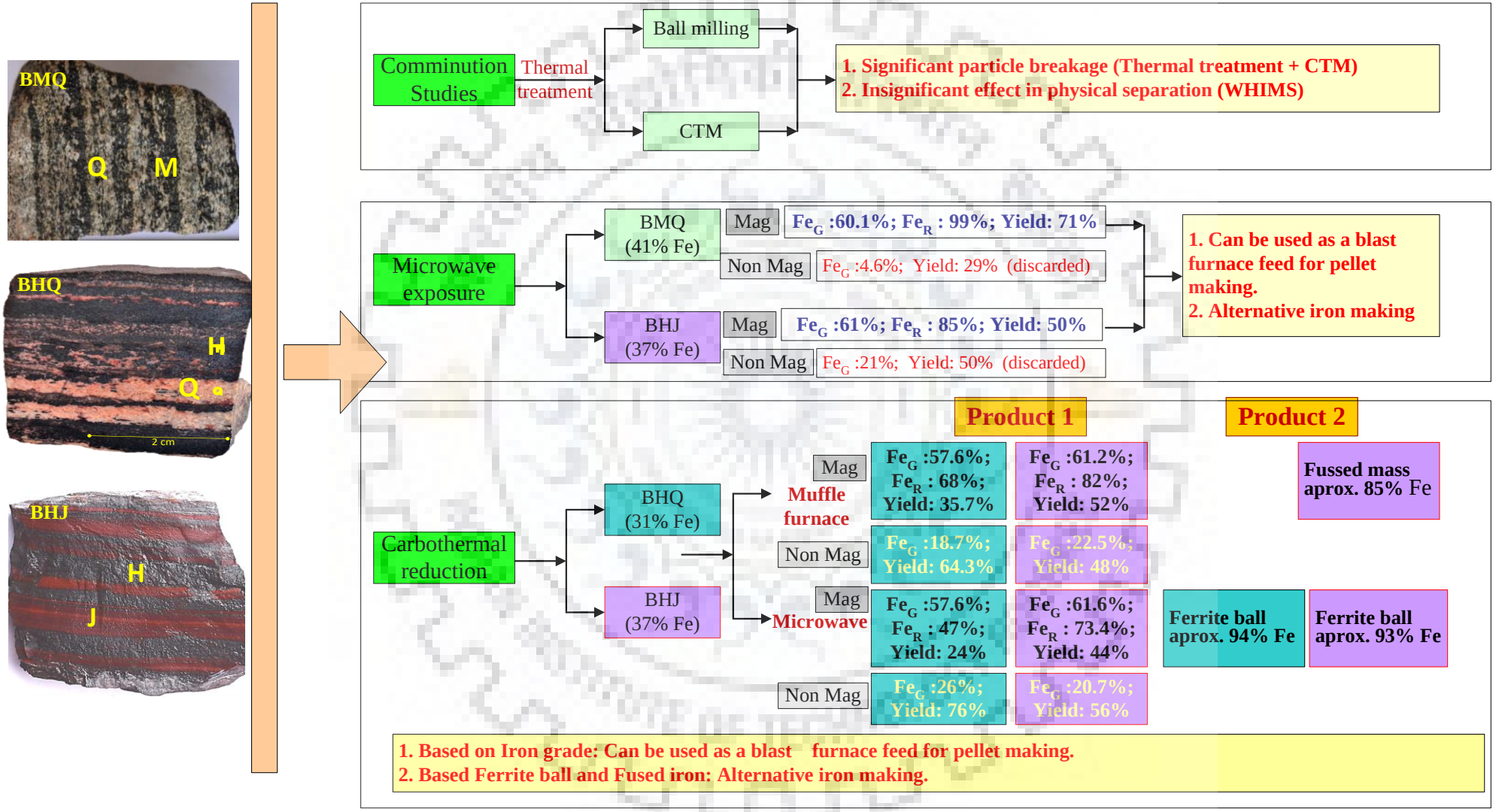

Figure 5.1 Overall flow sheet for the beneficiation of banded iron ores.

Suggestions for Future Research

1. The work should be done to identify the effect of different other alternative methods like high voltage, ultrasonic and high power microwave treatment with different mono-size particles.
2. To improvise further the iron grade and recovery, it is required to perform large scale experiments at higher power with the addition of higher charcoal dosage.
3. Controlled gaseous reduction experiments can be carried out to avoid the oxidation of reduced phases.
4. It is required to conduct thorough experimental studies to identify other alternative reductants to minimize the cost of the process.
5. Experiments should be carried to find conditions for fayalite breakdown.

LIST OF PUBLICATIONS FROM THIS RESEARCH WORK

PUBLISHED JOURNAL PAPERS

1. **Rayapudi, V.,** Agrawal, S., and Dhawan, N., 2019, Investigation of microwave exposure on beneficiation of low grade banded iron ore" Mining Metallurgy Exploration, 36 (2), pp.327-334.
2. **Rayapudi, V.,** and Dhawan, N., 2019, Microwave processing of banded magnetite quartzite ore for iron recovery, Transactions of the Indian Institute of Metals, DOI: 10.1007/s12666-019-01637-9
3. **Rayapudi, V.,** Agrawal, S., and Dhawan, N., 2019, Optimization of microwave carbothermal reduction for processing of banded hematite jasper ore, Minerals Engineering, 138 (9), pp. 204-214.
4. **Rayapudi, V.,** and Dhawan, N., 2019, Processing of banded hematite quartzite ore for recovery of iron values, Accepted, Mining, Metallurgy & Exploration DOI: 10.1007/s42461-019-00117-4.
5. **Rayapudi,** V., and Dhawan, N. Microwave-assisted carbothermal reduction of banded hematite jasper ore, Journal of Sustainable Metallurgy. **DOI:** 10.1007/s40831-019-00244-8.
6. **Rayapudi,** V., and Dhawan, N. Investigation of microwave reduction for ferrite formation from low-grade banded iron ores", Mineral Processing and Extractive Metallurgy. DOI: 10.1008/25726641.2019.1668662.
7. **Rayapudi,** V., Agrawal, S. and Dhawan, N. Evaluation of carbothermal reduction for processing of banded hematite jasper ore. Powder Technology. Accepted 30th September 2019.

COMMUNICATED JOURNAL PAPERS

1. **Rayapudi,** V., and Dhawan, N. Evaluation of microwave reduction for processing of banded hematite quartzite iron ore. CMQ Quarterly-Canadian Journal of Metallurgy and Materials Science.

CONFERENCE PROCEEDINGS

1. **Rayapudi, V.,** and Dhawan, N. (2018). Up-gradation of banded iron ores for pellet grade concentrate. Materials Today: Proceedings, 5(9), 17035-17072.
2. **Rayapudi, V.,** and Dhawan, N. (2017). Rayapudi,V., Dhawan,V., Mishra, B.K. (2017). Evaluation of compression breakage for banded hematite quartzite iron ore. Proceedings of

the 3rd International Conference on Science and Technology on Ironmaking & Steelmaking, pp. 291-294.

3. **Rayapudi, V.,** and Dhawan, N. (2019). Evaluation of groundnut shell as a reductant for microwave reduction of low grade banded iron ore. In IOP conference series: Materials Science and Engineering, 641(1), 012008-012017.

REFERENCES

1. Agacayak, T. (2011). Effect of microwave heating on magnetic separation: Kesikkpr magnetite deposits in Ankara, Central Turkey. Scientific Research and Essays, 6(8), pp.1856-1864.
2. Abouzeid, A.M., & Fuerstenau, D.W. (2009). Grinding of mineral mixtures in high-pressure grinding rolls. International journal of mineral processing, 93(1), 59–65.
3. Amini, A., Ohno, K.I., Maeda, T., & Kunitomo, K. (2018). Effect of the Ratio of Magnetite Particle Size to Microwave Penetration Depth on Reduction Reaction Behaviour by H 2. Scientific reports, 8(1), 15023.
4. Austin, L. G., & Luckie, P. T. (1972). Methods for determination of breakage distribution parameters. *Powder Technology*, *5*(4), 215-222.
5. Bhattacharyya, A., Tuzcu, E. T., & Rajamani, R. (2016). Experimental study on non-linear behavior of breakage rates due to fines generation in wet batch milling. *Minerals Engineering*, *99*, 19-29.
6. Barani, K., Koleini, S.J. & Rezaei, B., (2011). Magnetic properties of an iron ore sample after microwave heating. Separation and Purification Technology, 76(3), 331-336.
7. Cheng, J., Roy, R., & Agrawal, D. (2002). Radically different effects on materials by separated microwave electric and magnetic fields. Materials Research Innovations, 5(3-4), 170-177.
8. Crangle, J., and G. M. Goodman. "The magnetization of pure iron and nickel." Proceedings of the Royal Society of London. A. Mathematical and Physical Sciences 321, no. 1547 (1971): 477-491.
9. Das, S. K., Prasad, R., & Singh, R. P. (2018). Characterisation-Assisted Reduction Roasting of BHJ, West Singhbhum, Jharkhand, India. Transactions of the Indian Institute of Metals, 71(6), 1357-1362.
10. Das, S. K., Prasad, R., & Singh, R. P. (2018). Characterisation-Assisted Reduction Roasting of BHJ, West Singhbhum, Jharkhand, India. Transactions of the Indian Institute of Metals, 71(6), 1357-1362.
11. Das, B., Mishra, B. K., Prakash, S., Das, S. K., Reddy, P. S. R., & Angadi, S. I. (2010). Magnetic and flotation studies of banded hematite quartzite (BHQ) ore for the production

of pellet grade concentrate. International Journal of Minerals, Metallurgy, and Materials, 17(6), 675-682.

12. Huston, D. L., & Logan, G. A. (2004). Barite, BIFs and bugs: evidence for the evolution of the Earth's early hydrosphere. Earth and Planetary Science Letters, 220(1-2), 41-55.

13. Fuerstenau, D. W., & Abouzeid, A. Z. (2002). The energy efficiency of ball milling in comminution. International Journal of Mineral Processing, 67(1-4), 161-185.

14. Fuerstenau, D. W., De, A., & Kapur, P. C. (2004). Linear and nonlinear particle breakage processes in comminution systems. International Journal of Mineral Processing, 74, S317-S327.

15. Fuerstenau, D. W., & Kapur, P. C. (1995). Newer energy-efficient approach to particle production by comminution. Powder Technology, 82(1), 51-57.

16. Fruehan, R. J. (1977). The rate of reduction of iron oxides by carbon. Metallurgical Transactions B, 8(1), 279-286.

17. Faris, N., Tardio, J., Ram, R., Bhargava, S., & Pownceby, M. I. (2017). Investigation into coal-based magnetizing roasting of an iron-rich rare earth ore and the associated mineralogical transformations. Minerals Engineering, 114, 37-49.

18. Fuerstenau, D. W., & Vazquez-Favela, J. (1997). On assessing and enhancing the energy efficiency of comminution processes. Mining, Metallurgy & Exploration, 14(1), 41-48.

19. Gutsche, O., Kapur, P. C., & Fuerstenau, D. W. (1993). Comminution of single particles in a rigidly-mounted roll mill Part 2: Product size distribution and energy utilization. Powder technology, 76(3), 263-270.

20. HERBST, J. A. (1968). The zero-order production of fine sizes in comminution and its implications in simulation. Trans. AIME, 241, 538-549.

21. Hartlieb, P., Kuchar, F., Moser, P., Kargl, H., & Restner, U. (2018). Reaction of different rock types to low-power (3.2 kW) microwave irradiation in a multimode cavity. Minerals Engineering, 118, 37-51.

22. Hartlieb, P., Toifl, M., Kuchar, F., Meisels, R., & Antretter, T. (2016). Thermo-physical properties of selected hard rocks and their relation to microwave-assisted comminution. Minerals Engineering, 91, 34-41.

23. Haque, K. E. (1999). Microwave energy for mineral treatment processes—a brief review. International journal of mineral processing, 57(1), 1-24.

24. Hayashi, M., Takeda, K., Kashimura, K., Watanabe, T., & Nagata, K. (2013). Carbothermic reduction of hematite powders by microwave heating. ISIJ international, 53(7), 1125-1130.
25. Hayashi, M., Yokoyama, Y., & Nagata, K. (2010). Effect of particle size and relative density on powdery Fe3O4 microwave heating. Journal of Microwave Power and Electromagnetic Energy, 44(4), 198-206.
26. IBM, Indian Bureau of Mines, Indian Minerals Yearbook (2017) (Part- III: Mineral Reviews) 56th edition IRON ORE.
27. Iwasaki, I., & Prasad, M. S. (1989). Processing techniques for difficult-to-treat ores by combining chemical metallurgy and mineral processing. Mineral Procesing and Extractive Metallurgy Review, 4(3-4), 241-276.
28. Ishizaki, K., & Nagata, K. (2008). Microwave Induced Solid–Solid Reactions between Fe3O4 and Carbon Black Powders. ISIJ international, 48(9), 1159-1164.
29. Jena, S. K., Dhawan, N., Rath, S. S., Rao, D. S., & Das, B. (2016). Investigation of microwave roasting for potash extraction from nepheline syenite. Separation and Purification Technology, 161, 104-111.
30. Kapur, P. C. (1982). An improved method for estimating the feed-size breakage distribution functions. *Powder Technology*, *33*(2), 269-275.
31. Kato, T., Kobayashi, K., Yoshikawa, N., & Taniguchi, S. (2011). Microstructure Analysis of Fe3O4 Heated by Microwaves in a TE10 Mode Cavity: Surface and Volume Characterization. Journal of Microwave Power and Electromagnetic Energy, 45(2), 79-85.
32. Kingman, S. W., & Rowson, N. A. (2000). The effect of microwave radiation on the magnetic properties of minerals. Journal of Microwave Power and Electromagnetic Energy, 35(3), 144-150.
33. Kelly, E. G., & Spottiswood, D. J. (1990). The breakage function; what is it really?. Minerals Engineering, 3(5), 405-414.
34. King, R. P. (2012). Modeling and simulation of mineral processing systems. Elsevier.
35. Long, H., Meng, Q., Chun, T., Wang, P., & Li, J. (2016). Preparation of metallic iron powder from copper slag by carbothermic reduction and magnetic separation. Canadian Metallurgical Quarterly, 55(3), 338-344.

36. Liu, L., Tan, Q., Li, W., & Lv, L. (2017). Comparison of grinding characteristics in high-pressure grinding roller (HPGR) and cone crusher (CC). Physicochemical Problems of Mineral Processing, 53.

37. Montgomery, D. C., & Runger, G. C. (2016). *Applied statistics and probability for engineers, (With CD)*. John Wiley & Sons.

38. Mendoza, A. L., & Gómez, J. D. (2017). Effect of Microwave Pretreatment on Grinding of Iron Ore. Asian Journal of Chemistry, 29(5), 983.

39. Matijašic, G., & Glasnovic, A. (2009). Batch Grinding in Laboratory Ball Mills: Selection Function. Chemical Engineering & Technology: Industrial Chemistry-Plant Equipment-Process Engineering-Biotechnology, 32(10), 1560-1566.

40. Malghan SG (1976) "The scale up of ball mills using population balance models", Ph D, University of California, Berkeley, California, USA.

41. Mineral commodity summaries (2016). US Geological Survey.

42. Makhija, D., Mukherjee, A. K., & Ghosh, T. K. (2013). Preconcentration feasibility of gravity and magnetic techniques for banded hematite jasper. Int J Min Eng Miner Process, 2, 8-15.

43. Mishra, S., & Roy, G. G. (2016). Effect of amount of carbon on the reduction efficiency of iron ore-coal composite pellets in multi-layer bed rotary hearth furnace (RHF). Metallurgical and Materials Transactions B, 47(4), 2347-2356.

44. Omran, M., Fabritius, T., Elmahdy, A. M., Abdel-Khalek, N. A., El-Aref, M., & Elmanawi, A. E. H. (2014). Effect of microwave pre-treatment on the magnetic properties of iron ore and its implications on magnetic separation. Separation and Purification Technology, 136, 223-232.

45. Peng, Z., Hwang, J. Y., Andriese, M., Bell, W., Huang, X., & Wang, X. (2011). Numerical simulation of heat transfer during microwave heating of magnetite. ISIJ international, 51(6), 884-888.

46. Peng, Z., Hwang, J. Y., Park, C. L., Kim, B. G., & Onyedika, G. (2012). Numerical analysis of heat transfer characteristics in microwave heating of magnetic dielectrics. Metallurgical and Materials Transactions A, 43(3), 1070-1078.

47. Peng, Z., Li, Z., Lin, X., Yang, M., Hwang, J. Y., Zhang, Y., & Jiang, T. (2017). Microwave power absorption in materials for ferrous metallurgy. Jom, 69(2), 178-183.

48. Pickles, C. A. (2009). Microwaves in extractive metallurgy: Part 2–A review of applications. Minerals Engineering, 22(13), 1112-1118.

49. Napier-Munn, T. J., Morrell, S., Morrison, R. D., & Kojovic, T. (1996). Mineral comminution circuits: their operation and optimisation..
50. Poveromo, J. J. (1999). Iron Ores. The Making, Shaping, and Treating of Steel: Ironmaking, 2, 547–550.
51. Rath, S. S., Sahoo, H., Dhawan, N., Rao, D. S., Das, B., & Mishra, B. K. (2014). Optimal recovery of iron values from a low grade iron ore using reduction roasting and magnetic separation. Separation Science and Technology, 49(12), 1927-1936.
52. Ray, N., Nayak, D., Dash, N., & Rath, S. S. (2018). Utilization of low-grade banded hematite jasper ores: recovery of iron values and production of ferrosilicon. Clean Technologies and Environmental Policy, 20(8), 1761-1771.
53. Rajavaram, R., Lee, J., Oh, J. S., Kim, H. G., & Lee, J. (2016). Microwave heating characteristics of magnetite ore. Metals and Materials International, 22(6), 1116-1120.
54. Ray N, Nayak D, Dash N, et al. Utilization of low-grade banded hematite jasper ores: recovery of iron values and production of ferrosilicon. Clean Technol Envir Policy. 2018:1-11, https://doi.org/10.1007/s10098-018-1566-7.
55. Rayapudi, V., Agrawal, S., & Dhawan, N. (2019). Investigation of Microwave Exposure on Beneficiation of Low-Grade Banded Iron Ore. *Mining, Metallurgy & Exploration*, *36*(2), 327-334.
56. Renato de Castro, E., Breda Mourão, M., Jermolovicius, L. A., Takano, C., & Thomaz Senise, J. (2012). Carbothermal reduction of iron ore applying microwave energy. steel research international, 83(2), 131-138.
57. Rath, S. S., Dhawan, N., Rao, D. S., Das, B., & Mishra, B. K. (2016). Beneficiation studies of a difficult to treat iron ore using conventional and microwave roasting. Powder technology, 301, 1016-1024.
58. Rao, R. B., Narasimhan, K. S., & Rao, T. C. (1991). Effect of additives on grinding of magnetite ore. Mining, Metallurgy & Exploration, 8(3), 144-151.
59. Singh, S., Sahoo, H., Rath, S. S., Palei, B. B., & Das, B. (2015). Separation of hematite from banded hematite jasper (BHJ) by magnetic coating. Journal of Central South University, 22(2), 437-444.
60. Singh, S., Sahoo, H., Rath, S. S., Palei, B. B., & Das, B. (2015). Separation of hematite from banded hematite jasper (BHJ) by magnetic coating. Journal of Central South University, 22(2), 437-444.
61. Singh, V., Venugopal, R., Tripathy, S. K., & Saxena, V. K. (2017). Comparative analysis of the effect of microwave pretreatment on the milling and liberation characteristics of

mineral matters of different morphologies. Minerals & Metallurgical Processing, 34(2), 65-75.

62. Srinivasan, N. S., & Lahiri, A. K. (1977). Studies on the reduction of hematite by carbon. Metallurgical transactions B, 8(1), 175-178.
63. Sahoo, H., Rath, S. S., Rao, D. S., Mishra, B. K., & Das, B. (2016). Role of silica and alumina content in the flotation of iron ores. International Journal of Mineral Processing, 148, 83-91.
64. Standish, N., & Huang, W. (1991). Microwave application in carbothermic reduction of iron ores. ISIJ international, 31(3), 241-245.
65. Standish, N., Worner, H. K., & Obuchowski, D. Y. (1991). Particle size effect in microwave heating of granular materials. Powder Technology, 66(3), 225-230.
66. Schonert, K. (1986). Advances in the physical fundamentals of comminution. Advances in mineral processing, 28.
67. Tavares, L. M., & King, R. P. (1999). Evaluation of thermally-assisted fracture of particles using microscale fracture measurements. KONA Powder and Particle Journal, 17, 163-172.
68. Tavares, L. M. (2004). Optimum routes for particle breakage by impact. Powder Technology, 142(2-3), 81-91.
69. Tripathy, A., Bagchi, S., Rao, D. S., Nayak, B. K., Rout, P. K., & Biswal, S. K. (2018). Recovery of magnetite from low grade banded magnetite quartzite (BMQ) ore. Metallurgical Research & Technology, 115(3), 302.
70. Uwadiale, G. G. O. O. (1992). Magnetizing reduction of iron ores. Mineral Processing and Extractive Metullargy Review, 11(1-2), 1-19.
71. Veasey, T. J., & Wills, B. A. (1991). Review of methods of improving mineral liberation. Minerals Engineering, 4(7-11), 747-752.
72. Walkiewicz, J. W., Clark, A. E., & McGill, S. L. (1991). Microwave-assisted grinding. IEEE Transactions on industry applications, 27(2), 239-243.
73. Youssef, M. A., & Morsi, M. B. (1998). Reduction roast and magnetic separation of oxidized iron ores for the production of blast furnace feed. Canadian metallurgical quarterly, 37(5), 419-428.
74. Yoshikawa, N., Cao, Z., Louzguin, D., Xie, G., & Taniguchi, S. (2009). Micro/nanostructure observation of microwave-heated Fe 3 O 4. Journal of Materials Research, 24(5), 1741-1747.

75. Yu, J., Han, Y., Li, Y., & Gao, P. (2017). Beneficiation of an iron ore fines by magnetization roasting and magnetic separation. International Journal of Mineral Processing, 168, 102-108.
76. Walkiewicz, J. W., Clark, A. E., & McGill, S. L. (1991). Microwave-assisted grinding. IEEE Transactions on industry applications, 27(2), 239-243.
77. Wills, B. A., & Finch, J. (2015). Wills' mineral processing technology: an introduction to the practical aspects of ore treatment and mineral recovery. Butterworth-Heinemann.
78. Zhu, D. Q., Zhao, Q., Qiu, G. Z., Pan, J., Wang, Z. Q., & Pan, C. J. (2010). Magnetizing roasting-magnetic separation of limonite ores from Anhui province in east China. Journal of University of Science and Technology Beijing, 32(6), 713.
79. Zhong, C., Xu, C., Lyu, R., Zhang, Z., Wu, X., & Chi, R. A. (2018). Enhancing mineral liberation of a Canadian rare earth ore with microwave pretreatment. Journal of Rare Earths, 36(2), 215-224.

APPENDIX

1. **Primary, Secondary jaw crushing and roll Crushing procedure:**

   a. Thoroughly clean the jaw crusher and roll crusher to avoid contamination.

   b. Adjust the jaw gap to appropriate distance by lever to ensure the effective crushing operation.

   c. The large feed sample size will be unacceptable for crushing and will slip on the jaw/roll surface. It is recommended to break the large sample using hammer.

   d. It is necessary to ensure the constant feeding rate of the feed material to prevent choking or breakage of jaw/roll crusher.

   e. To obtain the desirable size fraction it is recommended to further process the material using secondary jaw crusher and roll crusher.

   f. Sieve the crushed sample to obtain P_{100} of particle size passing 6.35 mm sieve. This size was used to prepare a representative sample.

2. **Calculation for feed mass in ball milling process.**

   Dimensions:

   Diameter of the jar, D = 10 inch. = 25.4 cm = 0.254 m

   Length of the jar, L = 11.5 inch. = 29.21 cm = 0.2921 m

   Volume of the jar, $V_{jar} = \frac{\pi D^2 L}{4} = \pi x 25.4^2 x 29.21/4 = 14800.9254 cm^3$

   Therefore, Total volume of Balls and Solids should be filled, $x = V_{Balls} + V_{jar}$

   Mass of Balls to be filled:

   fractional Ball Filling, $J = \frac{M_{ball}}{(\rho_{ball} x\, V_{jar})} x \frac{1}{0.6}$

   If fraction of ball filling, J = 0.3 ; Therefore, ===> $0.3 = \frac{M_{ball}}{(7.85 \times 14800.9254)} X \frac{1}{0.6}$

   Mass of Ball, M_{ball}= 20.913 kg

   Mass of Powder to be filled:

   Fraction of powder to be filled, $f_c = \frac{\text{Mass of Powder}}{(\text{Density of Powder x volume of jar})} X \frac{1}{0.6}$

   If, J= 0.3, then f_c= 0.9 x 0.3 x 0.3 = 0.081

   Therefore ===> $0.081 = \frac{\text{Mass Powder}}{(2.5 \times 14800.9254)} x \frac{1}{0.6}$

   Mass of powder to be filled, m_p = 1798.31 g = 1.79 kg.

3. Procedure for magnetic separation

a) Turn on DC power supply in control panel and ensure that the output current and voltage are set to "0" value.

b) Fix the matrix (steel wool/Rod) in between magnetic poles before setting the magnetic intensity (Gauss value).

c) Allow the output voltage and current to stabilize before commencement of experiment.

d) The matrix selection for the magnetic separation is based on the particle size used. (steel wool for less than 150 µm and rod matrix for particle size between 150 µm to 500 µm).

e) Prepare the sample slurry by mixing sample in distilled water at fixed solid to liquid ratio, powder: water ratio should at least 1:10.

f) Pour the slurry through the matrix, and then collect the non-magnetic portion which is coming down through the matrix. Pour fresh water afterwards to ensure the separation of non-magnetic particles trapped in the matrix.

g) Then slowly decrease the voltage to reduce the GAUSS Value and turn off the DC power supply to collect the magnetic portion which is trapped in the matrix.

4. Procedure for spiral concentrator

a) Switch on electrical power and turn on the spiral concentrator.

b) Considering the particle size, the spiral concentrator should be allowed to use only less than one mm in particle size.

c) Thoroughly mix sample and liquid (water) to make uniform slurry. The solid to liquid ratio should be 1:8 to 1:10.

d) Run the machine 15 to 20 min continuously to make uniform flow of the slurry in spiral profile.

e) The Lighter particles will move towards the outer periphery of the spiral profile and heavier particles will move towards the centre of the axis of the spiral profile due to the centrifugal force acts on it.

f) The lighter particles report to the tailing section, while the coarser particles reports to the concentration section.

g) Proper cleaning is required to avoid the contaminations before and after the experiment.

5. Procedure for reduction studies

a) Reduction studies were conducted in a domestic microwave (LG brand, 900 Watts, 2.45 GHz, and MC2846SL) and in conventional muffle furnace (Carbolite brand, CWF 1200).

b) The ground iron ores sample was thoroughly mixed with the reductant (dosage: stoichiometric value) and poured it in refractory crucible.

c) Place the crucible covered with lid in muffle furnace. Whereas in microwave carbothermal reduction the crucible was placed at centre of the microwave, since, microwave radiation concentrates at the centre of the cavity. The attained temperature was measured with K- type thermocouple.

d) The reduced samples were taken out from furnace and immediately water quenched to avoid oxidation of the reduced samples, once the experiment completes.

e) The water was decanted and the reduced sample was dried in a hot oven for 30 min at 70 ºC. And the dried reduced sample was pulverised in pistol mortar to sieve with a screen size 75 µm.

f) The pulverized sample was subjected to wet low intensity magnetic separation (Applied magnetic intensity, for BHJ/BHQ=1800 Gauss and for BMQ=1000 Gauss).

g) All the obtained concentrate were characterized to study the phase transformation through XRD and magnetic properties through VSM, elemental analysis through SEM-EDAX, microscopic tests through optical microscopy.

6. Determination of total iron

0.25gm of powdered sample was taken in a conical flask and ~25ml of concentrated HCl was added to it and allowed to boil. When the iron ore completely dissolved, a 10% $SnCl_2$ solution was added slowly into the boiling solution until the yellow (Fe-III) colour disappears. Then 2 drops of excess $SnCl_2$ solution was added. Then the solution was cooled under tap water. After that, 10 ml of saturated $HgCl_2$ solution was added rapidly to obtain a small quantity of white precipitate. After 2-3 min, ~10 ml of acid mixture (H_2SO_4, H_3PO_4 and deionized water mixture) was added. Then the solution was diluted with distilled water and cooled under tap water. Then 2 to 3 drops of 1% barium

diphenylamine sulphonate indicator was added slowly followed by titration with 0.1 N $K_2Cr_2O_7$ solutions. The end point was noted to the first permanent violet from a blue-green, through a greyish tinge. The % Fe was calculated from the volume of the $K_2Cr_2O_7$ solution consumed.

Calculation:

$$Total\ iron\ \% = \frac{\text{Burret reading X Normality of } K_2Cr_2O_7 \text{ X } 0.05585 \text{ X } 100}{\text{Weight of the sample}}$$

7. Determination of metallic iron

The method is based on the selective dissolution of metallic iron in $CuSO_4$ solution. The sample (0.2-0.4 g) is taken in the 500ml reaction flask of the apparatus. Then 30ml of 10% aqueous $CuSO_4$ solution is added and the mixture is refluxed for 30min. The dissolution of metallic iron in $CuSO_4$ solution is carried out in presence of K_2SO_4 to prevent the hydrolysis of the $CuSO_4$ solution. The flask is then connected to the filtration assembly and filtration is carried out under carbon dioxide atmosphere. The residue is washed with distilled water. The acidity of the filtrate is adjusted to 4M with respect to hydrochloric acid and the solution is titrated against N/10 $K_2Cr_2O_7$, N-phenylanthranilic acid (NPA) is used as indicator.

$$Metallic\ iron\ \% = \frac{\text{B. R. x Normality of } K_2Cr_2O_7 \text{x } 0.05585 \text{ x } 100}{\text{Weight of the sample}}$$

8. Stoichiometric calculations

The following sequential wise equations for the calculation of

$C+O_2 \leftrightarrow CO_2$ (1)

$CO_2+C \leftrightarrow CO_2$ (2)

$Fe_2O_3+3CO = 2Fe + 3CO_2$ (3)

- 12 g of Carbon gives 44 g of CO_2

  12 g C ➔ 44 g CO_2

- 44 g of Carbon dioxide ➔ 56 g of CO

  44g CO_2 ➔ 56 g CO

- According to equation 3, 160 g of Fe_2O_3 requires 84 g CO to transform to metallic iron

  160g Fe_2O_3 ➔ 84 g CO

  56 g of CO ➔ 12 g of C

  1g of CO ➔ (12/56) g of C

  - Therefore 84 g of CO = 84 x (12/56) g of C

84 g of Co ➔18 g of C

- Therefore 160 g of Fe_2O_3 ➔ 18 g of C

  Since BHJ contains 53.6 g of Fe_2O_3

  So, 53.6 g of Fe_2O_3 ➔ (18/160) x 53.6 ➔6.03 g of C

- Therefore, as per stoichiometric calculations to convert the hematite in ore to metallic iron it requires 6.03% Carbon.

9. Energy Calculation for microwave and muffle furnace

Microwave energy calculations:

Frequency, f = 2.45 GHz
Density of iron ore, ρ = 3.5 g/cm^3

Mass, m = 25 gram
Time, t = 10 min
Microwave efficiency = 35%

Microwave dimensions,
Length, l = 0.4 m
Breadth, b = 0.26 m
Height, h = 0.16m

Energy input, $E_{in} = p \times t = 0.9 \times \frac{10}{60} = 0.15\ kWh$

Actual energy, $E_{act} = \eta \times E_{in} = 0.35 \times 0.15 = 0.0525\ kWh$

$$Number\ of\ microwaves\ generated\ in\ 10\ min = \frac{0.0525}{(6.64 \times 10^{-34}) \times (2.45 \times 10^{9}) \times (2.77 \times 10^{-7})} = \frac{0.0525}{(45.06 \times 10^{-32})}$$

$$= 1.165 \times 10^{29}\ no\ of\ waves$$

As per the theoretical assumptions,
Microwaves generated is proportional to the surface area of the chamber,
Surface area of microwave, a = 2 (lb+bh+hl) = 0.736 m^2
Density = mass/volume
The crucible in which the sample was kept is of hemispherical shape.
Therefore, volume=25/3.5 = 7.14 = 2/3 πr^3 => radius of sample = 1.50 cm
Area of sample = $2\pi r^2 = 2 \times \pi \times (1.50 \times 10^{-2})^2$= 0.00142 m^2
Waves absorbed by sample, $= \frac{0.00142}{0.736} \times 1.165 \times 10^{29} = 2.247 \times 10^{26}$
Energy consumed during microwave reduction for 25 g sample at 900 W,
$= (2.247 \times 10^{26})(6.64 \times 10^{-34})(2.45 \times 10^{9})(2.77 \times 10^{-7}) = 101.25 \times 10^{-6}\ kWh$

Energy consumed per tonne = 405.02 kWh/ton for 10 min

Table Microwave energy calculations with respect to its power (Sample density: 3.5 g/cc)

Power (Watts)	Energy consumed (kWh/tonne)
900	405.02
720	324
540	243.08
360	144
180	81.03

Muffle furnace energy calculation for BHJ

Assumptions,	
Mass of sample, m = 500 g	Specific heat of ore, S_{ore} = 0.2 kcal/kgK=0.836 kJ/kgK
Initial temperature, T_i = 30 ºC = 303 K	Final temperature, T_f = 900 ºC = 1173 K

Heat absorbed by ore, $Q_1 = mS_{ore}\Delta T = 0.5 \times 0.836 \times 870 = 363.67\ kJ$
Loss of ignition ore = 1.42%
Loss of ignition for 1 tonne of ore = 14.2 kg
Energy consumed by water (Q_2),
$= 14.2 \times 1.007 \times 75 = 1072.45 \frac{kcal}{ton\ of\ ore}$ (Assuming, from 25 ºC to 100 ºC)
Energy consumed during vaporization, $= 14.2 \times 540 = 7668 \frac{kcal}{ton\ of\ ore}$
Energy consumed by sample (iron ore), (Assuming, C_p of ore, = 0.213 kcal) (Q_3)

$$= 985.8 \times 875 \times 0.213 = 183728.5 \frac{kcal}{ton\ of\ ore}$$

Total energy consumed, $= 192468.95 \frac{kcal}{ton\ of\ ore} = 223.7 \frac{kWh}{ton\ of\ ore}$

Muffle furnace energy calculation for BHQ

Assumptions,	
Mass of sample, m = 500 g	Specific heat of ore, S_{orre} = 0.2 kcal/kgK=0.836 kJ/kgK
Initial temperature, T_i = 30 ºC = 303 K	Final temperature, T_f = 900 ºC = 1173 K

Heat absorbed by ore, $Q_1 = mS_{ore}\Delta T = 0.5 \times 0.836 \times 870 = 363.67\ kJ$
Loss of ignition ore = 0.45%
Loss of ignition for 1 ton of ore = 14.2 kg
Energy consumed by water,
$= 4.5 \times 1.007 \times 75 = 339.86 \frac{kcal}{ton\ of\ ore}$ (Assuming, from 25 ºC to 100 ºC)
Energy consumed during vaporization, $= 4.5 \times 540 = 2430 \frac{kcal}{ton\ of\ ore}$
Energy consumed by sample (iron ore), (Assume C_p of ore, = 0.213 kcal)

$$= 995.5 \times 875 \times 0.213 = 185536.31 \frac{kcal}{ton\ of\ ore}$$

Total energy consumed, $= 188306.18 \frac{kcal}{ton\ of\ ore} = 218.85 \frac{kWh}{ton\ of\ ore}$

10. Other supporting experimental data:

Table: Effect of charcoal dosage on various response parameters of BHQ ore

Charcoal dosage (%)	Fe_G (%)	Yield (%)	Fe_R (%)	M-Fe	Phases identified	VSM (emu/g)	wt. of balls (g)
12	41.33	72.3	99.6	17.64	Q, Ht, Mt, Fay, Cri, Fe, Wu	28.07	0.53
16	43.56	84.85	86.8	16.1	Q, Ht, Mt, Fay, Cri, Fe, Wu	23.82	--
20	44.01	91.06	98.34	17.64	Fe, Mt, Fay, Cri, Q, Wu	28.73	--

Table: Effect of charcoal dosage on various response parameters of BHJ ore

Charcoal dosage (%)	Fe_G (%)	Yield (%)	Fe_R (%)	M-Fe	Phases identified	VSM (emu/g)	wt. of balls (g)
12	43.34	69.10	80.94	19.18	Q, Ht, Mt, Fay, Cri, Fe, Wu	35.39	0.76
16	43.56	83.84	80.18	18.48	Q, Ht, Mt, Fay, Cri, Fe, Wu	38.17	0.37
20	43.12	93.86	99.75	24.36	Q, Mt, Fay, Cri, Fe, Wu	46.64	--

The effect of increase in sample quantity on responses.

	Feed sample wt. (g)	Fe_G (%)	Yield (%)	Fe_R (%)	balls	Fe values in feed	Fe values recoverd through ferrite balls	% of Fe recovered through ferrite balls
BHQ	25	44.68	55.54	82.72	0.2	7.5	2.46	32.86
	50	32.84	75.01	82.11	0.19	15	1.17	7.80
	75	34.85	77.74	90.30	0.49	22.5	2.01	8.94
BHJ	25	43.34	69.10	80.94	0.76	9.25	7.34	79.36
	50	38.65	76.79	98.92	1.12	18.5	5.41	29.24
	75	36.19	78.57	94.78	1.8	27.75	5.80	20.88